A MICROMECHANICAL MODEL FOR VISCOELASTIC-VISCOPLASTIC

ANALYSIS OF PARTICLE REINFORCED COMPOSITE

A Dissertation

by

JEONG-SIK KIM

Submitted to the Office of Graduate Studies of
Texas A&M University
in partial fulfillment of the requirements for the degree of

DOCTOR OF PHILOSOPHY

December 2009

Major Subject: Mechanical Engineering

A MICROMECHANICAL MODEL FOR VISCOELASTIC-VISCOPLASTIC

ANALYSIS OF PARTICLE REINFORCED COMPOSITE

A Dissertation

by

JEONG-SIK   KIM

Submitted to the Office of Graduate Studies of
Texas A&M University
in partial fulfillment of the requirements for the degree of

DOCTOR OF PHILOSOPHY

Approved by:

Chair of Committee,	Anastasia Muliana
Committee Members,	Ozden Ochoa
	Xin-Lin Gao
	Amine Benzerga
Head of Department,	Dennis O'Neal

December 2009

Major Subject: Mechanical Engineering

ABSTRACT

A Micromechanical Model for Viscoelastic-Viscoplastic Analysis of Particle Reinforced

Composite. (December 2009)

Jeong-Sik Kim, B.S., Dong-A University, Pusan, South Korea;

M.S., Pusan National University, Pusan, South Korea

Chair of Advisory Committee: Dr. Anastasia Muliana

This study introduces a time-dependent micromechanical model for a

viscoelastic-viscoplastic analysis of particle-reinforced composite and hybrid composite.

The studied particle-reinforced composite consists of solid spherical particle and

polymer matrix as constituents. Polymer constituent exhibits time-dependent or inelastic

responses, while particle constituent is linear elastic. Schapery's viscoelastic integral

model is additively combined with a viscoplastic constitutive model. Two viscoplastic

models are considered: Perzyna's model and Valanis's endochronic model. A unit-cell

model with four particle and polymer sub-cells is generated to obtain homogenized

responses of the particle-reinforced composites. A time-integration algorithm is

formulated for solving the time-dependent and inelastic constitutive model for the

isotropic polymers and nested to the unit-cell model of the particle composites.

Available micromechanical models and experimental data in the literature are used to

verify the proposed micromechanical model in predicting effective viscoelastic-

viscoplastic responses of particle-reinforced composites. Filler particles are added to

enhance properties of the matrix in the fiber reinforced polymer (FRP) composites. The combined fiber and particle reinforced matrix forms a hybrid composite. The proposed micromechanical model of particle-reinforced composites is used to provide homogenized properties of the matrix systems, having filler particles, in the hybrid composites. Three-dimensional (3D) finite element (FE) models of composite's microstructures are generated for two hybrid systems having unidirectional long fiber and short fiber embedded in cubic matrix. The micromechanical model is implemented at the material (Gaussian) points of the matrix elements in the 3D FE models. The integrated micromechanical-FE framework is used to examine time-dependent and inelastic behaviors of the hybrid composites.

TABLE OF CONTENTS

LIST OF FIGURES

Page

LIST OF TABLES

CHAPTER I

INTRODUCTION

Polymer based materials have been utilized in many engineering applications

since they can be customized to meet a desired performance while maintaining low cost.

However, time-dependent characteristic, poor impact resistance, and low fracture

toughness are often considered as major drawbacks in using polymers. Nano or micro

size particles are then added as fillers to increase crack resistance and improve fracture

toughness. Various types of fibers or particles have also been used to reinforce polymers.

The combined fibers and particles dispersed in a homogeneous constituent form a hybrid

composite. For example, fillers and particles are dispersed in the polymer matrix, which

is then reinforced with fibers. Under relatively high stress levels, polymer composites

exhibit time-dependent and inelastic deformations. The time-dependent and inelastic

deformations become more pronounced at elevated temperatures and hostile moisture

conditions. Depending on the applications, composites are often subject to various

histories of loading and environmental conditions. To accurately predict an overall

_____

This dissertation follows the style of International Journal of Solids and Structures.

performance and lifetime of polymer composites, it is necessary to model time-dependent and inelastic responses of the constituents[1] and to incorporate micro-structural characteristics of the composites, such as size, shape, and compositions of the constituents.

Micromechanical models have been widely used to determine effective mechanical responses of composites by taking into account detailed micro-structural geometries and constitutive models of the constituents. While micromechanical formulations that include detailed micro-structural characteristics can give good response characteristics; it is often difficult to obtain exact closed form solutions especially when material nonlinearity is also considered. Furthermore, it is necessary to integrate the time-dependent and inelastic responses of the composites to the structural analyses. This allows the engineers accurately analyzing performances of composite structures subject to external mechanical and non-mechanical stimuli while recognizing time-dependent and inelastic responses of the constituents.

---

[1] This study deals with a general constitutive relation for modeling a combined viscoelastic and viscoplastic response of isotropic materials undergoing a small deformation gradient. It should be noted that the presented constitutive model is capable of incorporating effects of different loading rates in a quasi-static typed loading, including that of cyclic loadings, on the deformations of polymers. When a material is subjected to high strain/stress rates, in which the inertia effect cannot be ignored like in impact or dynamic loading, it might be necessary to choose different constitutive models.

This study introduces a simplified micromechanical formulation for predicting combined viscoelastic and viscoplastic responses of particle reinforced composites. The micromechanical formulation is designed to be compatible with a general displacement based finite element (FE) framework. Thus, it can be used to analyze performances of composite structures while recognizing histories of deformation in the micro-structural constituents. Time-integration algorithms are formulated to simultaneously solve the governing equations of the viscoelastic and viscoplastic deformations at every material and structural scales. This forms a concurrent multi-scale framework, which is required due to the dependence of the constituent properties on the external mechanical loadings. The proposed micromechanical model of particle reinforced composites is also used to determine effective time-dependent and inelastic responses of matrix systems in hybrid composites. The studied hybrid composites consist of unidirectional fiber reinforcements embedded in a polymer matrix. The polymer matrix consists of particle fillers. The fibers and particles are modeled as linear elastic and the polymer matrix system exhibits time-dependent and inelastic responses. FE meshes of representative microstructures of hybrid composites are generated. The simplified micromechanical model of particle reinforced composites is implemented, via a user material (UMAT, ABAQUS)

subroutine, at each material point in every matrix element of the FE micro-structural

models.

This chapter provides a state of the art knowledge in mechanical behaviors of

polymer composites having particle reinforcements and micromechanical modeling of

particle reinforced composites exhibiting viscoelastic and viscoplastic responses. Studies

of hybrid composites are also discussed. The research objectives are presented in the

second part of this chapter.

1.1 State of the art knowledge in the nonlinear constitutive modeling of particle

   reinforced composite

1.1.1 Mechanical behaviors of particle reinforced polymer composites

Nano and micro size particles are commonly added as fillers to the polymeric

material in order to increase crack resistance and improve fracture toughness in

composite systems (Takahashi et al., 1983; Young et al., 1986). For polymers reinforced

with micro scale spherical beads, it was found that decreasing particle sizes at a constant

particle volume fraction increases the strength of the composites; while increasing

volume fractions at fixed particle size decreases the composite's strength (Leiden and

Woodhams, 1974; Wong and Ait-Kadi, 1995, and Cho et al., 2006). In addition, surface

treatment on particles increases the overall strength due to improvement in the interface

adhesion (Kinloch et al., 1985 and Wong and Ait-Kadi, 1995). On the other hand, the

effective moduli of the composites depend strongly on the particle volume contents and

are less influenced by the particle sizes (Wong and Ait-Kadi, 1995; Chawla et al., 2004;

Yang et al., 2004, and Cho et al., 2006). These phenomena are observed for composites

made of rigid particles and soft matrix and also for composites having soft particles and

stiffer matrix. Wong and Ait-Kadi (1995) also found that the effect of particle size on the

composite's failure strain is insignificant, while surface treatment on the particles

reduces the composite's failure strain. For composites containing nano particles, their

effective moduli are not only influenced by the volume contents of particles but also on

the size of the particles. Cho et al. (2006) showed that the elastic modulus increases with

decreasing particle sizes at the nano scale.

Polymer based composites exhibit viscoelastic behaviors. Their viscoelastic

responses become more significant under high load levels and severe environmental

conditions and are often accompanied by inelastic deformations. Limited experimental

studies have been done on understanding the viscoelastic behaviors of particulate

reinforced polymer composites (Alberola and Mele, 1996; Tsou and DelleFave, 1996; Park and Schapery, 1997 and Aniskevich and Hristova, 2000). Aniskevich and Hristova (2000) conducted four month creep tests on polyester resin reinforced with diabase and marble spherical particles. The average volume fraction of the studied composites was 28%. Creep tests were also performed on the unreinforced polyester resin. It was shown that after four month testing periods, the creep compliance for the polyester resin increased 400% compared to the one measured at 20 hour; while the compliances of the diabase/polyester and marble/polyester composites showed nearly 240% increase. Park and Schapery (1997) showed significant viscoelastic behaviors of rubber matrix having 70 percent volume contents of aluminum particles. The creep tests were performed at four different temperatures (25°C,-10°C,-25°C, and-40°C). It was shown that viscoelastic responses were more pronounced at elevated temperatures. Belayachi et al. (2008) investigated viscoplastic responses of spherical rubber particles embedded in glassy polymer matrix (PMMA). Composites with 10, 20, and 45% particle contents were tested under constant strain rates. The test were performed for different strain rates ($10^{-2} s^{-1}, 10^{-3} s^{-1}$, and $10^{-4} s^{-1}$) and temperatures (25°C, 60°C, and 80°C). It was

observed that the yield stress decreases with increasing particle contents and increases

with increasing temperatures and strain rates.

1.1.2 Micromechanical models of composites having particle reinforcements

Two classes of analytical modeling approaches have been proposed to evaluate

the effective mechanical responses of composites having various micro-structural

geometries and in-situ material properties. The first class treats the overall composite

system as a homogeneous medium with continuous stress and strain fields. The

constitutive material models are developed for the overall composite behaviors without

recognizing detailed microstructures and constituent properties. The second class uses a

micromechanical modeling concept which allows incorporating various micro-structural

geometries and properties of the constituents. Each constituent is represented by a

homogeneous and continuous medium. Homogenization schemes based on the dilute-

distribution method (Eshelby, 1957), self-consistent model (Kerner, 1956; Hill, 1965;

Willis, 1977 and Christensen and Lo, 1979), variational method (Hashin and Shtrikman,

1962), differential scheme (McLaughlin, 1977), and periodically distributed

microstructures (Aboudi, 1991) have been proposed to evaluate effective elastic and

inelastic responses of composites. These micromechanical models are formulated in

terms of exact stress-strain fields of the micro-structural geometries. Boundary value

problems (BVPs) are solved to determine the stress, strain, and deformation fields

throughout the constituents of the composites. Volume average scheme is then used to

obtain effective properties of composites. These micromechanical models are best for

providing overall properties when each constituent is made of a linear elastic material.

However, it is often difficult to obtain the exact closed form solutions especially when

material nonlinearity or inelastic behaviors are also considered. Extensive reviews and

formulations of micromechanical models can be found in Mura (1987); Nemat-Nasser

and Hori (1999) and Eroshkin and Tsukrov (1995) which focus on predicting mechanical

properties of composites.

Haj-Ali and Pecknold (1996) formulated a simplified unit-cell model for fiber

reinforced composites, derived from periodically distributed microstructures. The unit-

cell model consisted of several constituent sub-cells. The micromechanical

homogenization schemes were formulated in terms of the average stress-strain relations

in the sub-cells. For composite systems with nonlinear constitutive models in the

individual constituents, stress correction schemes were added to satisfy both the

micromechanical constraints and the nonlinear constitutive equations. The linearized

homogenization and corrector schemes have been successfully applied to model

nonlinear and time-dependent behaviors of composite materials having unidirectional

and randomly oriented fiber reinforcement (Haj-Ali and Muliana, 2003, 2004), and have

been extended for predicting overall response of particle reinforced composites. Ghosh

et al. (1991) have proposed Voronoi Cell Finite Element Method (VCFEM) to predict

effective properties of heterogeneous materials. A representative microstructure of

materials was divided into a network of multi sided convex elements called "Voronoi

polygons or Cells". These Voronoi polygons are treated as elements in the FE scheme.

To model multi-phase materials, heterogeneities or inclusions can be included to each

Voronoi polygon. The Voronoi element has been coupled to an asymptotic

homogenization scheme for multi-scale analyses of heterogeneous materials. Ghosh and

Moorthy (1995) have extended the VCFEM for analyzing elastic-plastic behavior of

heterogeneous materials.

Limited micromechanical models have been developed for predicting effective

viscoelastic behaviors of particle reinforced composites. Christensen (1969) presented

closed form analytical solutions for upper and lower bounds of the composite's complex

shear modulus. The studied composites consisted of perfectly rigid spherical inclusions

embedded in a linear viscoelastic matrix. The viscoelastic model followed a hereditary

integral form for an isotropic case. The effective properties of elastic composites were

converted directly to viscoelastic composites by replacing the elastic moduli with the

complex moduli. Li and Weng (1993) developed a micromechanical model for

predicting strain-rate sensitivity, relaxation behavior, and complex moduli of randomly

oriented spherical particles in a viscoelastic matrix. A linear viscoelastic behavior based

on four-parameter Maxwell model was incorporated for the matrix. They found that the

relaxation behavior of the composite having spherical particles were more pronounced

than those reinforced composites with other inclusion shapes. Yang et al. (1994) used

Eshelby's (1957) solution to derive effective elastic and viscoelastic properties of

composites. The simplified averaging method was applied only for rigid particle

reinforced composites. Hashin (1983) presented a review of homogenization methods for

determining effective properties of composites having particle reinforcements. Effective

properties were obtained for elastic and viscoelastic moduli, thermal expansion, moisture

swelling, and conductivity. Alberola and Mele (1996) used percolation concept to

include phase interaction in modeling viscoelastic behaviors of polymers reinforced with

spherical particles. A three concentric phase micromechanical model was used. The

effective responses of the composites are formulated based on the self-consistent method.

The inner and outer phases were designated for non-percolated and percolated matrix,

respectively, while the middle phase was the filler particle. Both rigid and soft particles

were studied and taken as linear elastic materials. A linear viscoelastic constitutive

model is used for the polymeric phases. Experimental data on the storage modulus and

loss tangent (damping factors) of glass/polystyrene composites having 15% and 50%

volume fraction were compared with the proposed micromechanical model. It was

shown that this micromechanical model was able to incorporate mechanical coupling

between phases at large composite volume fraction and model bond interaction at the

particle/polymer interface. Levesque et al. (2004) proposed a linearized homogenization

scheme for predicting nonlinear viscoelastic responses of particulate reinforced

composites. The homogenized micromechanical model of the Mori and Tanaka (1973)

was used. The particle was modeled as linear elastic, while the Schapery nonlinear

viscoelastic model (1969) was applied for the matrix phase. Moreover, a detailed

composite FE micromechanical model with 15 particles embedded in the polymeric

matrix was generated to validate their linearized homogenization scheme.

Micromechanical model formulations for predicting elastic-plastic or viscoplastic responses of particle reinforced composites have been derived for metal-matrix composites. Some of these micromechanical models have been extended to predict inelastic or viscoplastic behaviors of polymer based composites. Weng (1993) used the self consistent method for analyzing effective creep behavior of composites. A spherical inclusion is embedded in polycrystal matrix. Inclusion and matrix exhibit different linear viscoelastic behavior. It was assumed that the inclusion creeps less than the matrix creeps. Ju and Chen (1994) presented a micromechanical framework to predict effective elasto-plastic behavior of two-phase particle reinforced metal matrix composites. An overstress concept was used for the plastic response. Particle was assumed to be linear elastic and matrix exhibited an elasto-plastic behavior. To obtain effective responses, the eigen-strain concept of Eshelby (1957), ensemble volume average concept, and closed form micromechanical equation with interaction between the particle and matrix were used. Ju and Tseng (1996) presented a micromechanical framework to predict an effective elastoplastic behavior of particle reinforced ductile matrix composite. They used the micromechanical model proposed by Ju and Chen (1994) having Hill's concentration tensor (1963) and the inter-particle interaction tensor. The effects of

particle constituent and interaction between particles on the deformation in the matrix

constituent were statistically incorporated through the inter-particle interaction tensor.

The micromechanical predictions were verified using experimental data for composites

with several particle volume contents.

Seelig and van der Giessen (2002) investigated elasto-plastic responses of

acrylonitrile-butadiene-styrene (ABS) particles embedded in a polycarbonate (PP). The

ABS rubber particles were considered as voids because of their low modulus. PP matrix

exhibits elasto-viscoplastic behavior. The equivalent elasto-viscoplastic responses of

ABS are obtained via the Mori-Tanaka model. The homogenized elasto-viscoplastic

responses are compared to the ones obtained from the representative volume element

(RVE) models of the composites. The RVE models were generated using 2D FE.

Danielsson et al. (2007) used the Voronoi cell model to predict elasto-viscoplastic

responses of rubber toughened glassy polymers. Periodic boundary condition is imposed

to the representative microstructure of the composites. The viscoplastic flow of the

porous glassy polymer is characterized by a plastic strain rate potential, which followed

a power-law model of Hutchinson (1976). Pierard et al. (2007) developed a linearized

homogenization method to predict elasto-viscoplastic response of particle reinforced

composites. A total strain for a small deformation gradient problem was decomposed into elastic and viscoplastic components. The Laplace-Carson transformation was used to obtain a time dependent response from the thermo-elasticity solution. The mechanical and thermal strain concentration tensors were defined following the Hill's concentration tensor for linear elastic problems. The Mori-Tanaka homogenization method was applied to provide the effective properties. The effective responses from the homogenization procedure were compared with the ones determined from detailed FE microstructures. Mareau et al. (2009) used the self-consistent scheme to incorporate microstructural geometries and constituents' time-dependent behavior of particle reinforced composite. The constitutive models of the constituents were represented by spring-dashpot mechanical analog models. The Laplace-Carson transform was used to determine elastic, elastoplastic, and viscoplastic behaviors.

Some polymers used as constituents in composite systems exhibit combined viscoelastic-viscoplastic responses, e.g. high density polyethylene (Lai and Bakker, 1995) and polycarbonate (Frank, 1998). These combined responses can occur at early loading (small stress/strain levels). However, micromechanical models for a combined viscoelastic-viscoplastic response are very limited. Megnis et al. (2003) used Schapery's

nonlinear viscoelastic-viscoplastic material model for off-axis laminated composite

having unidirectional glass fiber and epoxy. The micromechanical concentric cylindrical

assembly model (Hashin, 1966) was used. The viscoelastic and viscoplastic material

parameters are determined experimentally from the off-axis creep tests. Aboudi (2005)

has developed a micromechanical model to predict the viscoelastic-viscoplastic

responses of multiphase materials. The viscoelastic-viscoplastic model for polymer

developed by Frank and Brockman (2001) is implemented in the multiphase composites.

An asymptotic expansion homogenization (AEH) method is used to obtain effective

properties. Depending on the complexity of the composite's microstructure the AEH

method could result in high computational cost.

FE methods are often used for modeling detailed microstructures of particulate

reinforced composites. The FE method allows generating composite systems having

certain particle numbers with detailed particle size and shape, easily incorporating

different constitutive material models for all the constituents, and modeling various

mechanisms between the constituents (Chen and Mai, 1998; Dommelen et al., 2002;

Chawla et al., 2004; Levesque et al., 2004 and Kari et al., 2007). In addition, unit-cell FE

models have been generated for simulating defect and failure mechanism, such as

particle/fiber and matrix debonding, matrix cracking, fiber breakage, void formation, etc.

Simulating overall composite behaviors by incorporating detailed micro structural

mechanism is often computationally expensive. Moreover, it is not always necessary or

possible to generate detailed micro structural geometries for evaluating overall

composite behaviors.

1.1.3 Responses of hybrid composites

Several experimental studies have been conducted on understanding performance

of hybrid composites. Young et al. (1986) examined elastic moduli of hybrid composites

at different temperatures. The studied hybrid composite consisted of glass fiber, rubber

particle, and epoxy matrix. The elastic moduli of the composite increased with

increasing fiber and particle volume contents and decreasing temperatures. It was also

concluded that the surface treatment of glass fibers significantly influenced the effective

elastic moduli. Friend et al. (1991) examined short-fiber and particulate metal matrix

hybrid composites. The strength and hardness of the hybrid composite are controlled by

the total volume contents of the fibers and particles, while the fracture toughness

depends on the particle contents. It was also found that the ultimate tensile strength and

toughness decreased with increasing particle sizes. Yilmazer (1992) studied a hybrid composite consisting of glass fiber (GF), glass bead (GB) and acrylonitrile butadieve styrene (ABS). It was shown that increasing GF or GB contents in the ABS matrix increased the ultimate strength of the composite. Increasing GB contents in the ABS matrix decreased the failure strain of the composite. Moreover, increasing GF in the ABS matrix increased the flexural strength and tensile strength of the composite, but increasing GB in ABS decreased the flexural strength. Oh et al. (2007) studied failure behavior of a short-fiber/particle hybrid composite. Increasing particle contents increased the fracture toughness and fatigue thresholds of the composite systems. They concluded that the combined short-fiber and particle hybrid composite could increase damage tolerance in the composites. Arunachaleswaran et al. (2007) examined creep behaviors of hybrid composites having alumina short-fiber (saffil) and SiC particle in an alloy AE42 matrix at different temperatures. They compared the creep resistant of a composite having 10% short-fiber volume contents of saffil and 10% particle volume contents of SiC to the one with 15% saffil and 5% SiC. They concluded that the hybrid composite with 10% saffil and 10% SiC exhibited better creep resistance than the one with 15% Saffil and 5% SiC. Mondal et al. (2008) also studied creep and recovery

responses of saffil, SiC, and AE42 hybrid composites in the longitudinal fiber direction. They compared creep resistant at different temperatures and stress levels between the composite filled with only 20% volume contents of saffil short-fiber and the hybrid composite having 15% saffil and 5% particle. Replacing a part of the expensive saffil short-fiber by the cheap SiC particle is beneficial in reducing cost while maintaining similar performance. They also found that permanent deformation is associated with the fiber breakage and dislocation of matrix.

Limited micromechanical modeling approaches of hybrid composites have been developed for predicting effective elastic behaviors. Liu (1998) presented multiple-step homogenization method using the rule of mixture for determining elastic responses of fiber and particle reinforced hybrid composites. The cylinder model is used for the fiber reinforcement, and the sphere model is used for the particle reinforcement. Kanaun et al. (2001) used an effective field approach for a three phase hybrid composite to predict overall elastic response. This method used the Mori-Tanaka micromechanical relation. The composite is divided into sub-regions. The overall elastic responses are predicted by the influence of inclusions and correlation of sub regions. Halpin et al. (1971) developed a laminate analogy approach (LAA) to predict effective mechanical properties of a

laminated system that consists of layers of short fiber composites. This laminate analogy

approach is extended for 2D and 3D composite systems consisting of short fiber

reinforcements. Fu et al. (2002) applied the LAA for predicting effective properties of a

short fiber and particle hybrid composite. The particle filled matrix is considered as an

effective matrix and then they applied the LAA to the short fiber and particle reinforced

hybrid composite. Fu et al. (2002) also used a rule of hybrid mixture (RoHM) to obtain

the elastic modulus of hybrid particle/fiber/polymer matrix composite. The hybrid

composite systems were divided into two systems which are unidirectional fiber

reinforced composite and particle reinforced system.

1.1.4 Viscoelastic and viscoplastic behaviors of polymer

Creep tests on some polymers such as high density polyethylene (Lai and Bakker,

1995), polycarbonate (Frank 1998), and aramid and polyester fibers (Chailleux and

Davies, 2003, 2005) at several stress levels show combined viscoelastic and viscoplastic

responses even at room temperature (20°C) and short periods (around 30 minutes). It is

also shown that the material properties of these polymers depend strongly on the stress

magnitude. To predict the responses of structures made of these polymers, one needs to use proper constitutive model of combined viscoelastic and viscoplastic responses.

Constitutive material models of viscoelastic solids with non-constant properties has been proposed for isotropic materials undergoing small deformation gradients, which can be found in Green and Rivlin (1957), Christensen (1971), Lockett (1972), and Findley et al. (1976). The Schapery (1969) single integral form has been widely used to characterize nonlinear (stress or strain dependent) viscoelastic behaviors of polymers. This viscoelastic model additively combines the elastic (instantaneous) and time dependent (transient) responses, and it consists of four nonlinear (stress or strain dependent) parameters that can be calibrated from a set of creep tests at various stresses or from a set of relaxation tests at various strains. The Schapery model has been extended for isotropic and anisotropic material responses. Levesque et al. (2007) has discussed constraints on the nonlinear material parameters in the Schapery's integral model. These constraints are required to maintain thermodynamically admissible constitutive relations. Several integration algorithms within FE frameworks have been formulated for solving the Schapery's integral model. At each incremental time step, a linearized strain solution is obtained at the material level and equilibrium equations at

the structural level are solved in an iterative manner. Such approach can be found in

Henriksen (1984), Lai and Bakker (1996), Kennedy (1998), Poon and Ahmad (1999),

Haj-Ali and Muliana (2004), Muliana and Khan (2008) and Sawant and Muliana (2008).

Haj-Ali and Muliana (2004) have shown that it is also necessary to include a correction

scheme in addition to the linearized strain solution at the material level in order to avoid

divergence at the structural level, especially for highly nonlinear responses. They also

show that adding iterative solver at the material level can accelerate convergence at the

structural level.

Constitutive relations for time-dependent and inelastic behaviors based on an

overstress function have been extensively developed for materials undergoing small

deformation gradients. The models can be classified into two categories. The first

category additively combines linear viscoelastic and plastic constitutive relations, e.g.,

Landau et al. (1960), Naghdi and Murch (1963), Drozdov (1999). In this category, the

viscoelastic strain rates depend upon loading histories and time, and the plastic strain

rates depend only upon loading path histories. Another category combines linear elastic

and viscoplastic constitutive relations, such as the models proposed by Perzyna (1966,

1971), Perzyna and Wojno (1975), Bodner and Partom (1975). The above constitutive

relations were primarily proposed to model viscoplastic behaviors of metals. Chailleux

and Davies (2003, 2005) have shown that the Perzyna viscoplastic model is able to

describe viscoplastic responses of aramid and polyester fibers. Recently, viscoplastic

constitutive models of polymers based on an overstress having nonlinear rate dependent

behaviors have been formulated, e.g., Krempl and Ho (2000), Colak (2005), Hall (2005).

Reviews on the recently developed constitutive viscoplastic models for polymers can be

found in Colak (2005). Valanis et al. (1971) proposed an endochronic viscoplastic model

based on an irreversible thermodynamics. The viscoplastic strain is expressed by

intrinsic time and internal variables. This model does not require determining yield stress

which is suitable for materials that exhibit inelastic responses at low stresses. With a

proper choice of intrinsic time function, the Valanis model can be related to overstress

based plastic behaviors e.g. Von-Misses plasticity.

To date, limited studies have been done on modeling combined viscoelastic-

viscoplastic behaviors of polymers. Schapery (1997) presented a constitutive equation

for the viscoelastic and viscoplastic behaviors of polymer derived from thermodynamics

principle. The thermodynamics state is defined by the following independent variables:

stress, temperature, moisture, time, and internal state variables. The internal state

variables are attributed to the viscoelastic and viscoplastic strains. The time dependent

modulus and strain hardening parameter are modeled as stress-dependent. It is shown

that even for small deformation gradient problems. The material nonlinearity can arise

from changes in the free energy. Frank and Brockman (2001) proposed a constitutive

model of an isotropic viscoelastic-viscoplastic response of glassy polymers under small

deformation gradient, which additively combines the viscoelastic and viscoplastic

components. The viscoelastic part is expressed by single integral equations of the

deviatoric and volumetric relaxation functions and the Bodner and Partom (1975) model

is used for the viscoplastic component. The nonlinear stress and strain dependent

relaxation functions are incorporated through a time shift factor in the reduced time

equation. The nonlinear softening is also incorporated in the deviatoric relaxation

function. Drozdov and Christiansen (2008) derived a viscoelastic-viscoplastic

constitutive model, which is expressed by exponential terms and seven adjustable

parameters including time and temperature dependent parameters. Incompressible

material behavior is assumed to simply the analysis. A plastic flow is described by an

assumption that deviatoric strain rate linearly increases with increasing total strain rate.

Numerical algorithms within the FE framework have been formulated for solving

the combined linear elastic-viscoplastic models of Perzyna. Examples can be found in

Zienkiewicz and Cormeau (1972, 1974), Wang et al. (1997), Simo and Hughes (1998),

and Heeres et al. (2002). The additive combinations of the elastic and viscoplastic

responses are applied on both strain and strain rate. Zienkiewicz and Cormeau (1972)

presented a time-stepping method to approximate incremental viscoplastic strains at each

time interval by keeping a constant state of stress. To obtain a good approximation and

an efficient computation, the incremental time is suggested to be 0.1-0.2 of the ratio of

the magnitude of the total strains to the magnitude of the viscoplastic strain rates. Wang

et al. (1997) formulated incremental viscoplastic stress-strain relations that are

compatible with the displacement based FE. A one-step Euler integration method is used

to obtain viscoplastic strain rate at the end of the current time interval (t+Δt). The goal is

to calculate the current stress ($\sigma_{t+\Delta t}$). In addition, the local iterative stress-update

algorithm is performed to minimize residual arising from the linearization of the plastic

multiplier, which is associated to the magnitude of the viscoplastic strain rate. Heeres et

al. (2002) show that the incremental plastic multiplier at the current time interval $\Delta t_{t+\Delta t}$

can be directly formed using the following relation $\Delta\lambda_{t+\Delta t} \approx \dot{\lambda}_{t+\Delta t}\Delta t_{t+\Delta t}$ without the need to

discrete the differential equation of the plastic multiplier. To accelerate convergence at

the structural level a consistent tangent stiffness matrix is also formulated. In general, the

consistent tangent stiffness matrix is non-symmetric, as discussed in Ju (1990, 1992) and

Simo and Hughes (1998). Implicit time integrations algorithm based on the consistent

tangent stiffness, initial strain prediction, and mid-point integration methods also have

been developed for other typed of elastic-viscoplastic constitutive models, e.g., Levy and

Pifko (1981), Hornberger and Stamm (1989), and Simo and Hughes (1998). It is shown

that by defining consistent tangent moduli at the material levels can fast converge at the

structural level.

1.2 Research Objective

This study presents a concurrent micromechanical formulation for predicting

overall viscoelastic and viscoplastic responses of particle reinforced polymer matrix

composites. The studied composites consist of linear elastic solid spherical particles and

viscoelastic-viscoplastic polymer matrix constituent. The polymer constituent exhibit

time-dependent and inelastic responses and its material parameters are allowed to change

with stress. The microstructure of the particle reinforced composite is idealized by

uniformly distributed cubic particles embedded in a polymer matrix. A representative

volume element (RVE) is modeled as a single particle placed in the center of a cubic

matrix and a periodic boundary condition is imposed to the RVE. By considering

symmetry conditions in the RVE, a unit-cell model (micromechanical model) is

generated. Each unit cell is divided into a number of sub-cells. The micromechanical

formulation is derived by imposing perfect bonding at the interfaces of the sub-cells. The

effective responses of the composite are formulated based on volume averages of stress

and strain in the constituents in the representative unit-cell model. Experimental data and

analytical solutions available in the literature are used to verify the micromechanical

model formulation. The responses obtained from the present micromechanical model

represent behaviors of a fictitiously homogenized composite. These responses are

compared to the ones of heterogeneous composites having detailed particle micro-

structural models. The heterogeneous composite models are generated using FE.

The concurrent micromechanical model is designed to be compatible with

general displacement based FE frameworks. This micromechanical model is beneficial

to new material and structural designs as performance and life-span of polymer

composites at various loading rates and histories can be simulated by varying constituent

properties and micro-structural arrangements. This method reduces the cost of the

material and structural design by reducing experimental trial and error process. The

proposed study on time-dependent and inelastic behaviors of solid spherical particle

composites can be extended to simulate time-dependent and inelastic behaviors of other

composite systems, such as fiber reinforced polymer composite.

Available studies on micromechanical formulations of hybrid composite systems

focus on predicting effective linear elastic properties. Polymer and aluminum, which are

often used as matrix in the hybrid composites, can exhibit time dependent and inelastic

responses. The time-dependent behavior becomes more pronounced at elevated

temperatures. This study also presents a simplified multi-scale model for predicting

nonlinear viscoelastic and viscoplastic responses of hybrid composites. The studied

hybrid systems consist of unidirectional fiber reinforcements embedded in a matrix

system, having particle fillers and polymer constituent. The concurrent micromechanical

formulation of particle reinforced composite is used to obtain effective properties of the

homogenized matrix system. This matrix system is then integrated to unit-cell models of

and RVE models unidirectional fiber composites, which are generated using the FE.

Limited experimental data available in the literatures are used for comparisons.

This dissertation consists of the following major components:

1)   A time-integration algorithm for solving the time-dependent and inelastic

constitutive material model for isotropic polymer is formulated. Focus will be on

small deformation gradient problems. The Schapery integral model for an isotropic

viscoelastic material with stress-dependent material parameters is used. This integral

model is additively combined with viscoplastic constitutive models, i.e., Perzyna's

(1967) model based on an overstress function and Valanis's (1971) endocronic

model without a yield surface, to simulate combined nonlinear time-dependent and

inelastic material responses.

2)   A concurrent micromechanical model for polymer composites having solid

spherical particles is developed. The composite microstructure is simplified by

periodically distributed cubic particles embedded in a matrix medium. A unit-cell

model with four particle and matrix sub-cells is generated to obtain homogenized

material responses of the composites. The time integration algorithm, derived in item

(1), is incorporated to the matrix sub-cells. Additional time-integration algorithm is

also formulated at the micromechanical level which is compatible with a general FE framework.

3) Viscoelastic-viscoplastic analyses of hybrid composites having fiber reinforcements and particle fillers dispersed in a homogeneous polymer constituent are performed. FE models of micro-structures of the fiber reinforced composites are generated. The effective properties of the matrix system that consists of solid spherical particle fillers and polymer constituent are obtained using the concurrent micromechanical model described in item (2). Performance of hybrid composites at various compositions and properties of fiber, particle, and polymer constituents are examined.

4) Limitation of the proposed model and assumptions made in developing the time-dependent and inelastic micromechanical model are summarized. Future research studies are discussed.

CHAPTER II

A TIME INTEGRATION METHOD FOR THE VISCOELASTIC-VISCOPLASTIC

RESPONSES OF ISOTROPIC MATERIALS

This chapter introduces a time integration algorithm for solving a combined

viscoelastic-viscoplastic constitutive equation of isotropic polymers. The material

parameters in the constitutive models are stress-dependent. The algorithm is derived

based on an implicit time integration method within a general displacement based FE

analysis and suitable for small deformation gradient problems. The Schapery integral

model is used for the 3D isotropic nonlinear viscoelastic responses. Two viscoplastic

models are considered: the Perzyna model, having a static yield condition of rate

dependent plastic material, and the Valanis endochronic model based on an irreversible

thermodynamics without a yield surface. The Valanis model is suitable for materials

when viscoplastic responses occur at early loadings (small stress levels). A recursive

method is employed to solve the viscoelastic-viscoplastic constitutive equation. During

each incremental time step within the recursive method, an iterative procedure is added

to minimize errors arising from the linearized stress-strain relation. A residual vector is

defined in terms of incremental total strain and magnitude of the incremental

viscoplastic strain. Furthermore, a consistent tangent stiffness matrix is formulated to

improve convergence and avoid divergence of the solutions. Available experimental data

on time-dependent and inelastic responses of high-density polyethylene (HDPE) are

used to verify the current numerical algorithm. The proposed time-integration scheme is

also examined in terms of its computational efficiency and accuracy.

2.1 Linearized Solution for the Nonlinear Viscoelastic-Viscoplastic Behaviors

A time integration scheme for the three-dimensional (3D) isotropic viscoelastic-

viscoplastic constitutive model having stress-dependent material properties is formulated.

Linearized solutions of the nonlinear constitutive equations and iterative schemes are

performed, both at the FE structural (global) and material (local) levels. The linearized

relation is used as a starting point to calculate trial stress-strain solutions in every time

increment. Material properties from the previous converged time are used to determine

the trial stress-strain solutions. The purpose of forming iterative schemes is to minimize

errors arising from the linearization; otherwise very small time increments are required.
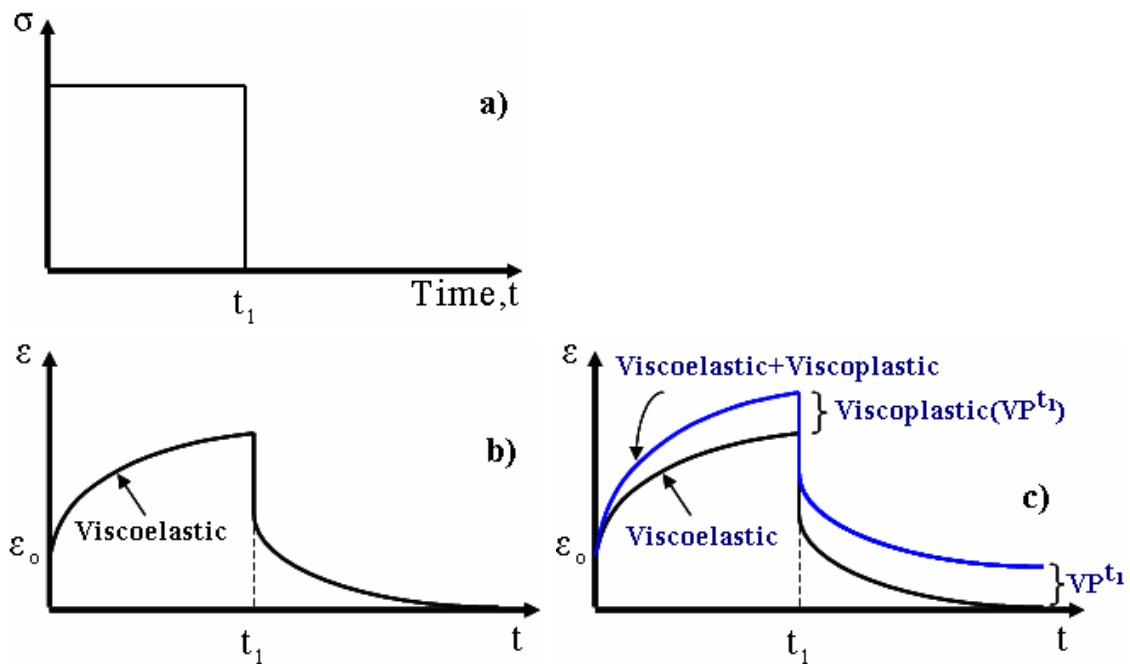
Figure 2-1. Viscoelastic (VE)-Viscoplastic (VP) responses due to a creep recovery loading a) Input loading history b) Viscoelastic response c) Viscoelastic-Viscoplastic response

Figure 2-1 illustrates one-dimensional viscoelastic-viscoplastic response of a

material subject to a creep-recovery loading. The input loading history is shown in Fig.

2-1a. A constant stress is applied at t=0 and held constant until t_1, and the load is

removed at t_1. The strain of a viscoelastic response returns to an original state when a

sufficient recovery time is given. When materials exhibit a combined viscoelastic and

viscoplastic response, the plastic deformation also increases with time during, and only

the viscoelastic strain is recovered during unloading. The accumulated plastic strain up

to time t_1 leads to a plastic strain after fully recovery of the viscoelastic strain is achieved.

In small deformation gradient theory, total strains and incremental strains at a

material point can be written as:

$$
\begin{aligned}
\varepsilon_{ij}^{t} &= \varepsilon_{ij}^{ve,t} + \varepsilon_{ij}^{vp,t} \\
\Delta\varepsilon_{ij}^{t} &= \Delta\varepsilon_{ij}^{ve,t} + \Delta\varepsilon_{ij}^{vp,t} \qquad \forall\ t \geq 0 \\
\varepsilon_{ij}^{t} &= \varepsilon_{ij}^{t\text{-}\Delta t} + \Delta\varepsilon_{ij}^{t} = \varepsilon_{ij}^{ve,t\text{-}\Delta t} + \Delta\varepsilon_{ij}^{ve,t} + \varepsilon_{ij}^{vp,t\text{-}\Delta t} + \Delta\varepsilon_{ij}^{vp,t}
\end{aligned}
\qquad (2\text{-}1)
$$

where $\varepsilon_{ij}^{ve,t}$ and $\varepsilon_{ij}^{vp,t}$ are the viscoelastic and viscoplastic strains at current time t,

respectively; $\Delta\varepsilon_{ij}^{ve,t}$ and $\Delta\varepsilon_{ij}^{vp,t}$ are the current incremental viscoelastic and viscoplastic

strains respectively. The rest of this manuscript will denote time-dependence of variables

with superscript of the time variable.

2.1.1 Schapery viscoelastic model

A single-integral constitutive equation derived from the thermodynamics of

irreversible process, Schapery (1969), is used for the viscoelastic component. This

integral model is suitable for small deformation gradient problems and allows

incorporating stress or strain dependent viscoelastic responses. The stress or strain

dependent parameters can be determined from a set of creep or relaxation data. The

Schapery single integral equation is generalized for a nonlinear isotropic viscoelastic

response and is written as:

$$\varepsilon_{ij}^{ve,t} = e_{ij}^{ve,t} + \frac{1}{3}\delta_{ij}\varepsilon_{kk}^{ve,t} \tag{2-2}$$

$$e_{ij}^{ve,t} = \frac{1}{2}g_0(\bar{\sigma}^t)J_0S_{ij}^t + \frac{1}{2}g_1(\bar{\sigma}^t)\int_0^t \Delta J^{(\psi^t-\psi^\tau)} \frac{d[g_2(\bar{\sigma}^\tau)S_{ij}^\tau]}{d\tau}d\tau \tag{2-3}$$

$$\varepsilon_{kk}^{ve,t} = \frac{1}{3}g_0(\bar{\sigma}^t)B_0\sigma_{kk}^t + \frac{1}{3}g_1(\bar{\sigma}^t)\int_0^t \Delta B^{(\psi^t-\psi^\tau)} \frac{d[g_2(\bar{\sigma}^\tau)\sigma_{kk}^\tau]}{d\tau}d\tau \tag{2-4}$$

It is assumed that loading starts at time t=0 and the material is non-aging. The

parameters J_o and B_o are the instantaneous elastic shear and bulk compliances,

respectively. The terms ΔJ and ΔB are the time-dependent (transient) shear and bulk

compliances, respectively. The non-linear parameters g_0, g_1, and g_2 of the multi-axial

behaviors are modeled as a function of the current effective stress $\bar{\sigma}^t$. The corresponding

linear elastic Poisson's ratio, ν obtained from the creep test is assumed to be time

independent. The shear and bulk compliances are expressed as:

$$\begin{aligned} J_0 &= 2(1+\upsilon)D_0 \quad, & B_0 &= 3(1-2\upsilon)D_0 \\ \Delta J^{\psi^t} &= 2(1+\upsilon)\Delta D^{\psi^t} \quad, & \Delta B^{\psi^t} &= 3(1-2\upsilon)\Delta D^{\psi^t} \end{aligned} \tag{2-5}$$

A Prony series of exponential functions is used for the transient part due to the advantage

of this representation in solving the integral form in Eqs. (2-3) and (2-4) in a recursive

manner. The uniaxial transient compliance is expressed as:

$$\Delta D^{\psi^t} = \sum_{n=1}^{N} D_n(1-\exp[-\lambda_n\psi^t]) \tag{2-6}$$

where ψ is the reduced-time (effective time), given by:

$$\psi^t \equiv \psi(t) = \int_0^t \frac{ds}{a_{\overline{\sigma}}^s} \tag{2-7}$$

The parameter $a_{\overline{\sigma}}^t$ is the time-stress shift factor. It is also assumed that the time-dependent material properties and field variables before time t=0 are equal to zero. It is noted that Eqs. (2.2) ~ (2.4) are a non-standard form as the general nonlinear constitutive models are often defined in terms of deformation histories. However, in the linearized viscoelastic responses, stress and strain based constitutive models are interchangeable. It has also been shown that the above constitutive equations are suitable only for small deformation gradient problems (Rajagopal and Srinivasa, 2005). A recursive-iterative method is used for solving the nonlinear viscoelastic model in Eqs. (2-3) and (2-4). Detailed recursive-iterative algorithm for the nonlinear viscoelastic behaviors is presented in Haj-Ali and Muliana (2004). The incremental viscoelastic strain derived from the recursive-iterative approach is summarized as:

$$\Delta\varepsilon_{ij}^{ve,t} = \left[\overline{J}^t \sigma_{ij}^t + \frac{1}{3}\delta_{ij} \left\{ \overline{B}^t - \overline{J}^t \right\} \sigma_{kk}^t \right] - \left[\overline{J}^{t-\Delta t} \sigma_{ij}^{t-\Delta t} + \frac{1}{3}\delta_{ij} \left\{ \overline{B}^{t-\Delta t} - \overline{J}^{t-\Delta t} \right\} \sigma_{kk}^{t-\Delta t} \right]$$
$$- A_{ij}^t - \frac{1}{3}B^t \delta_{ij} \tag{2-8}$$

$$\overline{J}^t = \frac{1}{2}\left[g_0^t J_0 + g_1^t g_2^t \sum_{n=1}^N J_n - g_1^t g_2^t \sum_{n=1}^N J_n \frac{1-\exp[-\lambda_n \Delta\psi^t]}{\lambda_n \Delta\psi^t} \right] \tag{2-9}$$

$$\overline{B}^t = \frac{1}{3}\left[g_0^t B_0 + g_1^t g_2^t \sum_{n=1}^{N} B_n - g_1^t g_2^t \sum_{n=1}^{N} B_n \frac{1-\exp[-\lambda_n \Delta\psi^t]}{\lambda_n \Delta\psi^t} \right] \tag{2-10}$$

$$A_{ij}^t = \frac{1}{2}\sum_{n-1}^{N} J_n (g_1^t \exp[-\lambda_n \Delta\psi^{t-\Delta t}] - g_1^{t-\Delta t}) q_{ij,n}^{t-\Delta t} + \frac{1}{2} g_2^{t-\Delta t} \sum_{n=1}^{N} J_n$$
$$\times \left[g_1^{t-\Delta t} \left(\frac{1-\exp[-\lambda_n \Delta\psi^{t-\Delta t}]}{\lambda_n \Delta\psi^{t-\Delta t}} \right) - g_1^t \left(\frac{1-\exp[-\lambda_n \Delta\psi^t]}{\lambda_n \Delta\psi^t} \right) \right] S_{ij}^{t-\Delta t} \tag{2-11}$$

$$B^t = \frac{1}{2}\sum_{n-1}^{N} B_n (g_1^t \exp[-\lambda_n \Delta\psi^{t-\Delta t}] - g_1^{t-\Delta t}) q_{kk,n}^{t-\Delta t} + \frac{1}{2} g_2^{t-\Delta t} \sum_{n=1}^{N} B_n$$
$$\times \left[g_1^{t-\Delta t} \left(\frac{1-\exp[-\lambda_n \Delta\psi^{t-\Delta t}]}{\lambda_n \Delta\psi^{t-\Delta t}} \right) - g_1^t \left(\frac{1-\exp[-\lambda_n \Delta\psi^t]}{\lambda_n \Delta\psi^t} \right) \right] \sigma_{kk}^{t-\Delta t} \tag{2-12}$$

Material parameters $\overline{J}^t$ and $\overline{B}^t$ are the shear and bulk compliances that depend on the effective stress at the current time t, while A_{ij}^t and B^t are the strain components that contain history variables. The incremental reduced time is expressed by

$\Delta\psi^t \equiv \psi^t - \psi^{t-\Delta t}$. Variables $q_{ij,n}^{t-\Delta t}$ and $q_{kk,n}^{t-\Delta t}$ are the shear and volumetric hereditary variables for every Prony series term at the end of the previous time, t-Δt. At the end of each time interval, the hereditary variables are updated and stored, which will be used for the next time integration step. The updated hereditary variables are:

$$q_{ij,n}^t = \exp[-\lambda_n \Delta\psi^t] q_{ij,n}^{t-\Delta t} + (g_2^t S_{ij}^t - g_2^{t-\Delta t} S_{ij}^{t-\Delta t}) \frac{1-\exp[-\lambda_{ij,n}\Delta\psi^t]}{\lambda_{ij,n}\Delta\psi^t} \tag{2-13}$$

$$q_{kk,n}^t = \exp[-\lambda_n \Delta\psi^t] q_{kk,n}^{t-\Delta t} + (g_2^t \sigma_{kk}^t - g_2^{t-\Delta t} \sigma_{kk}^{t-\Delta t}) \frac{1-\exp[-\lambda_{ij,n}\Delta\psi^t]}{\lambda_{ij,n}\Delta\psi^t} \tag{2-14}$$

2.1.2 Perzyna viscoplastic model

Many structural materials are often exposed to long-term mechanical loading and

elevated temperatures. Under such loading and environmental conditions, materials

could experience significant time-dependent and inelastic deformations. Several

viscoplastic constitutive models, based on an overstress assumption, have been

formulated to describe time-dependent and inelastic behaviors of metallic materials.

Perzyna's viscoplastic model has been used to predict responses of metals under a wide

range of strain rates and temperature changes. The Perzyna viscoplastic model is shown

to be applicable to simulate time-dependent and inelastic responses of some polymer

(Chailleux and Davis 2003, 2005). The viscoplastic strain rate in the Perzyna (1966,

1971) model for isotropic material is expressed as:

$$\dot{\varepsilon}_{ij}^{vp,t} = \dot{\lambda}^t \frac{\partial F(\bar{\sigma}^t, k^t)}{\partial \sigma_{ij}^t} \qquad (2\text{-}15)$$

where $\dot{\varepsilon}_{ij}^{vp,t}$ is the viscoplastic strain rate at current time t and $\dot{\lambda}^t$ is the magnitude of the

viscoplastic strain rate, also known as a plastic multiplier. In general, a rate dependent

yield function $F(\bar{\sigma}^t, k^t)$ is expressed in terms of an effective stress. During the plastic

deformation, the stress in the stress space remains on the subsequent yield surface and

$\dot{\lambda}$ is greater than 0. Let $f(\bar{\sigma}^t, \sigma_y)$ be a yield function of a general plastic material. Thus,

during a plastic loading, the yield function needs to be updated such that $f(\bar{\sigma}^t, \sigma_y) = 0$.

During unloading or neutral loading, the following conditions should be met:

$f(\bar{\sigma}^t, \sigma_y) \leq 0$ and $\dot{\lambda} = 0$. It is seen that for all types of loading, the yield function and

plastic multiplier can be written as $f(\bar{\sigma}^t, \sigma_y) \leq 0$ and $\dot{\lambda} \geq 0$, respectively. Thus, the

following relation should be hold: $\dot{\lambda} f(\bar{\sigma}^t, \sigma_y) = 0$ which is known as the Kuhn-Tucker

complementary condition. Let us define $f(t) = f(\bar{\sigma}^t, \sigma_y)$ and $f(t) \leq 0$. For all $\Delta t > 0$,

$\dot{f} \equiv \dfrac{df}{dt}$ should be less than or equal to zero, otherwise $f(t + \Delta t)$ would be greater than

zero, which violates the condition $f(t) \leq 0$. Therefore, the following condition should

also be fulfilled: $\dot{\lambda} \dot{f}(\bar{\sigma}^t, \sigma_y) = 0$, which is the consistency (persistency) condition.

The variable $\dot{\lambda}^t$ is also referred to a consistency parameter (Simo and Hughes,

1998). Vector $\partial F / \partial \sigma$ describes the direction of the viscoplastic strain rate, which is

the normal direction at the stress point on the yield surface F. The viscoplastic yield

function based on an overstress function for isotropic hardening materials is given as:

$$F(\bar{\sigma}^t, k^t) = \bar{\sigma}^t - \sigma_y^o - hk^t \qquad (2\text{-}16)$$

The parameter σ_y^o is the initial yield stress measured from a uniaxial loading and h is

the hardening material constant. The hardening material parameter can also depend on

the current effective stress $\bar{\sigma}^t$. The parameter k^t is the accumulated effective

viscoplastic strain, expressed as:

$$k^t = \int_0^t \dot{k}^s ds = \int_0^t \dot{\bar{e}}^{vp,s} ds \tag{2-17}$$

$$\dot{k}^t = \dot{\bar{e}}^{vp,t} = \sqrt{\frac{2}{3} \dot{e}_{ij}^{vp,t} \dot{e}_{ij}^{vp,t}} \tag{2-18}$$

Using Eq. (2-16), the direction of the viscoplastic strain rate is expressed as:

$$\frac{\partial F(\bar{\sigma}^t, k^t)}{\partial \sigma_{ij}} = \frac{\partial F}{\partial \bar{\sigma}^t} \frac{\partial \bar{\sigma}^t}{\partial \sigma_{ij}} = \frac{3}{2\bar{\sigma}^t} (\delta_{ik} \delta_{jl} - \delta_{ij} \delta_{kl}) S_{kl}^t \tag{2-19}$$

S_{kl}^t is the current deviatoric stress. Substituting Eq. (2-19) into (2-15) leads to:

$$\dot{\varepsilon}_{ij}^{vp,t} = \dot{\lambda}^t \frac{3}{2\bar{\sigma}^t} (\delta_{ik} \delta_{jl} - \frac{1}{3} \delta_{ij} \delta_{kl}) S_{kl}^t = \dot{\lambda}^t \frac{3}{2\bar{\sigma}^t} I'_{ijkl} S_{kl}^t \tag{2-20}$$

Next, the plastic multiplier is obtained from the following equation:

$$\dot{\lambda} \approx \frac{\Delta\lambda}{\Delta t} = \frac{1}{\eta_P} \langle \Phi(F) \rangle \left(\exp(-\frac{h(\bar{\sigma}^t)}{\eta_p} \hat{t}) - \exp(-\frac{h(\bar{\sigma}^t)}{\eta_p} (\hat{t} - \Delta\hat{t})) \right) \tag{2-21}$$

where η_p is the viscosity coefficient during the viscoplastic deformation, $\langle \; \rangle$

represents the Macauley bracket, the function $\langle \Phi(F) \rangle$ depends on the distance of the

current stress point to the yield surface (Bathe, 1996; Simo and Hughes, 1998). Perzyna

(1966) proposed different functions for $\Phi(F)$, e.g., linear, power law, and exponential

forms. The function can be characterized by fitting available experimental data. For

example, Kojic and Bathe (2005) have shown that a power law model can be used to fit

viscoplastic strains based on creep tests. Following Kojic and Bathe (2005), for an

isotropic hardening viscoplastic model the function $\Phi(F)$ is defined by:

$$\Phi(F) = \left[\frac{\bar{\sigma}^t - \sigma_y^o - hk^t}{\sigma_y^o} \right]^n \tag{2-22}$$

where n, h, and σ_y^o are material constants, which need to be calibrated by fitting

experimental data. An incremental formulation of the Perzyna viscoplastic constitutive

model is formed based on the following approximations:

$$\dot{\varepsilon}_{ij}^{vp} \approx \frac{\Delta\varepsilon_{ij}^{vp}}{\Delta t} \qquad \dot{\lambda} \approx \frac{\Delta\lambda}{\Delta t} \qquad \dot{k} \approx \frac{\Delta k}{\Delta t} \qquad \sigma_{ij}^t \approx \sigma_{ij}^{t-\Delta t} + \Delta\sigma_{ij}^t \tag{2-23}$$

The magnitude of the accumulated viscoplastic strain from the previous time step is

written as:

$$k^t = \int_0^{t-\Delta t} \dot{k}^s ds + \int_{t-\Delta t}^t \dot{k}^s ds = k^{t-\Delta t} + \Delta k^t \tag{2-24}$$

where $k^{t-\Delta t}$ is the magnitude of the accumulated viscoplastic strain from the previous

time step, which is stored as a history variable. This value is updated at the end of time

increment during the plastic deformation. Wang et al. (1997) have discussed that by

substituting $\dot{\varepsilon}_{ij}^{vp,t}$ in Eq. (2-20) into k in Eq. (2-18) results in $\dot{k} = \dot{\lambda}$. The incremental

form of the magnitude of the viscoplastic strain rate is written as:

$$\Delta \lambda^t = \frac{\Delta t}{\eta_p} \langle \Phi(F) \rangle \left(\exp(-\frac{h(\bar{\sigma}^t)}{\eta_p} \hat{t}) - \exp(-\frac{h(\bar{\sigma}^t)}{\eta_p}(\hat{t} - \Delta\hat{t})) \right) \tag{2-25}$$

The incremental viscoplastic strain for the Perzyna is given as:

$$\Delta\varepsilon_{ij}^{vp,t} = \frac{\Delta t}{\eta_p} \langle \Phi(F) \rangle \left(\exp(-\frac{h(\bar{\sigma}^t)}{\eta_p} \hat{t}) - \exp(-\frac{h(\bar{\sigma}^t)}{\eta_p}(\hat{t} - \Delta\hat{t})) \right) \frac{3}{2\bar{\sigma}^t} \left(\delta_{ik}\delta_{jl} - \frac{1}{3}\delta_{ij}\delta_{kl} \right) S_{kl}^t \tag{2-26}$$

The current stress is determined from the stress at previous time step and the incremental

stress at current time $(\sigma_{ij}^t = \sigma_{ij}^{t-\Delta t} + \Delta\sigma_{ij}^t)$, and the plastic strain is updated similarly. In Eq.

(2-25) and Eq. (2-26), the current $\Phi(F)$ in an incremental formulation is defined as:

$$\Phi(F) = \left[\frac{(\bar{\sigma}^{t-\Delta t} + \Delta\bar{\sigma}^t) - \sigma_y^o - h(k^{t-\Delta t} + \Delta k^t)}{\sigma_y^o} \right]^n \tag{2-27}$$

Substituting Eq. (2-8) and (2-26) into Eq. (2-1), the total incremental strains $\Delta\varepsilon_{ij}^t$ is

obtained.

2.1.3   Spring-dashpot-slider model
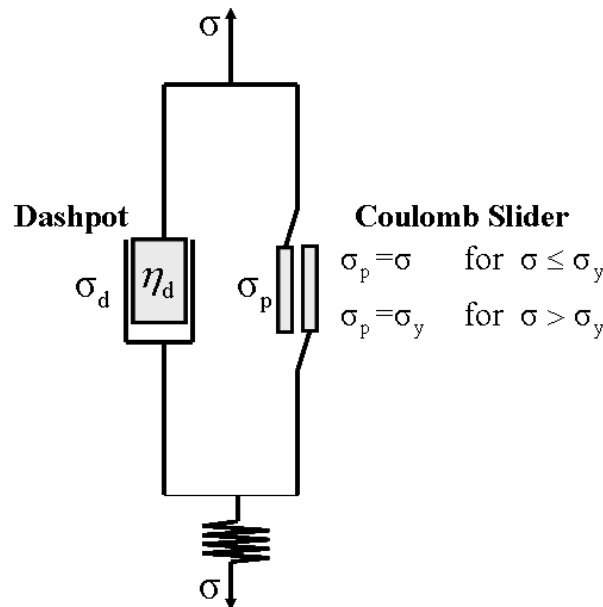
Figure 2-2. One dimensional mechanical analog model

A viscoplastic constitutive model based on an overstress function can be visualized

by a parallel arrangement of a dashpot and a slider (Zienkiewicz and Cormeau, 1972;

Kojic and Bathe, 2005) as illustrated in Fig. 2-2. Kojic and Bathe (2005) presented an

analytical solution of a creep function by solving a governing differential equation of the

spring-dashpot-slider mechanical analog model. The uniaxial creep strain is expressed

by:

$$\varepsilon^t = \frac{\overline{\sigma}^t}{E} + \left\langle \frac{\overline{\sigma}^t - \sigma_y^o}{h(\overline{\sigma}^t)} \right\rangle \left[1 - \exp\left(-\frac{h(\overline{\sigma}^t)}{\eta_p}\hat{t} \right) \right] \tag{2-28}$$

The second term of Eq. (2-28) describes the viscoplastic creep strain. The effective time

$\hat{t}$ is a relative time measured when the plastic deformation starts. The incremental form

of the uniaxial strain is written as:

$$\Delta\varepsilon^{vp,t} = \Delta t \left\langle \frac{\overline{\sigma}^t - \sigma_y^o}{h(\overline{\sigma}^t)} \right\rangle \exp\left(-\frac{h(\overline{\sigma}^t)}{\eta_p}\hat{t} \right) \tag{2-29}$$

Eq. (2-29) can be extended for a 3D isotropic case, as discussed in Kojic and Bathe

(2005). It is assumed that the direction of viscoplastic strain is normal to the yield

surface. Thus, the strain components are expressed using a normal tensor:

$$\Delta\varepsilon_{ij}^{vp,t} = \Delta t \left\langle \frac{\overline{\sigma}^t - \sigma_y^o}{h(\overline{\sigma}^t)} \right\rangle \exp\left(-\frac{h(\overline{\sigma}^t)}{\eta_p}\hat{t} \right) n_{ij}^t \tag{2-30}$$

where n_{ij}^t is normal tensor to the yield surface and written as:

$$n_{ij}^t = \frac{S_{ij}^t}{\|\mathbf{S}^t\|} \tag{2-31}$$

where the yield function f is given as:

$$f = <\overline{\sigma}^t - \sigma_y^0> \tag{2-32}$$

The incremental form of the magnitude of the viscoplastic strain of the dashpot-slider

model is expressed as:

$$\Delta\lambda^t = \sqrt{\Delta\varepsilon_{ij}^{vp,t}\Delta\varepsilon_{ij}^{vp,t}} = \Delta t \left\langle \frac{\bar{\sigma}^t - \sigma_y^o}{h(\bar{\sigma}^t)} \right\rangle \exp\left(-\frac{h(\bar{\sigma}^t)}{\eta_p}\hat{t} \right) \frac{\sqrt{S_{ij}^t S_{ij}^t}}{\|\mathbf{S}^t\|} \qquad (2\text{-}33)$$

Eq. (2-30) together with Eqs. (2-6) and (2-7) give the total incremental strain at current

time t.

2.1.4   Valanis viscoplastic model

Most of plasticity and viscoplasticity theories are derived from the concept of

overstress function that requires the existence of yield stress. In some polymers and

metals at high temperatures, inelastic deformation occurs at a very low stress level. In

such cases, it is quite difficult to accurately define the yield point. Haythornthwaite

(1968) proposed several criteria to define a yield point as illustrated in Fig. 2-3. The first

definition assumes a yield point as the last point of a linear stress-strain state. The second

definition identifies a yield point as the point at the smallest measurable plastic strain.

The third definition takes a yield point as the point, at which the stress-strain curve

intersects with a line having a slope of 90~95% of the initial slope of the first definition.

The fourth definition takes a yield point as the point, at which the stress axis intersects

with the post yield slope. The fifth definition of the yield point is the point of

intersection of the post yield slope with the elastic slope of the first definition. In the

sixth definition, a yield stress is defined as a stress point in the stress-strain curve that

gives permanent strain of 0.2% after removal of the stress. It should be noted that

various definitions of yield points of materials result in different inelastic response of the

materials.
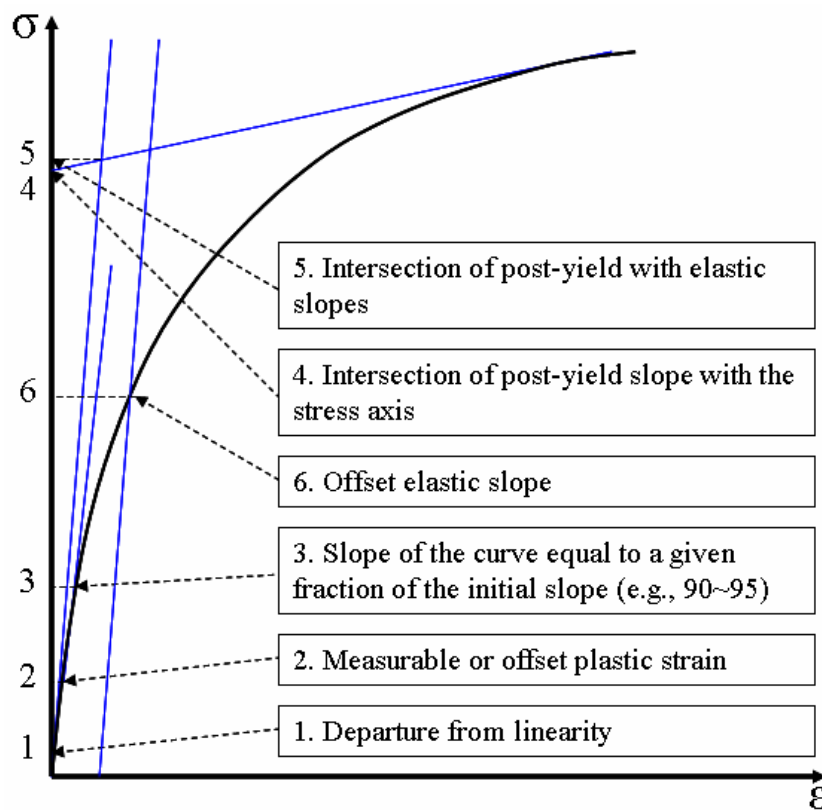
Figure 2-3. Various definitions for yield point in a uniaxial representation

Inelastic deformations of polymers and aluminum at high temperatures could start at low stress points. Valanis (1971) proposed an endochronic viscoplastic model based on the irreversible thermodynamics concept for isotropic materials. The endochronic viscoplastic model is suitable for a class of metal or polymer materials when yield occurs at early loadings. Valanis's viscoplastic model is expressed as:

$$S_{ij}^t = 2G \int_0^z \rho(z-z') \frac{de_{ij}^{vp}}{dz'} dz' \tag{2-34}$$

where S_{ij}^t and $e_{ij}^{vp,t}$ are the deviators of the stress and viscoplastic strain, respectively, and G is the elastic shear modulus. The kernel $\rho(z)$ is a non-dimensional material function and z appearing in the equation is the intrinsic time. The kernel $\rho(z)$ can be written as:

$$\rho(z) = \rho_0 \delta(z) + \rho_1(z) \tag{2-35}$$

$$S_y^0 = 2G\rho_0 \tag{2-36}$$

where ρ_0 is a material constant related to an isotropic hardening, $\delta(z)$ is a Dirac delta function, ρ_1 is a nonsingular function that describes a kinematic hardening behavior, and the variable S_y^0 is a material constant which can be related to a yield stress. Substituting Eq. (2-35) and Eq. (2-36) into Eq. (2-34) yields:

$$S_{ij}^t = S_y^o \frac{de_{ij}^{vp,t}}{dz} + 2G \int_0^t \rho_1(z^t - z') \frac{de_{ij}^{vp,t}}{dz'} dz' \tag{2-37}$$

The variable z in Eq. (2-37) is the intrinsic time which is given by

$$dz = \frac{d\zeta}{f(\zeta)}$$

(2-38)

For an isotropic hardening model, the second term of Eq. (2-37) can be retrieved at all

times and Eq. (2-37) can be rewritten as:

$$S_{ij}^t = S_y^0 \frac{de_{ij}^{vp,t}}{dz} = S_y^0 \frac{de_{ij}^{vp,t}}{d\zeta} f(\zeta)$$

(2-39)

The parameter ζ is an intrinsic time scale that depends on the magnitude of the

incremental viscoplastic strain, and is defined as (Valanis, 1971; Khan and Huang,

1995):

$$d\zeta = \sqrt{de_{ij}^{vp,t} de_{ij}^{vp,t}}$$

(2-40)

It is possible to rewrite the intrinsic time in terms of the incremental viscoplastic strain

scale at the current time t remains as unknown. The above equation can be rewritten in

terms of known variables such as current stress, strain, and time. This expression will be

discussed later in this manuscript. The intrinsic time scale function $f(\zeta)$ can take

various forms (Valanis, 1971), such as:

$$\begin{aligned} f(\zeta) &= 1 + \beta\zeta & \text{(Linear form)} \\ f(\zeta) &= a + (1-a)e^{-b\zeta} & \text{(Exponential form)} \end{aligned}$$

(2-41)

The parameters $\beta, a, and \ b$ are material constants that have to be characterized from

experiments. The total work during the plastic deformation is defined by:

$$W^{vp,t} = \int_0^t S_{ij}^t de_{ij}^{vp,s} \tag{2-42}$$

The evolution of $W^{vp,t}$ can be obtained by differentiating equation (2-42).

$$dW^{vp,t} = S_{ij}^t de_{ij}^{vp,t} \tag{2-43}$$

Using Eqs. (2-39) and (2-40), the yield criterion is defined as (Valanis 1971, Khan and

Huang 1995):

$$\begin{aligned}
S_{ij}^t S_{ij}^t &= S_y^0 \frac{de_{ij}^{vp,t}}{d\zeta} f(\zeta) S_y^0 \frac{de_{ij}^{vp,t}}{d\zeta} f(\zeta) \\
&= \left(S_y^0\right)^2 \frac{de_{ij}^{vp,t} de_{ij}^{vp,t}}{(d\zeta)^2} \left(f(\zeta)\right)^2 \\
&= \left(S_y^0\right)^2 \left(f(\zeta)\right)^2
\end{aligned} \tag{2-44}$$

The parameter $f(\zeta)$ is a nonnegative function of the intrinsic time scale ζ,

with $f(\zeta) = 0$. If $f(\zeta)$ is equal to 1, Eq. (2-44) corresponds to the von Mises yield

function. Material responses during the deformation are categorized as:

$$\begin{aligned}
S_{ij}^t S_{ij}^t &\leq \left(S_y^0\right)^2 f^2(\zeta) \qquad && \text{(elastic or viscoelastic response)} \\
S_{ij}^t S_{ij}^t &= \left(S_y^0\right)^2 f^2(\zeta) \quad \text{and} \quad S_{ij}^t de_{ij}^{vp,t} > 0 \qquad && \text{(viscoplastic response)}
\end{aligned} \tag{2-45}$$

The time derivatives of the deviatoric and volumetric viscoplastic strains from Eq. (2-39),

are:

$$de_{ij}^{vp,t} = \frac{1}{S_y^0 f(\zeta)} S_{ij}^t d\zeta$$

$$d\varepsilon_{kk}^{vp,t} = 0$$

(2-46)

The incremental total strain is defined by adding the incremental (visco) elastic and

viscoplastic components. Using the expression of total incremental strain in Eq. (2-1),

the incremental stress for isotropic material model can be expressed by:

$$d\varepsilon_{ij}^t = d\varepsilon_{ij}^{ve,t} + d\varepsilon_{ij}^{vp,t}$$

(2-47)

$$dS_{ij}^t = 2G(de_{ij}^t - de_{ij}^{vp,t}) = 2Gde_{ij}^t - \frac{2G}{S_y^o f(\zeta)} S_{ij}^t d\zeta$$

(2-48)

The incremental deviatoric stress is related to the incremental deviatoric visco (elastic)

strain (Eq. (2-48)) by the value of G that is time-dependent. The time-dependent effect is

due to the viscoelastic part. If instead the elastic part is considered, the G value is the

linear elastic shear modulus. By differentiating Eq. (2-44), the endochronic consistency

condition is given as:

$$S_{ij}^t dS_{ij}^t = \left(S_y^o\right)^2 f(\zeta)f'(\zeta)d\zeta$$

(2-49)

Substituting Eq. (2-48) into Eq. (2-49) gives:

$$S_{ij}^t (2Gde_{ij}^t - \frac{2G}{S_y^o f(\zeta)} S_{ij}^t d\zeta) = \left(S_y^o\right)^2 f(\zeta)f'(\zeta)d\zeta$$

(2-50)

The strain increases monotonically by setting $f(\zeta)$ to be a monotonic decreasing

function of ζ. The incremental total strain is defined by additively combining the

incremental viscoelastic and viscoplastic components and also their deviatoric and

volumetric parts. The expression of $d\zeta$ can be found in Valanis (1971) and Khan and

Huang (1995), which are given as:

$$d\zeta = \frac{1}{\left(S_y^o\right)^2 f(\zeta) f'(\zeta)} \left[2G(S_{ij}^t de_{ij}^t) - 2GS_y^o f(\zeta) d\zeta\right]$$

$$\left[1 + \frac{2G}{S_y^o f'(\zeta)}\right] d\zeta = \frac{2G}{\left(S_y^o\right)^2 f(\zeta) f'(\zeta)} (S_{ij}^t de_{ij}^t) \tag{2-51}$$

Thus,

$$d\zeta = \frac{2G}{S_y^o f(\zeta) \ [2G + S_y^o f'(\zeta)]} (S_{ij}^t de_{ij}^t) \tag{2-52}$$

It should be noted that the expression $d\zeta$ in Eq. (2-38) is written in terms of unknown

incremental viscoplastic strain. In Eq. (2-52), the unknown variables are replaced with

total incremental deviatoric stress, incremental deviatoric strain, and intrinsic time. This

expression is suitable for implementation in a displacement based FE where the

components of an incremental total stain are the known variables. Substituting Eq. (2-

52) to (2-39), the time-derivative of the viscoplastic strain is:

$$de_{ij}^{vp,t} = \frac{2G}{(S_y^o)^2 f^2(\zeta)[2G + S_y^o f'(\zeta)]} (S_{mn}^t de_{mn}^t) S_{ij}^t \tag{2-53}$$

An incremental formulation of the Valanis viscoplastic constitutive model is formed by

assuming $de_{ij} \approx \dfrac{\Delta e_{ij}}{\Delta t}$. Eq. (2-53) is now written as:

$$\Delta e_{ij}^{vp,t} = \frac{2G}{(S_y^o)^2 f^2(\zeta)[2G + S_y^o f'(\zeta)]} (S_{mn}^t \Delta e_{mn}^t) S_{ij}^t \qquad (2\text{-}54)$$

The Valanis constitutive model is formulated in terms of stress histories, in which the

components of stress are taken as independent variables. In this study, the Valanis model

will be integrated to micromechanical models of composites, which will be implemented

in a general displacement based FE framework. In such cases, components of strains are

the known (independent) variables and we need to determine the corresponding stresses.

As the total strains consist of the recoverable elastic (viscoelastic) and irrecoverable

viscoplastic components, it is important to simultaneously determine these components

and the total stress. Linearized (trial) strains components are obtained and a residual

vector consisting of the incremental total strains is defined. The incremental form of the

magnitude of the Valanis viscoplastic strain is taken as:

$$\Delta \lambda^t = \frac{2G}{(S_y^o)^2 f^2(\zeta)[2G + S_y^o f'(\zeta)]} (S_{mn}^t \Delta e_{mn}^t) \sqrt{S_{ij}^t S_{ij}^t} \qquad i=1, 2, 3 \qquad (2\text{-}55)$$

Eq. (2-54) together with Eqs. (2-6) and (2-7) give the total incremental strain at current

time t. It is then necessary to correct the residual (error) from the linearized solutions.

2.2 Correction Algorithm

A time-integration algorithm with linearized predictor and corrector schemes is

formulated for the combined nonlinear viscoelastic and viscoplastic constitutive

equations. Haj-Ali and Muliana (2004) has shown that a nonlinear viscoelastic

constitutive model using a linearized stress-update alone at the material point leads to a

large residual strain, even though small time-increment is chosen. It was also concluded

that a structural (global) iterative correction alone is not adequate to reduce errors at the

element level. An iterative procedure at the material level is needed in order to minimize

the residual strain. Furthermore, a consistent tangent stiffness matrix is developed to

accelerate convergence and to avoid divergence.

1. **Input variables: (at the mth global iteration)**

$$\varepsilon_{ij}^{t-\Delta t}, \Delta\varepsilon_{ij}^{t,(m)}, \Delta t^{(m)} \qquad \text{History}: \sigma_{ij}^{t-\Delta t}, q_{ij,n}^{t-\Delta t}, q_{kk,n}^{t-\Delta t}, k^{k-\Delta t}, \varepsilon_{ij}^{ve,t-\Delta t}, \varepsilon_{ij}^{vp,t-\Delta t}$$

2. **Initial approximation variables:**

$$g_{\beta}^{t,tr} = g_{\beta}(\overline{\sigma}^{t-\Delta t}) \;\; ; \;\; \beta = 0,1,2 \qquad\qquad a^{t,tr} = a(\overline{\sigma}^{t-\Delta t})$$

$$\Delta\sigma_{ij}^{t,tr} = \Delta\sigma_{ij}^{t,tr}(\Delta S_{ij}^{t,tr}, \Delta\sigma_{kk}^{t,tr}) \qquad\qquad \sigma_{ij}^{t,(0)} = \sigma_{ij}^{t-\Delta t} + \Delta\sigma_{ij}^{t,tr}$$

$$\Delta\lambda^{t,tr} = \Delta\lambda^{t,(0)} = \Delta\lambda^{t}(\overline{\sigma}^{t-\Delta t}) = 0.0$$

3. **Iterate for k=1, 2, 3 ...   (k=local iteration counter)**

   3.1 **Compute incremental viscoelastic and viscoplastic strains:**

   $$\Delta\varepsilon_{ij}^{ve,t,(k)} \text{ from Eq. (2-8) and } \Delta\varepsilon_{ij}^{vp,t,(k)} \text{ from Eq.(2-26)}$$

   3.2 **Evaluate residual tensor:**

   $$R_{\Delta s_{ij}}^{t,(k)} \text{ from Eq. (2-57) and } R_{\Delta\lambda}^{t,(k)} \text{ from Eq.(2-58)}$$

   3.3 **Compute stress correction and plastic multiplier correction using Eq. (2-60):**

   $$\Delta\sigma_{ij}^{t,(k+1)} \quad \text{and} \quad \Delta\lambda^{t,(k+1)}$$

   $$\text{IF } \|R_{ij}^{t,(k)}\| \le \text{Tol Then GOTO 4 and EXIT}$$

   ENDIF GOTO 3

4. **Update stress, consistent tangent stiffness, and history variables:**

   $$\sigma_{ij}^{t} \leftarrow \sigma_{ij}^{t,(k+1)} \qquad q_{ij,n}^{t} \leftarrow q_{ij,n}^{t,(k+1)} \qquad q_{kk,n}^{t} \leftarrow q_{kk,n}^{t+(k+1)} \qquad C_{ijkl}^{t}$$

   $$k^{t} \leftarrow k^{t,(k+1)} \qquad \varepsilon_{ij}^{ve,t} \leftarrow \varepsilon_{ij}^{ve,t,(k+1)} \qquad \varepsilon_{ij}^{vp,t} \leftarrow \varepsilon_{ij}^{vp,t,(k+1)}$$

Figure 2-4. Integration algorithm for the incremental viscoelastic and viscoplastic responses

The numerical algorithm, which is used to provide the total stresses for viscoelastic and viscoplastic responses, is summarized in Fig. 2-4. This algorithm is compatible with the displacement based FE framework. The superscript (m) denotes the global iteration counter within the current incremental time step. At each structural (global) iteration within an incremental time step, $\Delta t^{(m)}$, the components of the incremental strain tensor $\Delta\varepsilon_{ij}^{t,(m)}$ are obtained from the micromechanical level or FE structural level. The goal is to

calculate stresses $\sigma_{ij}^{t,(m)}$ and consistent tangent stiffness $C_{ijkl}^{t,(m)}$ at the current time t. At

each time increment, it is also necessary to determine the components of the viscoelastic

and viscoplastic strains. All history variables ($Hist^{t-\Delta t}$) stored from the previous

converged solution at time (t-Δt), which are $q_{ij,n}^{t-\Delta t}, q_{kk,n}^{t-\Delta t}$, and $k^{t-\Delta t}$, are passed to the

material points and these history variables will be updated once the convergence is

achieved. The history variable $k^{t-\Delta t}$ is needed only for the Perzyna's model. For

simplicity, the superscript (m) will be dropped. The consistent tangent stiffness matrix

C_{ijkl}^{t} at the current time t will be used to provide incremental trial strains for the next

time step $(t+\Delta t)$. If at every time increment (Δt), the components of the current total

stress tensor σ_{ij}^{t} are the known variables, the stress-dependent incremental viscoelastic

strains in Eq. (2-8) and the incremental viscoplastic strains of the Perzyna model in Eq.

(2-26), Dashpot-slider model in Eq. (2-30), or Valanis model in Eq. (2-54) can be

directly calculated. However, the total incremental strains $\Delta\varepsilon_{ij}^{t}$ are the known variables

and the total stresses σ_{ij}^{t} are being calculated, while at the same time the strain

formulation depends on the current total stresses. One can solve this problem using a

linearized stress-strain relation with a constant stress within the time interval

(Zienkiewicz and Cormeau, 1972, 1974). The constant stress state can be obtained from

the previous converged solution at time $(t - \Delta t)$ and the material parameters can be

defined in terms of $\sigma_{ij}^{t-\Delta t}$. At this stage, trial incremental stresses can be obtained from

$\Delta \sigma_{ij}^{t,tr} = C_{ijkl}^{t-\Delta t} \Delta \varepsilon_{kl}^{t}$ and total trial stresses are defined by $\sigma_{ij}^{t,tr} = \sigma_{ij}^{t-\Delta t} + \Delta \sigma_{ij}^{t,tr}$. The

approximated or trial incremental stresses from the linearized viscoleastic strains, as

discussed in (Haj-Ali and Muliana, 2004), are expressed by:

$$\Delta S_{ij}^{t(0)} = \Delta S_{ij}^{t,tr} = \frac{1}{\bar{J}^{t,tr}} \left[\Delta e_{ij}^{t} + \frac{1}{2} g_1^{t,tr} \sum_{n=1}^{N} J_n (\exp[-\lambda_n \Delta \psi^t] - 1) q_{ij,n}^{t-\Delta t} \right] \qquad (2\text{-}56)$$

$$\Delta \sigma_{kk}^{t(0)} = \Delta \sigma_{kk}^{t,tr} = \frac{1}{\bar{B}^{t,tr}} \left[\Delta \varepsilon_{kk}^{t} + \frac{1}{3} g_1^{t,tr} \sum_{n=1}^{N} B_n (\exp[-\lambda_n \Delta \psi^t] - 1) q_{kk,n}^{t-\Delta t} \right] \qquad (2\text{-}57)$$

The terms $J^{t,tr}$ and $B^{t,tr}$ have the same form as in Eq. (2-9) and Eq. (2-10), respectively,

but with the non-linear parameters $(g_0, g_1, g_2, a_\sigma)$ are functions of the effective stress

from the previous converged step $(\bar{\sigma}^{t-\Delta t})$. Since the trial incremental viscoplastic strain

is obtained based on the stress state from the previous converged step, this also leads to

$\Delta \lambda^{t(0)} = \Delta \lambda^{t,tr} = 0.0$ at the beginning of the iteration.
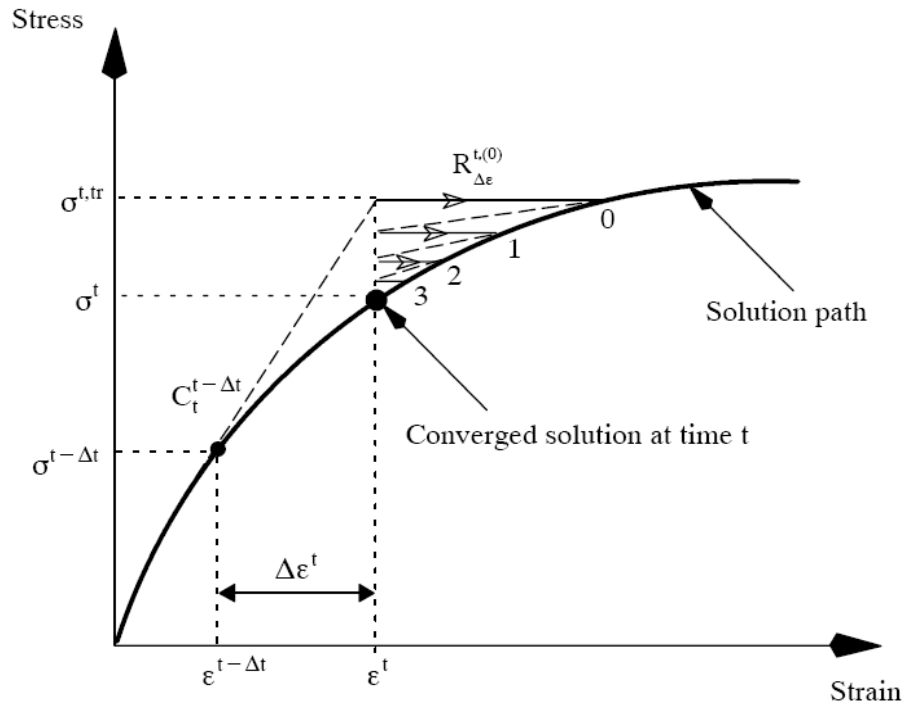
Figure 2-5. Convergence path during the iteration at the material level

The convergence path during each incremental time step in the material level is illustrated in Figure 2-5 (for a uniaxial representation). It is seen that unless the incremental strain $\Delta\varepsilon^t$ is very small, the calculated stress from the linearized relation can lead to a significant stress error, indicated by the trial stress $\sigma^{t,tr}$. Determining the incremental viscoelastic strain $\Delta\varepsilon_{ij}^{ve,t}$ in Eq. (2-8) and viscoplastic strains $\Delta\varepsilon_{ij}^{vp,t}$ of the Perzyna model in Eq. (2-26) or Valanis model in Eq. (2-54) based on the trial stress, will result in a residual strain $(\mathbf{R}_{\Delta\varepsilon}^{t,(0)})$. In addition, the linearized stress will cause error in

obtaining the plastic multiplier of the Perzyna model in Eq. (2-25) or the Valanis model

in Eq. (2-55). In this study, a correction scheme is formulated to minimize errors from

the linearization. The residual strains and plastic multiplier are defined in the following

linearized equations:

$$R_{\Delta\varepsilon_{ij}}^t = \Delta\varepsilon_{ij}^{ve,t} + \Delta\varepsilon_{ij}^{vp,t} - \Delta\varepsilon_{ij}^t \tag{2-58}$$

$$R_{\Delta\lambda} = \Delta\lambda^t - \frac{\Delta t}{\eta_p}\langle\Phi(F)\rangle\left(\exp(-\frac{h(\bar{\sigma}^t)}{\eta_p}\hat{t}) - \exp(-\frac{h(\bar{\sigma}^t)}{\eta_p}(\hat{t} - \Delta\hat{t}))\right) \quad \text{(for Perzyna)} \tag{2-59}$$

$$R_{\Delta\lambda} = 0 \qquad \text{(for Valanis)} \tag{2-60}$$

$$R_{\Delta\lambda} = 0 \qquad \text{(for Dashpot-slider)} \tag{2-61}$$

The goal is to calculate $\Delta\sigma_{ij}^t$ and update the total stress $\sigma_{ij}^t = \sigma_{ij}^{t-\Delta t} + \Delta\sigma_{ij}^t$. The Perzyna

model depends on the plastic multiplier $\Delta\lambda^t$, which at current time remains as an

unknown variable. To determine the total stress in the combined Schapery-Perzyna

model, we minimize each component of the residual tensors, $R_{\Delta\varepsilon_{ij}}$ and $R_{\Delta\lambda}$. It is noted

that the expressions of incremental viscoplastic strains for the Valanis model and

dashpot-slider model depend on unknown stress tensor and other material parameters

which are known (constant). Thus, it is not necessary to define the residual $R_{\Delta\lambda}$ for the

Valanis and dashpot-slider model as $\Delta\lambda^t$ will be determined once the correct stress has

been obtained. This study used the Newton-Raphson iterative method. At the

$(k+1)$ iteration, $\Delta\sigma_{ij}^t$ and $\Delta\lambda^t$ are calculated by:

$$\left\{\begin{array}{c} \Delta\boldsymbol{\sigma}^t \\ \Delta\boldsymbol{\lambda}^t \end{array}\right\}^{(k+1)} = \left\{\begin{array}{c} \Delta\boldsymbol{\sigma}^t \\ \Delta\boldsymbol{\lambda}^t \end{array}\right\}^{(k)} - \left[\frac{\partial\boldsymbol{R}^{t,(k)}}{\partial\boldsymbol{X}}\right]^{-1} \left\{\begin{array}{c} \boldsymbol{R}_{\Delta\varepsilon}^t \\ \boldsymbol{R}_{\Delta\lambda}^t \end{array}\right\}^{(k)} \qquad (2\text{-}62)$$

$$\frac{\partial\boldsymbol{R}}{\partial\boldsymbol{X}} = \left[\begin{array}{cc} \dfrac{\partial\boldsymbol{R}_{\Delta\varepsilon}}{\partial\Delta\boldsymbol{\sigma}} & \dfrac{\partial\boldsymbol{R}_{\Delta\varepsilon}}{\partial\Delta\boldsymbol{\lambda}} \\[3mm] \dfrac{\partial\boldsymbol{R}_{\Delta\lambda}}{\partial\Delta\boldsymbol{\sigma}} & \dfrac{\partial\boldsymbol{R}_{\Delta\lambda}}{\partial\Delta\boldsymbol{\lambda}} \end{array}\right]_{(7\times7)} \qquad (2\text{-}63)$$

Each component of the Jacobian matrix in Eq. (2-62) is given as follows:

$$\frac{\partial R_{\Delta\varepsilon_{ij}}}{\partial\Delta\sigma_{kl}} = \frac{\partial\Delta\varepsilon_{ij}^{ve,t}}{\partial\Delta\sigma_{kl}^t} + \frac{\partial\Delta\varepsilon_{ij}^{vp,t}}{\partial\Delta\sigma_{kl}^t} \qquad (2\text{-}64)$$

$\partial\Delta\varepsilon_{ij}^{ve,t}/\partial\Delta\sigma_{kl}^t$ is given in Haj-Ali and Muliana (2004), which is :

$$\frac{\partial \Delta \varepsilon_{ij}^{ve,t}}{\partial \Delta \sigma_{kl}^{t}} = \bar{J}^{t} \delta_{ik} \delta_{jl} + \frac{1}{3}(\bar{B}^{t} - \bar{J}^{t})\delta_{ij}\delta_{kl}$$

$$+ \frac{\partial \Delta \bar{\sigma}^{t}}{\partial \Delta \sigma_{kl}^{t}} \left\{ \frac{\partial \bar{J}^{t}}{\partial \Delta \bar{\sigma}^{t}} \sigma_{ij}^{t} + \frac{1}{3}(\frac{\partial \bar{B}^{t}}{\partial \Delta \bar{\sigma}^{t}} - \frac{\partial \bar{J}^{t}}{\partial \Delta \bar{\sigma}^{t}})\sigma_{kk}^{t}\delta_{ij} \right.$$

$$- \frac{1}{2}\frac{\partial g_{1}^{t}}{\partial \Delta \bar{\sigma}^{t}} \sum_{n=1}^{N} J_{n}\left[\exp[-\lambda_{n}\Delta\psi^{t}]q_{ij,n}^{t-\Delta t} - g_{2}^{t-\Delta t}\left(\frac{1-\exp[-\lambda_{n}\Delta\psi^{t}]}{\lambda_{n}\Delta\psi^{t}} \right)S_{ij}^{t-\Delta t} \right]$$

$$- \frac{1}{2}\frac{\partial a_{\sigma}^{t}}{\partial \Delta \bar{\sigma}^{t}} g_{1}^{t}\sum_{n=1}^{N} J_{n}\left[\exp[-\lambda_{n}\Delta\psi^{t}]\left(\frac{\lambda_{n}\Delta t q_{ij,n}^{t-\Delta t}}{a_{\sigma}^{t2}} + \frac{S_{ij}^{t-\Delta t}}{a_{\sigma}^{t}} \right) \right.$$

$$\left. -g_{2}^{t-\Delta t}\left(\frac{1-\exp[-\lambda_{n}\Delta\psi^{t}]}{\lambda_{n}\Delta\psi^{t}} \right)S_{ij}^{t-\Delta t} \right]$$

$$- \frac{1}{9}\frac{\partial g_{1}^{t}}{\partial \Delta \bar{\sigma}^{t}} \sum_{n=1}^{N} B_{n}\left[\exp[-\lambda_{n}\Delta\psi^{t}]q_{kk,n}^{t-\Delta t} - g_{2}^{t-\Delta t}\left(\frac{1-\exp[-\lambda_{n}\Delta\psi^{t}]}{\lambda_{n}\Delta\psi^{t}} \right)\sigma_{kk}^{t-\Delta t} \right]\delta_{ij}$$

$$- \frac{1}{9}\frac{\partial a_{\sigma}^{t}}{\partial \Delta \bar{\sigma}^{t}} g_{1}^{t}\sum_{n=1}^{N} B_{n}\left[\exp[-\lambda_{n}\Delta\psi^{t}]\left(\frac{\lambda_{n}\Delta t q_{kk,n}^{t-\Delta t}}{a_{\sigma}^{t2}} + \frac{\sigma_{kk}^{t-\Delta t}}{a_{\sigma}^{t}} \right) \right.$$

$$\left. \left. -g_{2}^{t-\Delta t}\left(\frac{1-\exp[-\lambda_{n}\Delta\psi^{t}]}{\lambda_{n}\Delta\psi^{t}} \right)\sigma_{kk}^{t-\Delta t} \right]\delta_{ij} \right\}$$

(2-65)

where

$$\frac{\partial \Delta \bar{\sigma}^{t}}{\partial \Delta \sigma_{kl}^{t}} = \frac{3}{2}\frac{\Delta S_{ij}^{t}}{\Delta \bar{\sigma}^{t}}\left(\delta_{ik}\delta_{jl} - \frac{1}{3}\delta_{ij}\delta_{kl} \right) = \frac{3}{2}\frac{\Delta S_{ij}^{t}}{\Delta \bar{\sigma}^{t}}I_{ijkl}'$$

(2-66)

For the Perzyna model, $\partial\Delta\varepsilon_{ij}^{vp,t}/\partial\Delta\sigma_{kl}^{t}$ is given as (Kim & Muliana, 2009):

$$
\frac{\partial\Delta\varepsilon_{ij}^{vp,t}}{\partial\Delta\sigma_{kl}^{t}} = \Delta\lambda^{t}\left\{\frac{1}{\exp(-\frac{h(\bar{\sigma}^{t})\hat{t}}{\eta_{p}})-\exp(-\frac{h(\bar{\sigma}^{t})(\hat{t}-\Delta\hat{t})}{\eta_{p}})}\times\right.
$$

$$
\left(-\frac{\hat{t}}{\eta_{p}}\exp(-\frac{h(\bar{\sigma}^{t})\hat{t}}{\eta_{p}})+\frac{(\hat{t}-\Delta\hat{t})}{\eta_{p}}\exp(-\frac{h(\bar{\sigma}^{t})(\hat{t}-\Delta\hat{t})}{\eta_{p}})\right)h'(\bar{\sigma}^{t})\times
$$

$$
\frac{9}{4\bar{\sigma}^{t}}I_{ijpq}S_{pq}\frac{\Delta S_{ij}^{t}}{\Delta\bar{\sigma}^{t}}I_{ijkl}+ \tag{2-67}
$$

$$
\left(\frac{n}{\sigma_{y}^{o}\phi}\left[1-(k^{t-\Delta t}+k^{\Delta t})h'(\bar{\sigma}^{t})\right]\right)\frac{9}{4\bar{\sigma}^{t}}I_{ijpq}S_{pq}\frac{\Delta S_{ij}^{t}}{\Delta\bar{\sigma}^{t}}I_{ijkl}-
$$

$$
\left.\frac{9}{4\bar{\sigma}^{t}}I_{ijpq}S_{pq}\frac{\Delta S_{ij}^{t}}{(\Delta\bar{\sigma}^{t})^{3}}I_{ijkl}+\frac{1}{2\Delta\bar{\sigma}^{t}}I_{ijpq}I_{pqkl}\right\}
$$

where $h'(\bar{\sigma}^{t})=\dfrac{dh(\bar{\sigma}^{t})}{d\bar{\sigma}^{t}}$, and $I'_{ijkl}=\delta_{ik}\delta_{jl}-\dfrac{1}{3}\delta_{ij}\delta_{kl}$

$$
\frac{\partial R_{\Delta\varepsilon_{ij}}}{\partial\Delta\lambda^{t}}=\frac{2\Delta\lambda^{t}}{3\bar{\sigma}^{t}}I'_{ijkl}S_{kl}^{t} \tag{2-68}
$$

$$
\frac{\partial R_{\Delta\lambda^{t}}}{\partial\Delta\sigma_{kl}^{t}}=-\frac{\Delta t}{\eta_{p}}\Phi^{n-1}\left\langle\frac{n}{\sigma_{y}^{0}}+\right.
$$

$$
\left.\Phi\left(-\frac{\hat{t}}{\eta_{p}}\exp(-\frac{h(\bar{\sigma}^{t})\hat{t}}{\eta_{p}})+\frac{(\hat{t}-\Delta\hat{t})}{\eta_{p}}\exp(-\frac{h(\bar{\sigma}^{t})(\hat{t}-\Delta\hat{t})}{\eta_{p}})\right)h'(\bar{\sigma}^{t})\right\rangle\frac{3\Delta\sigma_{kl}^{t}}{2\bar{\sigma}^{t}} \tag{2-69}
$$

$$
\frac{\partial R_{\Delta\lambda^{t}}}{\partial\Delta\lambda^{t}}=\frac{\Delta t}{\eta_{p}}\left\langle n\frac{n}{\sigma_{y}^{0}}\Phi(F)^{n-1}\right\rangle \tag{2-70}
$$

In Eq. (2-25) and (2-26), the incremental stress and the incremental magnitude of

plastic strain of the Perzyna model are expressed in terms of the stress and

accumulated plastic strain which are unknown variables. In Eq. (2-33) and Eq. (2-

55), the incremental viscoplastic strains of the Valanis and Dashpot-slider models

are expressed in terms of unknown stress variables. Thus, the components related to

the magnitude of plastic strain in Eq. (2-63) for the Valanis and dashpot-slider

models are neglected. The second term of Eq. (2-64) for the Valanis and Dashpot-

slider models are given as:

For the dashpot-slider model,

$$
\frac{\partial \Delta \varepsilon_{ij}^{vp,t}}{\partial \Delta \sigma_{kl}^{t}} = \Delta t \times \exp\left(-\frac{h(\bar{\sigma}^{t})}{\eta_{p}}\hat{t}\right) \times \left\{ \frac{3}{2h(\bar{\sigma}^{t})\Delta\bar{\sigma}^{t}} \frac{S_{ij}^{t}}{\|\mathbf{S}^{t}\|}\left(S_{pq}^{t} I'_{pqkl} - \frac{h'(\bar{\sigma}^{t})}{h(\bar{\sigma}^{t})} S_{rs}^{t} I'_{rskl} \right) + \right.
$$
$$
\left. \left(\frac{(\bar{\sigma}^{t} - \sigma_{y}^{o})}{h(\bar{\sigma}^{t})} \right)\left[\left(-\frac{h'(\bar{\sigma}^{t})}{\eta_{p}}\hat{t} \right) \frac{3 S_{ij}^{t} S_{tu}^{t}}{2h(\bar{\sigma}^{t})\|\mathbf{S}^{t}\|\Delta\bar{\sigma}^{t}} I'_{tukl} + \left(\frac{I'_{ijkl}}{\|\mathbf{S}^{t}\|} \right) \right] \right\}
$$

(2-71)

For the Valanis model,

$$
\frac{\partial \Delta \varepsilon_{ij}^{vp,t}}{\partial \Delta \sigma_{kl}^{t}} = \frac{2G}{(S_{y}^{o})^{2} f^{2}(\zeta)[2G + S_{y}^{o} f'(\zeta)]} \left[2 S_{ij}^{t} \Delta\varepsilon_{mn}^{t} I'_{mnkl} \right]
$$

(2-72)

Once the convergence is achieved, the consistent tangent stiffness matrix is calculated

using Eq. (2-74). The incremental viscoelastic and viscoplastic strains of the Perzyna,

Dashpot-slider, and Valanis models are obtained from Eqs. (2-8), (2-26), (2-30), and (2-

54), respectively. Detailed discussion on the consistent tangent moduli for a class of

viscoplastic constitutive model can be found in Ju (1990). Finally, the following

variables: $q_{ij,n}^{t}$, $q_{kk,n}^{t}$, k^{t}, $F(\overline{\sigma}^{t}, k^{t})$, $\varepsilon_{ij}^{ve,t}$, $\varepsilon_{ij}^{vp,t}$, and σ_{ij}^{t} are also updated. The

variables k^{t} and $F(\overline{\sigma}^{t}, k^{t})$ are needed for the Perzyna model.

$$\{R^{t}\} = \begin{Bmatrix} R_{\Delta\varepsilon}^{t} \\ R_{\Delta\lambda}^{t} \end{Bmatrix}, \qquad \left\| R^{t} \right\| \le Tol \tag{2-73}$$

$$C_{ijkl}^{t} = \left[\frac{\partial R_{kl}^{t}}{\partial \Delta\sigma_{ij}^{t}} \right]^{-1} \tag{2-74}$$

2.3 Numerical Implementation and Verification

The time-integration algorithm of the combined Schapery viscoelastic model and

viscoplastic model of the Perzyna, dashpot-slider, or Valanis models are verified using

experimental data on high density polyethylene (HDPE) reported by Lai and Bakker

(1995). Four loading histories, which are: 1) creep recovery tests at various stress levels,

2) two-step loadings, 3) loading-unloading at different constant stress rates; and 4) five

cycles of creep and long recovery loadings, are presented. All tests were performed at

fixed temperature 20°C. Lai and Bakker (1995) used creep-recovery data of HDPE at

various stress levels to calibrate the nonlinear viscoelastic and viscoplastic material

properties. In this study, the nonlinear viscoelastic material parameters calibrated by Lai

and Bakker (1995) are directly used as input to the numerical algorithm, while the

viscoplastic material parameters in the Perzyna, dashpot-slider, or Valanis model are

calibrated from the viscoplastic strains during the creep tests at various stresses. The

elastic modulus and the Poisson's ratio of the tested HDPE are 4535MPa and 0.3,

respectively. The time-dependent material parameters described in Eq. (2-6) are given in

Table 2-1. The stress-dependent viscoelastic material parameters defined in Eqs. (2-3)

and (2-4) are given in Fig.2-6. The viscoplastic material constants of Valanis's

endochronic model S_y^0 and β are 21 MPa and 10^{-7}, respectively. The parameter S_y^0

describes the increasing rate of the viscoplastic strain and β is time dependent

parameter in Eq. (2-41). The viscoplastic parameters of the Perzyna model η_p and n

are 35 [MPa/s] and 1.36, respectively, and the hardening parameter is stress dependent.

The viscoplastic parameter of dashpot slider model, η_p, is 35 [MPa/s]. The stress-

dependent hardening parameter $h(\bar{\sigma}^t)$ of the Perzyna model in Eq. (2-16) is given in Fig.

2-7. The initial yield stress S_y^0 for the Perzyna and dashpot-slider model is taken as 1

MPa.

Table 2-1

Prony series coefficients for the HDPE polymer

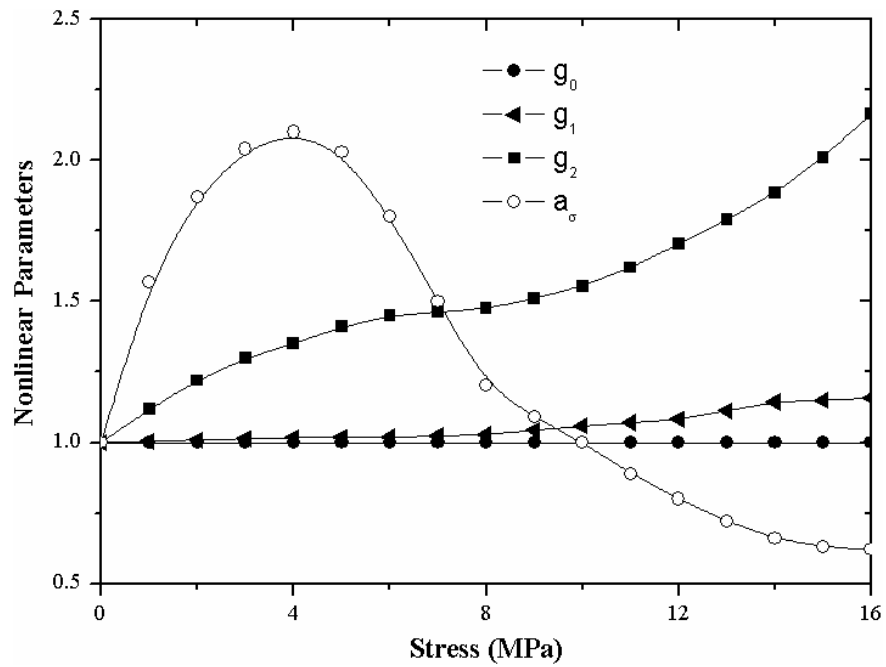| n	$\lambda_n \, (\sec^{-1})$	$D_n \times 10^{-4} \, (MPa^{-1})$
1	1	2.23
2	10^{-1}	2.27
3	10^{-2}	1.95
4	10^{-3}	3.50
5	10^{-4}	5.50
6	10^{-5}	5.50

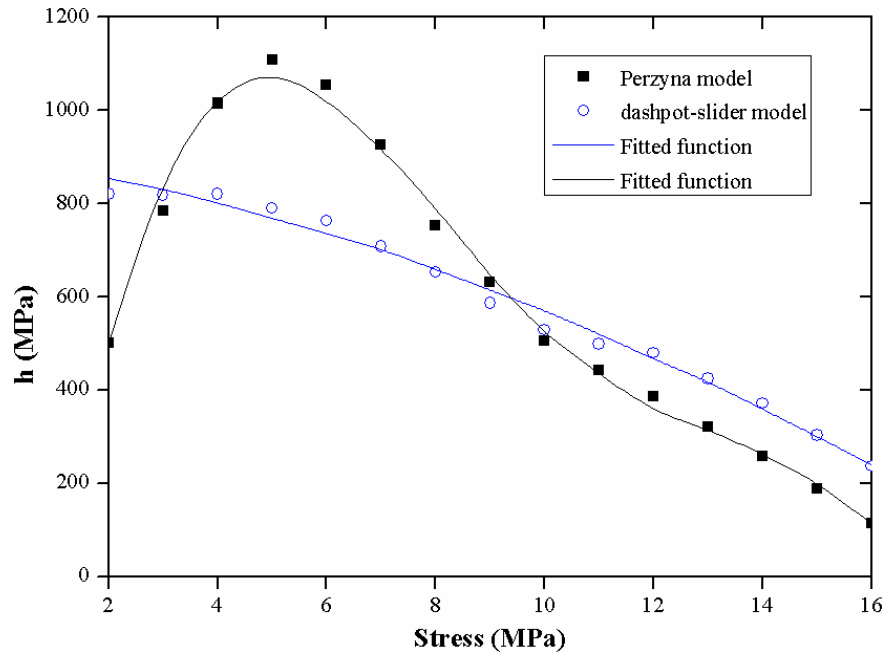Figure 2-6. Nonlinear stress dependent parameters of the Schapery viscoelastic model (Lai and Bakker, 1995)

Figure 2-7. Hardening parameters (calibrated from the viscoplastic creep strains)

2.3.1 Creep-recovery and two-step loading histories

The creep recovery responses at stresses: 2~16 MPa are shown in Fig. 2-8. The

numerical algorithm of the combined Schapery and Perzyna model predicts the

experimental data very well for all stress levels. Moreover, viscoplastic material

constants described by a dashpot-slider model in Eq. (2-54) are also characterized. The

calibrated stress-dependent hardening parameter is illustrated in Fig. 2-7 and the

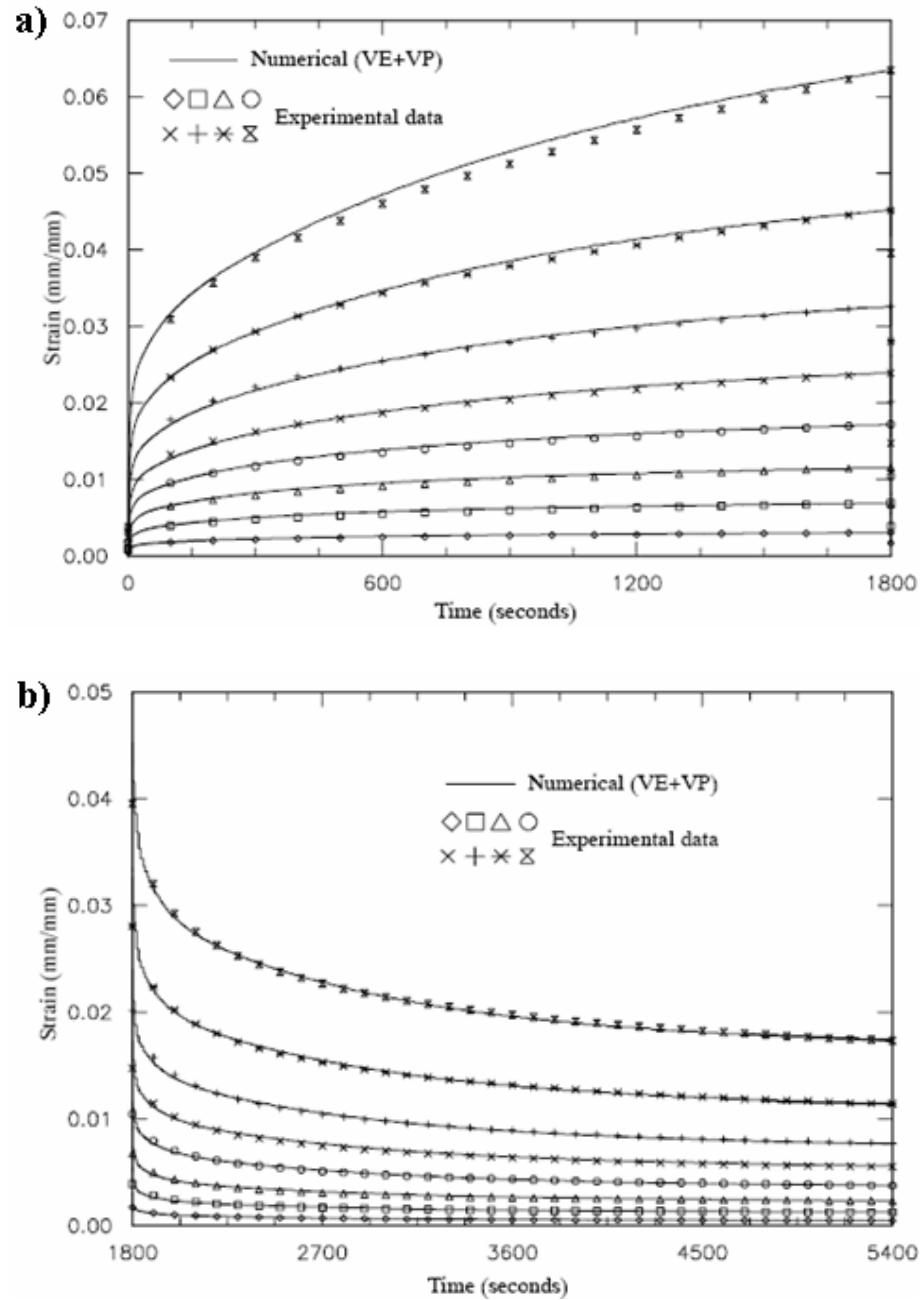viscoplastic material constant, η_p for Perzyna is 35 MPa/s.

Figure 2-8. Creep and Recovery strains at various stresses 2-16MPa (combined viscoelastic and viscoplastic strains) a) creep strain b) recovery strain

The numerical algorithm of the Schapery-Valanis model is verified with experimental data from the two step loading histories, which are given in Fig. 2-9. This response is also compared to the Schapery-Perzyna model. The first step loading is 10 MPa for 1800 seconds. This stress is reduced to 8, 6, 4, 2, and 0 MPa, respectively, and is held for another 1800 seconds. Good comparisons are shown for all cases. Next, numerical simulations of the two-step loading histories are performed by holding the second step stresses up to 8 hour, as illustrated in Figure 2-10. During the second loading step, the strain recovery is observed for a certain period of time and at the same time creep strain occurs due to the existence of the second stress. The recovery period is proportional to the amount of the stress reduction. When the stress from the first loading step is completely removed, fully recovery of the viscoelastic strain is exhibited and permanent strain from the accumulated viscoplastic strain in the first loading step is shown. The shortest recovery period occurs in this case for the stress level of 8MPa. In this case, the recovery strain is due to the 2 MPa stress removal and this strain is combined with the creep strain at 8 MPa.
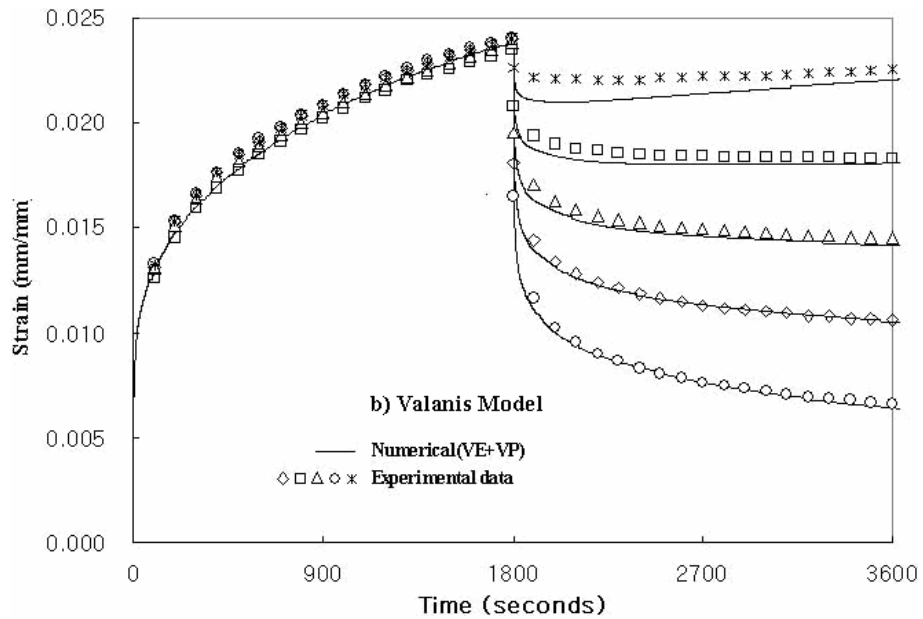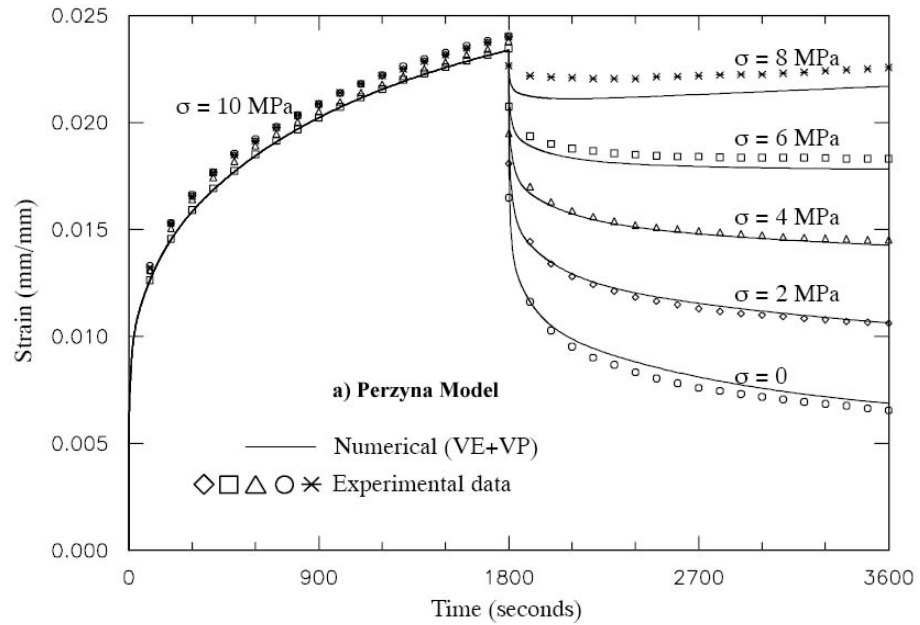
Figure 2-9. Total strains from the two-step loading histories a) Perzyna Model b) Valanis model
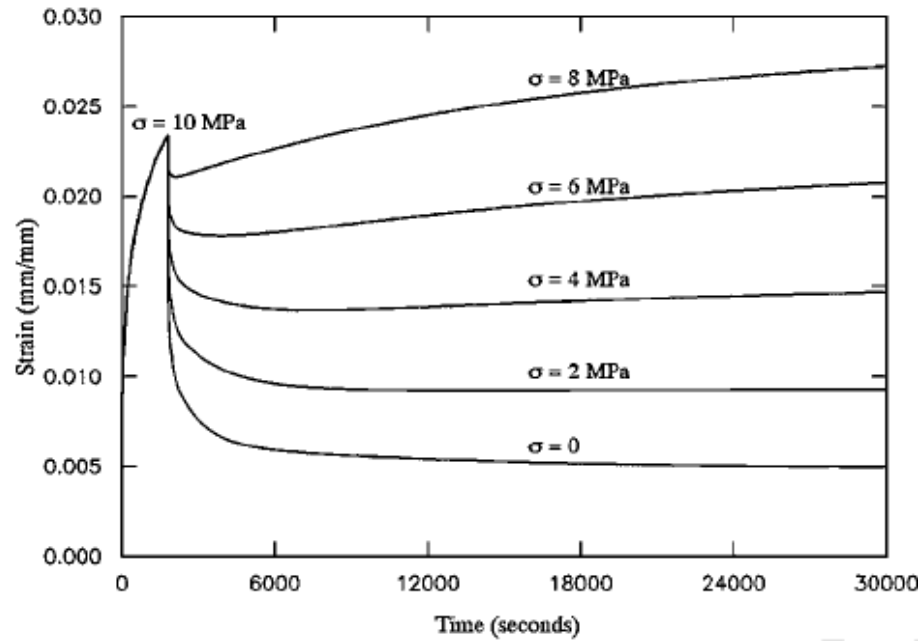
Figure 2-10. Responses of the two-step loading with longer time for the second loading

2.3.2 Loading-unloading at constant stress rates

Verification of the proposed time-integration algorithm at different loading rates is also performed. Lai and Bakker (1995) conducted tests with constant stress rates for the following uniaxial loading-unloading histories:

$$\sigma(t) = \begin{cases} rt & 0 \leq t \leq t_1 \\ r(2t_1 + t) & t_1 \leq t \leq 2t_1 \end{cases} \qquad (2\text{-}79)$$

where r is the constant stress rate and t_1 is the time, when a maximum load σ_{max} is reached, the unloading begins. The stress-strain responses of the Schapery-Perzyna and

Schapery-Valanis models are compared with experimental data in Fig. 2-11. Three

different constant stress rates and σ_{max} = 10 MPa are applied. For the fast loading (1

MPa/s), the viscoelastic-viscoplastic strain is less prominent. For the slower loadings

(rates 0.1MPa/s and 0.01 MPa/s), the viscoelastic-viscoplastic strains are more

pronounced. For the fast loading of 1 MPa/s, errors about 5% are observed between the

Perzyna and Valanis models and the experimental data. For the 0.1 MPa/s loading, errors

about 2% is observed during loading and errors about 10% is shown for the unloading.

For the slowest loading of 0.01 MPa/s, errors about 2% are shown during loading and

the unloading part has 5% error for the Perzyna model and 10% error for the Valanis

model. Overall, the time-integration algorithm for the viscoelastic-viscoplastic response

of the Schapery-Perzyna and Schapery-Valanis models predicts the experimental data

very well. It is seen that the Perzyna model give slightly better predictions than the

Valanis model. The advantage of the Valanis model is that it does not require defining an

initial yield stress, which is beneficial when plastic deformation occurs at a low stress
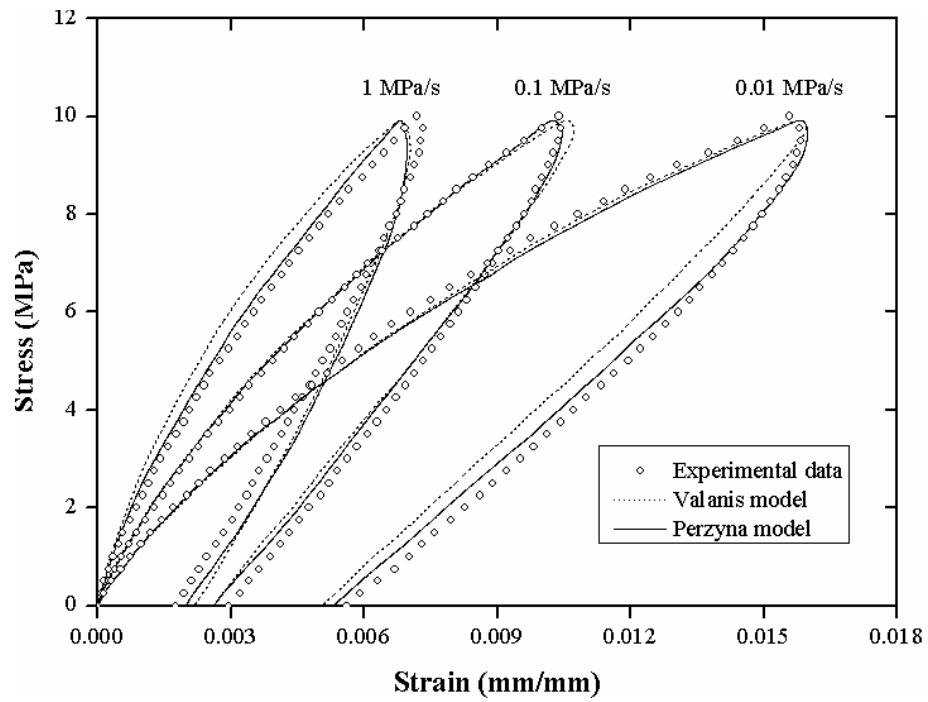
level.

Figure 2-11. Stress-strain relations under different constant stress rates (numerical results)

2.3.3 Five cycles of creep-long recovery loadings

The experimental data of 600 second creep loading at 8 MPa followed by nearly 7

hour recovery are also used to verify the proposed time-integration algorithm. The creep-

long recovery process is repeated five times. Comparisons of the recovery strains after

the first and fifth cycles obtained from the numerical algorithm and the ones from the

experimental tests are shown in Fig. 2-12. Both Perzyna and dashpot-slider viscoplastic

models are used. The time-integration algorithm shows relatively good prediction of the

experimental data. Deviation in the recovery period of the fifth cycle is perhaps due to

the time-dependent material parameters that are calibrated from short-term data. Finally,

the total strains during the creep loading at 100, 300, and 600 seconds are also recorded

at every cycle. Figure 2-13 illustrates comparisons of the isochronous strains obtained

from the numerical algorithm and the ones from the experiment. Significant mismatch is

shown by the dashpot-slider model at 600 second after the first cycle. This is perhaps

due to the limited time-dependent material data. Moreover, the use of only one dashpot-

slider element limits the retardation time to a short-duration. To capture longer time

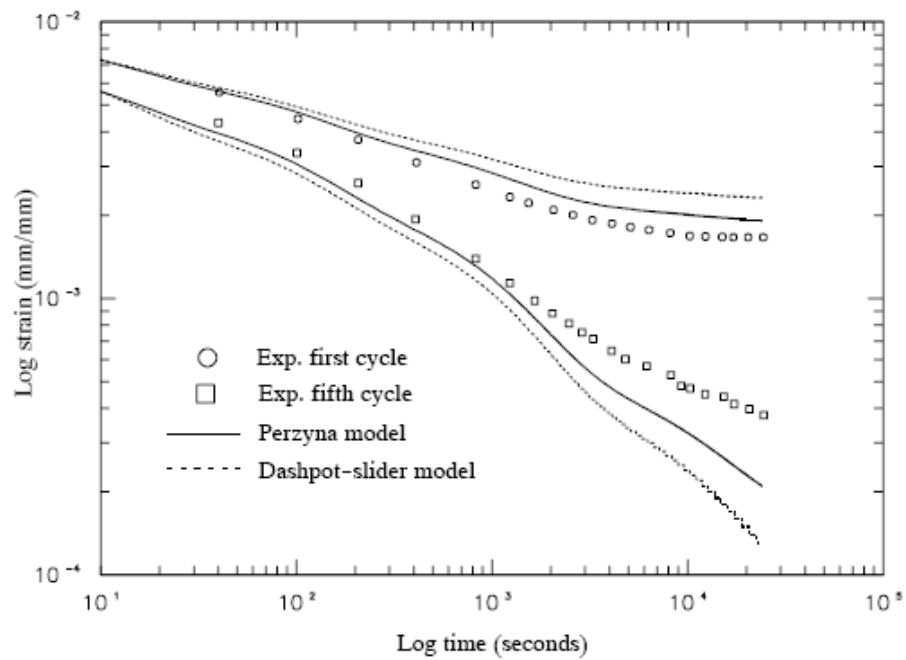responses, several dashpot-slider elements may be added in series arrangement.

Figure 2-12. Recovery strains during the first and fifth cycles
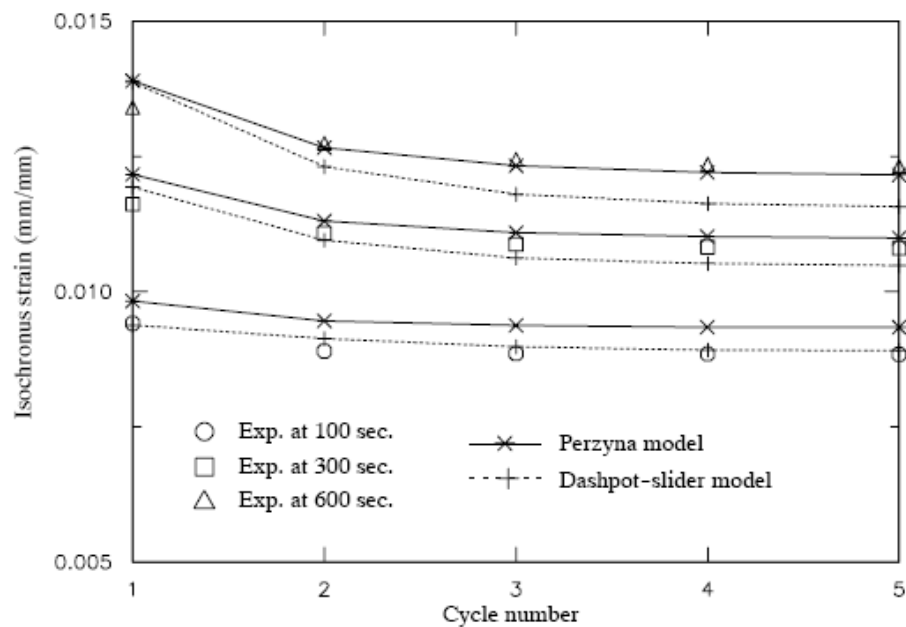
Figure 2-13. Isochronous strains during the creep-long recovery cycles

2.3.4 Convergence study of recursive-iterative algorithm

The convergence behaviors at the material (local) level during the creep-recovery numerical analysis under 10 MPa uniaxial loading are monitored. The viscoelastic and viscoplastic material parameters are reported in section.2.3.1. The residuals (Eqs. 2-58 ~ 2-61) are evaluated at early loading (t=0.0035s), prior to the removal of the load (t=1793s), and sometime during the recovery stage (t=2670s).

Figure 2-14. Convergence behaviors at the material (local) levels during creep-recovery at 10MPa.

Figure 2-15 shows the magnitude of the strain residual from the Schapery-Perzyna and Schapery-Valanis models at three different times. T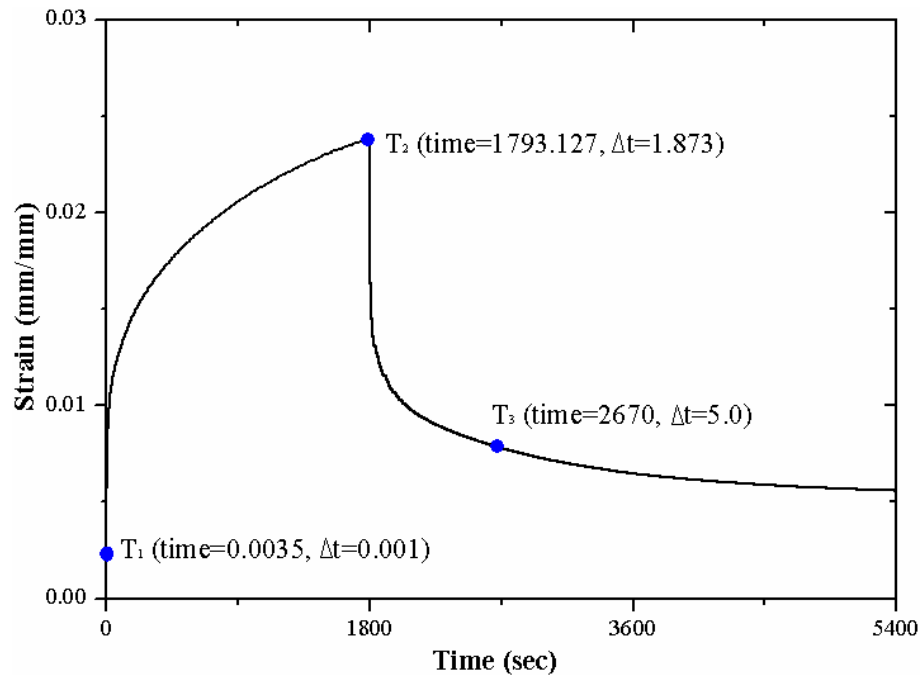he incremental time steps corresponding to the above times are 0.001, 2, and 5 second, respectively. Tolerance, 10^{-6}, which is equivalent to 1 micron-strain $(1\mu\varepsilon)$, is used for the convergence criterion. It is seen that using a linearized stress-update alone can result in residual strain error up to 0.1% (1000 micron-strain), indicated by the residual from the first iteration. Figure 2-16 compares the creep-recovery strains for the combined viscoelastic and viscoplastic responses when different tolerances at the material level are used. The analyses have the same global (structural) iterations and the same time increments are maintained. Figure 2-16 shows that bypassing the iteration at the material level, indicated by Tolerance of 500 $\mu\varepsilon$, results in significant strain errors, which are propagated to the structural level and accumulated to the next time intervals. It is also seen that by tightening the tolerance to 250 $\mu\varepsilon$, in which we allow two iterations at the material level, tremendously reduces the residual as indicated by overall strain responses in Figure 2-16. This result shows the efficiency of the proposed algorithm in minimizing residual. It is also seen that the magnitude of the residual in the Perzyna model at the first iteration is higher than that of the Valanis model (Fig 2-15) leading to higher

mismatches in the overall creep response (Fig 2.16). This is due to the fact that the

residual vector in the Perzyna model consists of 6 strain component and the plastic

multiplier, while in the Valanis model the residual of the plastic multiplier during the

iteration is zero (Eqs 2-58 ~ 2-61).

Convergence behaviors at the material (local) and at the structural element (global)

levels during 1800 second creep and 3600 second recovery are also monitored for two

stress levels: 4 and 16 MPa, as given in Tables 2-2 and 2-3. These values are reported for

the Perzyna viscoplastic model. An efficient integration algorithm at the material level

can accelerate convergence at the element (global) level. Quadratic convergence rates

are shown in most loading periods, except at highly non-linear responses (close to 1800
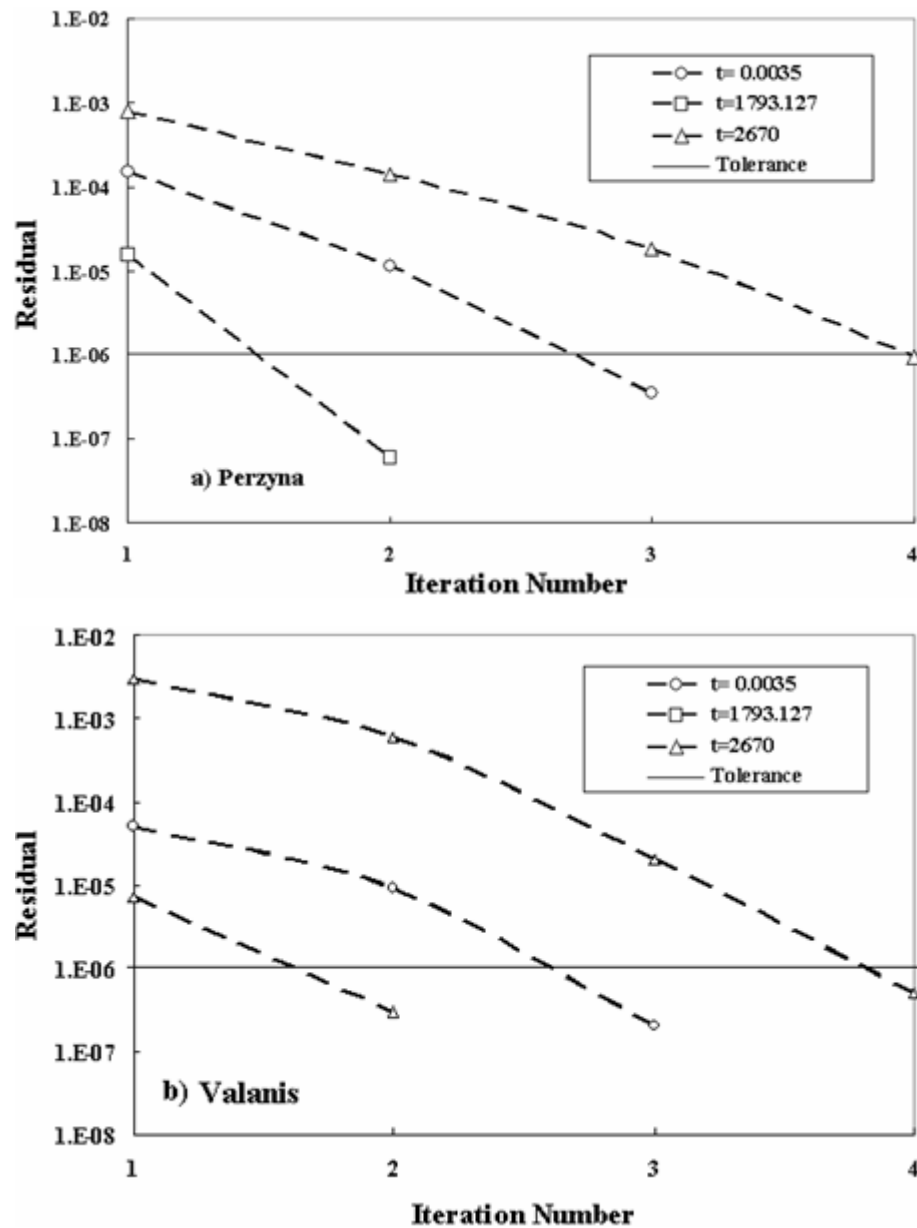
second).

Figure 2-15. Convergence behaviors at the material (local) levels during creep-recovery at 10MPa.   a) Perzyna model b) Valanis model
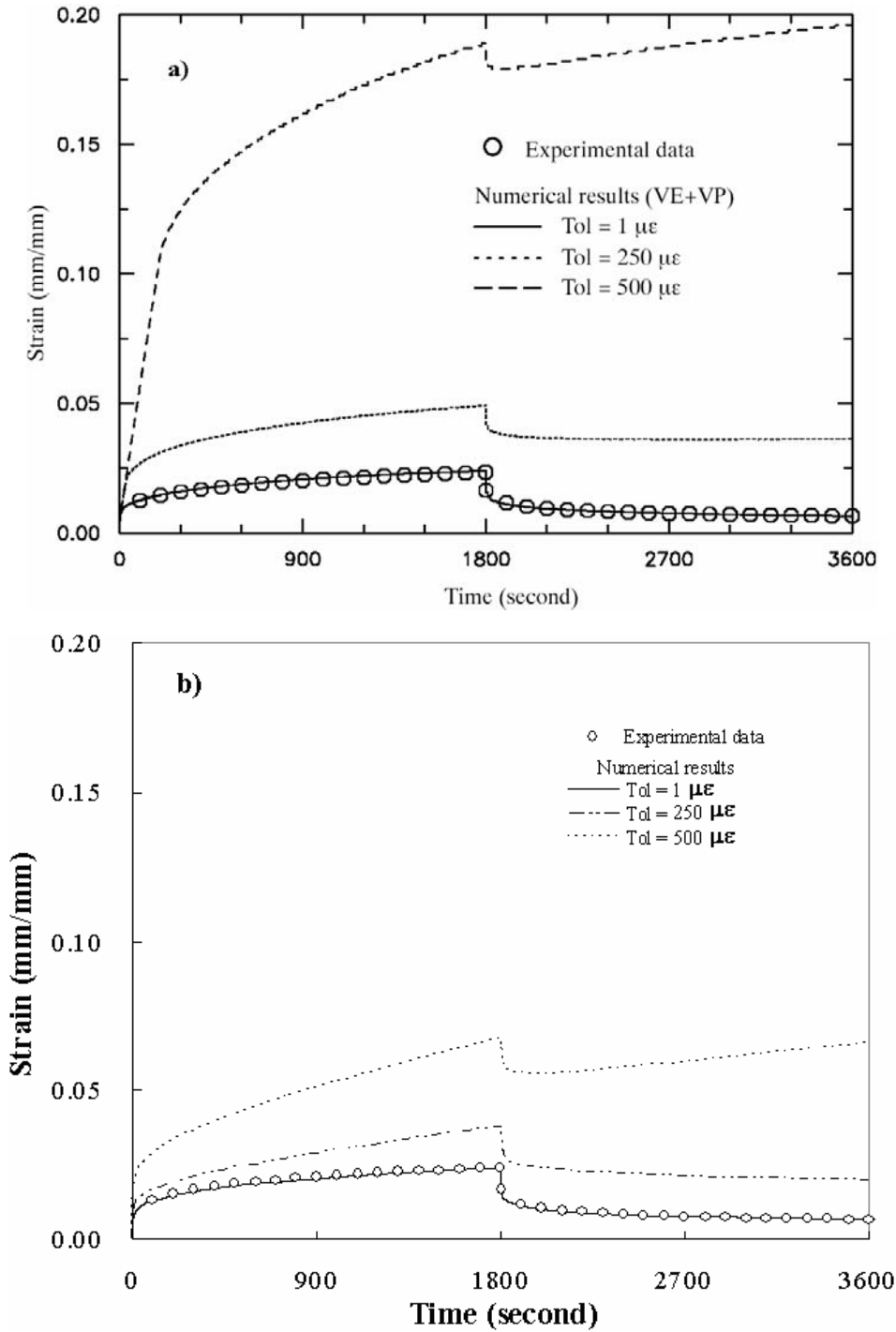
Figure 2-16. Responses of the creep-recovery at 10MPa under various tolerance at the material (local) level. a) Perzyna model   b) Valanis model

Table 2-2

Residual and Iteration of Local stiffness level for Creep recovery loading

Iteration	4 MPa-0 MPa			16 MPa-0 MPa		
	1.5 (sec)	1796.5 (sec)	2937.3 (sec)	1.5 (sec)	1796.5 (sec)	2937.3 (sec)
1	0.173E-03	1.432E-06	1.775E-04	0.103E-02	2.084E-05	2.464E-06
2	0.155E-05	6.440E-07	9.234E-06	0.433E-04	1.679E-06	9.108E-22
3	0.163E-08		4.804E-07	0.193E-06	1.360E-07	
4						

Table 2-3

Residual and Iteration of Global stiffness level for Creep recovery loading

Iteration	4 MPa-0 MPa			16 MPa-0 MPa		
	1.5 (sec)	1796 (sec)	2937	1.5 (sec)	1793 (sec)	2937 (sec)
1	1.089E-02	3.307E-03	3.712E-01	8.319E-01	7.492E-03	4.182E-04
2	6.040E-04		2.208E-02	1.487E-01		
3			1.210E-03	2.073E-03		

CHAPTER III

A CONCURRENT MICROMECHANICAL MODEL FOR PARTICLE REINFORCED

COMPOSITES

A micromechanical model is presented for modeling time-dependent and inelastic

responses of composites having solid spherical reinforcements. The solid spherical

particles are made of linear elastic materials and are assumed to have the same size

throughout the composites. Time-dependent and inelastic constitutive models are used

for the matrix constituent. Figure 3-1 illustrates a composite microstructure having

randomly distributed solid spherical particles in the homogeneous matrix. The composite

microstructure is idealized as periodically distributed arrays of cubic particles. This

geometry representation is similar to the one proposed by Aboudi and co-authors (1996)

for composites with a non-uniform fiber spacing. It is also assumed that each particle is

fully surrounded by polymeric matrix and direct contact between particles is avoided. A

composite representative volume element (RVE) is defined by a cubic particle embedded

in the center of the matrix phase of a cubic domain. It is also assumed that changes in the

micro-structural geometries of the composites during deformation can be ignored. The

proposed micromechanical model is suitable for estimating responses of composites

having low to medium volume fractions, in which the effects of contact between

particles on the overall performance of composites are insignificant. A one eighth unit-

cell consisting of four particle and matrix sub-cells is modeled due to the three-plane

symmetry of the RVE. The first sub-cell represents a particle constituent, while sub-cells

2, 3, and 4 represent a matrix constituent. The homogenization scheme is derived in

terms of average strains and stresses in the sub-cells. Perfect bond is assumed at the sub-

cell's interface which requires imposing the traction continuity and displacement

compatibility at the sub-cells' interfaces. The micromechanical relations provide

equivalent homogeneous material responses of heterogeneous composites and

simultaneously predict nonlinear behaviors of the individual constituents due to

prescribed boundary conditions at the composite (macro) structures. The two-ways

micro-macro mechanical relations refer to a concurrent micromechanical model.
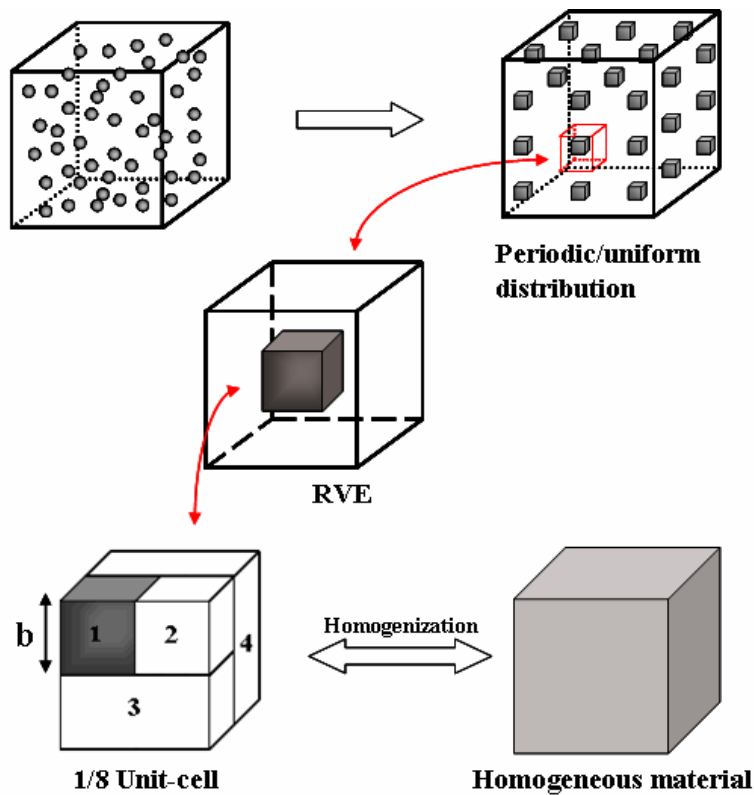
Figure 3-1. Representative unit-cell model for the particulate reinforced polymers

A linearized micromechanical model and a corrector scheme are presented for

modeling time-dependent and inelastic responses of polymer composites having solid

spherical reinforcements. Due to the nonlinear and time-dependent responses in the

polymeric matrix, the linearized micromechanical relations often lead to error in

predicting the nonlinear constitutive equations. A stress–strain correction algorithm is

formulated to satisfy both micromechanical constraints and nonlinear constitutive

equations. A time-integration algorithm that is developed for the viscoelastic-

viscoplastic matrix constituents (Chapter II), is nested to the upper-scale time-integration

algorithm of the unit-cell model, which is compatible with FE structural analysis

framework.

3.1 Linearized Micromechanical Relations

The effective properties of a heterogeneous medium are approximated using a

volume average of the properties of the individual constituents. The average stresses and

strains are defined by:

$$\bar{\sigma}_{ij}^t = \frac{1}{V} \int_V \sigma_{ij}^t(x_k)dV \qquad\qquad i,j = 1,2,3 \qquad\qquad (3\text{-}1)$$

$$\bar{\varepsilon}_{ij}^t = \frac{1}{V} \int_V \varepsilon_{ij}^t(x_k)dV \qquad\qquad i,j = 1,2,3 \qquad\qquad (3\text{-}2)$$

where $\sigma_{ij}^t(x_k)$ and $\varepsilon_{ij}^t(x_k)$ are the components of stress and strain fields in the

representative unit-cell model. An over-bar indicates effective field quantities. For a

small deformation gradient problem, the strain is expressed by $\varepsilon_{ij}^t = \frac{1}{2}[u_{i,j}^t + u_{j,i}^t]$, where

u_i^t is the component of the displacement at time t. In a heterogeneous periodic medium,

a basic unit-cell that represents geometrical and material characteristics can be defined.

Each unit-cell is divided into a number of sub-cells and the spatial variation of the

displacement field in each sub-cell is assumed such that the stresses and deformations

are spatially uniform. Traction continuity at an interface between sub-cells is satisfied in

an average sense. Thus, the average stresses and strains in the unit-cell model are defined

by:

$$\bar{\sigma}_{ij}^t = \frac{1}{V}\sum_{\alpha=1}^{N} \int_{V^{(\alpha)}} \sigma_{ij}^{(\alpha),t}(x_k^{(\alpha)})dV^{(\alpha)} \approx \frac{1}{V}\sum_{\alpha=1}^{N} V^{(\alpha)}\sigma_{ij}^{(\alpha),t} \tag{3-3}$$

$$\bar{\varepsilon}_{ij}^t = \frac{1}{V}\sum_{\alpha=1}^{N} \int_{V^{(\alpha)}} \varepsilon_{ij}^{(\alpha),t}(x_k^{(\alpha)})dV^{(\alpha)} \approx \frac{1}{V}\sum_{\alpha=1}^{N} V^{(\alpha)}\varepsilon_{ij}^{(\alpha),t} \tag{3-4}$$

The superscript $[\alpha]$ denotes the sub-cell number and N is the total number of sub-cells.

The stress $\sigma_{ij}^{(\alpha),t}$ and strain $\varepsilon_{ij}^{(\alpha),t}$ are the average stress and strain at current time within

each sub-cell. The unit-cell total volume V is given as:

$$V = \sum_{\alpha=1}^{N} V^{(\alpha)} \tag{3-5}$$

To relate the stresses and strains in each sub-cell to the effective stress and strain of the

composites, concentration matrices are formulated. The concentration matrices were

proposed by Hill [1965] for linear elastic composites. In this study, the micromechanical

model is designed to be compatible with displacement based FE structural analyses, in

which the effective strains $\bar{\varepsilon}_{ij}^t$ are the independent known variables at time t. The sub-

cell strain-interaction (concentration) matrix ($\mathbf{B}^{(\alpha),t}$), which relates the sub-cell average

strains at time t, $\mathbf{\varepsilon}^{(\alpha),t}$, to the effective unit-cell average strain at time t, $\bar{\mathbf{\varepsilon}}^t$, is defined as:

$$\varepsilon_{ij}^{(\alpha),t} = B_{ijkl}^{(\alpha),t}\ \bar{\varepsilon}^t \tag{3-6}$$

Substituting Eq. (3-6) to (3-4) gives:

$$\bar{\varepsilon}_{ij}^t = \frac{1}{V}\sum_{\alpha=1}^{N}V^{(\alpha)}B_{ijkl}^{(\alpha),t}\ \bar{\varepsilon}_{kl}^t \tag{3-7}$$

It is also seen from Eq. (3-7) that the $\mathbf{B^{(\alpha),t}}$ matrices should satisfy the following

constraint:

$$\frac{1}{V}\sum_{\alpha=1}^{N}V^{(\alpha)}B_{ijkl}^{(\alpha),t} = \delta_{ik}\delta_{jl} \tag{3-8}$$

In order to derive the strain-interaction matrices for all sub-cells, the micromechanical

relations together with sub-cells constitutive material models must be imposed. Using

the strains defined in Eq. (3-6) and linearized constitutive relations for the constituents,

the sub-cell's average stress is:

$$\sigma_{ij}^{(\alpha),t} = C_{ijkl}^{(\alpha),t}\varepsilon_{kl}^{(\alpha),t} = C_{ijkl}^{(\alpha),t}B_{klrs}^{(\alpha),t}\ \bar{\varepsilon}_{rs}^t \tag{3-9}$$

where $\mathbf{C}^{(\alpha),t}$ is the consistent tangent stiffness matrix of the sub-cell at time t which is

obtained from the Eq. (2-74). Substituting Eq. (3-9) into Eq. (3-3), the effective stress is

given as:

$$\bar{\sigma}_{ij}^t = \frac{1}{V}\sum_{\alpha=1}^{N}V^{(\alpha)}C_{ijkl}^{(\alpha),t}B_{klrs}^{(\alpha),t}\ \bar{\varepsilon}_{rs}^t \tag{3-10}$$

The unit-cell effective stiffness matrix $\bar{\mathbf{C}}^t$ at time t is determined by:

$$\overline{C}_{ijrs}^{t} = \frac{1}{V}\sum_{\alpha=1}^{N}V^{(\alpha)}C_{ijkl}^{(\alpha),t}B_{klrs}^{(\alpha),t} \tag{3-11}$$

The micromechanical model of solid spherical particle reinforced composites is represented by a unit-cell model with four sub-cells, as illustrated in Fig. 3-1. The volume of the unit-cell is taken as one. The volume of the sub-cell 1, which is model as a cube of edge length b, represents the particle volume fraction of the composite systems. Thus, the magnitude of b is always less than one. The volumes of the four sub-cells are then expressed as

$$V^{(1)} = b^3, \ V^{(2)} = b^2(1-b), \ V^{(3)} = b(1-b), \ V^{(4)} = (1-b) \tag{3-12}$$

The micromechanical relations within the four sub-cells are derived by assuming perfect bond along the interfaces of the sub-cells. Thus, displacement compatibility and traction continuity at the sub-cells' interface should be satisfied. The three-plane symmetries of the RVE make it possible for interchanging the principal axes in the micromechanical formulations, as illustrated in Fig. 3-2(a). The homogenized stress–strain relations within the sub-cells can be illustrated by the spring mechanical analog models, shown in Fig. 3-2(b). Each spring constant refers to the mechanical property of each sub-cell. In the case of both isotropic particle and matrix, the outcome of the homogenized micromechanical model is also isotropic. The homogenized strain relations are summarized as follows.
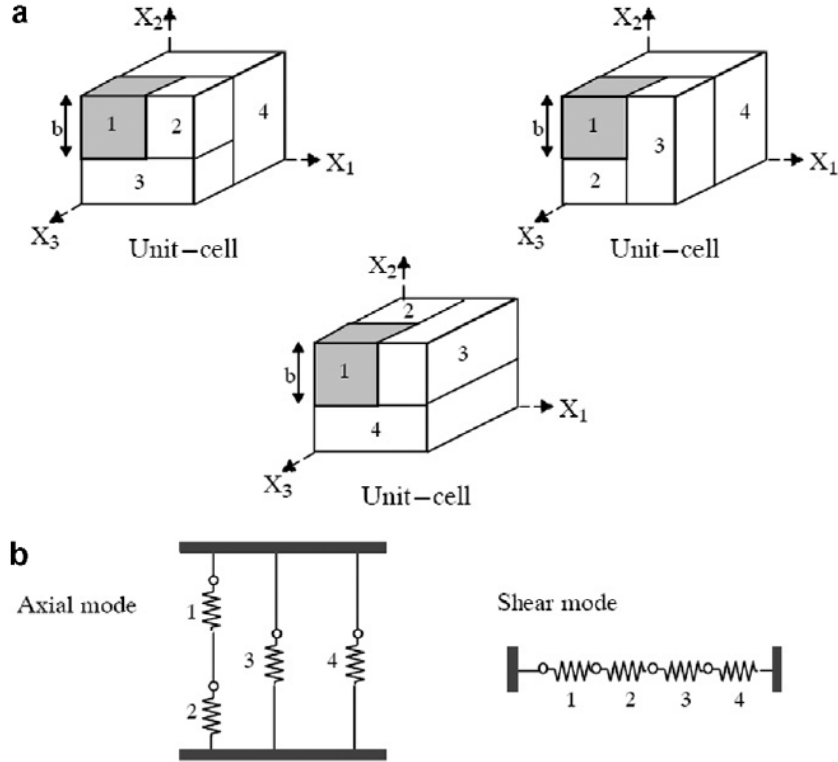
Figure 3-2. Homogenization schemes idealized with mechanical analog models. (a) Isotropic unit-cell model. (b) Micromechanical analog for stress-strain homogenization schemes.

$$\overline{\varepsilon}_{11}^{t} = \frac{1}{V^{(1)}+V^{(2)}}\left[V^{(1)}\varepsilon_{11}^{(1),t} + V^{(2)}\varepsilon_{11}^{(2),t}\right] = \varepsilon_{11}^{(3),t} = \varepsilon_{11}^{(4),t} \qquad (3\text{-}13)$$

$$\overline{\varepsilon}_{22}^{t} = \frac{1}{V^{(1)}+V^{(2)}}\left[V^{(1)}\varepsilon_{22}^{(1),t} + V^{(2)}\varepsilon_{22}^{(2),t}\right] = \varepsilon_{22}^{(3),t} = \varepsilon_{22}^{(4),t} \qquad (3\text{-}14)$$

$$\overline{\varepsilon}_{33}^{t} = \frac{1}{V^{(1)}+V^{(2)}}\left[V^{(1)}\varepsilon_{33}^{(1),t} + V^{(2)}\varepsilon_{33}^{(2),t}\right] = \varepsilon_{33}^{(3),t} = \varepsilon_{33}^{(4),t} \qquad (3\text{-}15)$$

$$\overline{\gamma}_{12}^{t} = V^{(1)}\gamma_{12}^{(1),t} + V^{(2)}\gamma_{12}^{(2),t} + V^{(3}\gamma_{12}^{(3),t} + V^{(4)}\gamma_{12}^{(4),t} \qquad (3\text{-}16)$$

$$\overline{\gamma}_{13}^t = V^{(1)}\gamma_{13}^{(1),t} + V^{(2)}\gamma_{13}^{(2),t} + V^{(3}\gamma_{13}^{(3),t} + V^{(4)}\gamma_{13}^{(4),t} \tag{3-17}$$

$$\overline{\gamma}_{23}^t = V^{(1)}\gamma_{23}^{(1),t} + V^{(2)}\gamma_{23}^{(2),t} + V^{(3}\gamma_{23}^{(3),t} + V^{(4)}\gamma_{23}^{(4),t} \tag{3-18}$$

The homogenized stresses are written in the following:

$$\begin{aligned} \overline{\sigma}_{11}^t &= V^{(A)}\sigma_{11}^{(A),t} + V^{(3)}\sigma_{11}^{(3),t} + V^{(4)}\sigma_{11}^{(4),t} \\ \sigma_{11}^{(a),t} &= \sigma_{11}^{(1),t} = \sigma_{11}^{(2),t} \end{aligned} \tag{3-19}$$

$$\begin{aligned} \overline{\sigma}_{22}^t &= V^{(A)}\sigma_{22}^{(A),t} + V^{(3)}\sigma_{22}^{(3),t} + V^{(4)}\sigma_{22}^{(4),t} \\ \sigma_{22}^{(A),t} &= \sigma_{22}^{(1),t} = \sigma_{22}^{(2),t} \end{aligned} \tag{3-20}$$

$$\begin{aligned} \overline{\sigma}_{33}^t &= V^{(A)}\sigma_{33}^{(A),t} + V^{(3)}\sigma_{33}^{(3),t} + V^{(4)}\sigma_{33}^{(4),t} \\ \sigma_{33}^{(A),t} &= \sigma_{33}^{(1),t} = \sigma_{33}^{(2),t} \end{aligned} \tag{3-21}$$

$$\overline{\tau}_{12}^t = \tau_{12}^{(1),t} = \tau_{12}^{(2),t} = \tau_{12}^{(3),t} = \tau_{12}^{(4),t} \tag{3-22}$$

$$\overline{\tau}_{13}^t = \tau_{13}^{(1),t} = \tau_{13}^{(2),t} = \tau_{13}^{(3),t} = \tau_{13}^{(4),t} \tag{3-23}$$

$$\overline{\tau}_{23}^t = \tau_{23}^{(1),t} = \tau_{23}^{(2),t} = \tau_{23}^{(3),t} = \tau_{23}^{(4),t} \tag{3-24}$$

In Eqs. (3-19) - (3-21), the total volume of sub-cell 1 and 2 is $V^{(A)} = V^{(1)} + V^{(2)}$. Next,

the strain concentration matrices $\mathbf{B}^{(\alpha),t}$ can be formed using the strain compatibility

relations in Eqs.(3-13) - (3-18), traction continuity conditions in Eqs.(3-19) - (3-24), and

the constitutive equations for each sub-cell. Six components of strains need to be

determined for every sub-cell. Thus, a total of 24 strain components is defined, which

requires forming 24 sets of equations. The first twelve equations are formulated from the

strain compatibility equations, which are expressed as:

$$\left\{ \begin{array}{c} R_{Disp} \\ (12x1) \end{array} \right\} = \left[\begin{array}{c} A_1 \\ (12x24) \end{array} \right] \left\{ \begin{array}{c} \varepsilon^{(1),t} \\ \varepsilon^{(2),t} \\ \varepsilon^{(3),t} \\ \varepsilon^{(4),t} \\ (24x1) \end{array} \right\} - \left[\begin{array}{c} D_1 \\ (12x6) \end{array} \right] \{ \overline{\varepsilon}^t \}_{(6x1)} \tag{3-25}$$

where $[A_1]$ and $[D_1]$ are given as:

$$[A_1] = \begin{bmatrix} \frac{V^{(1)}}{V^{(A)}} I & 0 & \frac{V^{(2)}}{V^{(A)}} I & 0 & 0 & 0 & 0 & 0 \\ (3x3) & (3x3) & (3x3) & (3x3) & (3x3) & (3x3) & (3x3) & (3x3) \\ 0 & 0 & 0 & 0 & I & 0 & 0 & 0 \\ (3x3) & (3x3) & (3x3) & (3x3) & (3x3) & (3x3) & (3x3) & (3x3) \\ 0 & 0 & 0 & 0 & 0 & 0 & I & 0 \\ (3x3) & (3x3) & (3x3) & (3x3) & (3x3) & (3x3) & (3x3) & (3x3) \\ 0 & V^{(1)}I & 0 & V^{(2)}I & 0 & V^{(3)}I & 0 & V^{(4)}I \\ (3x3) & (3x3) & (3x3) & (3x3) & (3x3) & (3x3) & (3x3) & (3x3) \end{bmatrix} \tag{3-26}$$

$$[D_1] = \begin{bmatrix} I & 0 \\ (3x3) & (3x3) \\ I & 0 \\ (3x3) & (3x3) \\ I & 0 \\ (3x3) & (3x3) \\ 0 & I \\ (3x3) & (3x3) \end{bmatrix} \tag{3-27}$$

R_{Disp} is the residual vector arising from the strain compatibility conditions in the

linearized micromechanical relations. In the case of linear elastic responses are

considered for all sub-cells, the vector R_{Disp} is automatically reduced to zero. The second

set of equations is formed based on the traction continuity relations. Up to this stage, the

components of effective stress tensor $\bar{\sigma}_{ij}^t$ remain unknown, thus, rearranging Eqs. (3-19) - (3-24) should avoid the presence of $\bar{\sigma}_{ij}^t$. The equations based on the traction continuity relations within sub-cells are:

$$\{ \underset{(12x1)}{R_{Trac}} \} = [\underset{(12x24)}{A_2}] \begin{Bmatrix} \varepsilon^{(1)} \\ \varepsilon^{(2)} \\ \varepsilon^{(3)} \\ \varepsilon^{(4)} \end{Bmatrix}_{(24x1)} - [\underset{(12x6)}{O}] \{ \underset{(6x1)}{\bar{\varepsilon}} \}$$
(3-28)

where A_2 is given as:

$$A_2 = \begin{bmatrix} \underset{(3x3)}{-C_{ax}^{(1)}} & \underset{(3x3)}{0} & \underset{(3x3)}{C_{ax}^{(2)}} & \underset{(3x3)}{0} & \underset{(3x3)}{0} & \underset{(3x3)}{0} & \underset{(3x3)}{0} & \underset{(3x3)}{0} \\ \underset{(3x3)}{0} & \underset{(3x3)}{-C_{sh}^{(1)}} & \underset{(3x3)}{0} & \underset{(3x3)}{-C_{sh}^{(1)}} & \underset{(3x3)}{0} & \underset{(3x3)}{0} & \underset{(3x3)}{0} & \underset{(3x3)}{0} \\ \underset{(3x3)}{0} & \underset{(3x3)}{-C_{sh}^{(1)}} & \underset{(3x3)}{0} & \underset{(3x3)}{0} & \underset{(3x3)}{0} & \underset{(3x3)}{C_{sh}^{(3)}} & \underset{(3x3)}{0} & \underset{(3x3)}{0} \\ \underset{(3x3)}{0} & \underset{(3x3)}{-C_{sh}^{(1)}} & \underset{(3x3)}{0} & \underset{(3x3)}{0} & \underset{(3x3)}{0} & \underset{(3x3)}{0} & \underset{(3x3)}{0} & \underset{(3x3)}{C_{sh}^{(4)}} \end{bmatrix}$$
(3-29)

$C_{ax}^{(\alpha)}$ and $C_{sh}^{(\alpha)}$ are the (3 x 3) matrices for sub-cell ,and defined as:

$$C_{ax} = \begin{bmatrix} C_{1111} & C_{1122} & C_{1133} \\ C_{2211} & C_{2222} & C_{2233} \\ C_{3311} & C_{3322} & C_{3333} \end{bmatrix} \quad C_{sh} = \begin{bmatrix} C_{1212} & 0 & 0 \\ 0 & C_{1212} & 0 \\ 0 & 0 & C_{1212} \end{bmatrix}$$
(3-30)

The residual vector R_{Trac} arising from the traction continuity relations, which once again for linear elastic constituents, its components are zero. The matrix O is the zero matrix.

The $\mathbf{B}^{(\alpha),t}$ matrices in Eq. (3-6) are then formed using Eqs. (3-25) and (3-28), which in linearized relations are:

$$
\begin{bmatrix} \mathbf{B}^{(1)} \\ \mathbf{B}^{(2)} \\ \mathbf{B}^{(3)} \\ \mathbf{B}^{(4)} \end{bmatrix}_{(24x6)} = \begin{bmatrix} \mathbf{A}_1 \\ \mathbf{A}_2 \end{bmatrix}^{-1}_{(24x24)} \begin{bmatrix} \mathbf{D}_1 \\ \mathbf{O} \end{bmatrix}_{(24x6)} \tag{3-31}
$$

Once the $\mathbf{B}^{(a)}$ matrices are determined, the effective homogenized stresses and stiffness

matrix can be solved using Eqs.(3-9) and (3-10), respectively.

3.2 Stress Correction Algorithm

The linearized micromechanical relations are satisfied only when all sub-cells

exhibit linear elastic responses. Due to the nonlinear and time-dependent response in the

matrix sub-cells, the linearized micromechanical relations will usually violate the

constitutive equations or the nonlinear constitutive relations will violate the traction and

displacement continuity conditions. The iterative corrector scheme is formulated to

minimize errors from the linearization such that both the micromechanical constraints

and the nonlinear time dependent constitutive equations are satisfied. Otherwise, very

small time step is required to better approximate the nonlinear and time-dependent

responses. Moreover, keeping small time increments is computationally expensive.

Due to the nonlinear and time-dependent responses in the constituents, the

solutions for the deformation fields are performed incrementally. The incremental forms

of the effective stress and strain tensor at the current time are $\bar{\sigma}_{ij}^{t} = \bar{\sigma}_{ij}^{t-\Delta t} + \Delta\bar{\sigma}_{ij}^{t}$ and

$\bar{\varepsilon}_{ij}^{t} = \bar{\varepsilon}_{ij}^{t-\Delta t} + \Delta\bar{\varepsilon}_{ij}^{t}$, respectively. The incremental forms are also used for the stress- and

strain in each sub-cells (Chapter II). The linearized micromechanical relations in Eqs.(3-

12)-(3-24) are used to define trial stresses and strains for each sub-cell at the beginning

of time increment (backward Euler method). The nonlinear stress–strain relations and

time dependent responses in one or more of the sub-cells result in nonzero residual

vectors when the traction continuity and displacement compatibility at the inter-phase

are imposed. To minimize the residual vectors, the local stress–strain components in

each sub-cell need to be corrected. Since the stress and strain in each sub-cell are related

through the constitutive relations, the correction is performed only for 24 independent

variables. The Newton–Raphson (NR) typed iterative method is used to minimize the

residual. In this study, the components of strains in each sub-cell $\varepsilon_{ij}^{(\alpha),t} = \varepsilon_{ij}^{(\alpha),t-\Delta t} + \Delta\varepsilon_{ij}^{(\alpha),t}$

are chosen as independent variables, which are

$$\mathbf{X}^{T} = \left\{ \boldsymbol{\varepsilon}^{(1),t} \quad \boldsymbol{\varepsilon}^{(2),t} \quad \boldsymbol{\varepsilon}^{(3),t} \quad \boldsymbol{\varepsilon}^{(4),t} \right\}_{(1x24)} \tag{3-32}$$

The stress components in the sub-cells are defined as functions of the independent

variables X_{ij}. The residual vector $\mathbf{R}$ is then defined using both Eqs. (3-25) and (3-28).

These residuals are used to correct for the trial solution. This requires defining the

Jacobian tensor, which are given in Eq. (3-33).

$$\frac{\partial R_{ij}}{\partial X_{kl}} = \begin{bmatrix} C_{ax}^{(1)} & 0 & -C_{ax}^{(2)} & 0 & 0 & 0 & 0 & 0 \\ 0 & C_{sh}^{(1)} & 0 & C_{sh}^{(2)} & 0 & 0 & 0 & 0 \\ 0 & C_{sh}^{(1)} & 0 & 0 & 0 & -C_{sh}^{(3)} & 0 & 0 \\ 0 & C_{sh}^{(1)} & 0 & 0 & 0 & 0 & 0 & -C_{sh}^{(4)} \\ f_1 I & 0 & f_2 I & 0 & 0 & 0 & 0 & 0 \\ 0 & 0 & 0 & 0 & I & 0 & 0 & 0 \\ 0 & 0 & 0 & 0 & 0 & 0 & I & 0 \\ 0 & V^{(1)} I & 0 & V^{(2)} I & 0 & V^{(3)} I & 0 & V^{(4)} I \end{bmatrix}_{(24 \times 24)} \tag{3-33}$$

$$f_1 = \frac{V^{(1)}}{V^{(1)} + V^{(2)}}, \qquad f_2 = \frac{V^{(2)}}{V^{(1)} + V^{(2)}} \tag{3-34}$$

where I and O are the 3x3 identity and zero matrices, respectively. A converged solution

is achieved when all residual vectors R_{Disp} and R_{Trac} defined for the micromechanical

model and for the time-dependent and inelastic constitutive equations are diminished.

The calculation of $\bar{\sigma}_{ij}^{t,(m)}$ and $\bar{C}_{ijkl}^{t,(m)}$ is summarized in Eq. (3-35).

1. Input variables : $\Delta\bar{\varepsilon}_{ij}^{t,(m)}$; $\Delta t^{(m)}$; $\bar{\sigma}_{ij}^{t-\Delta t}$; $\bar{\varepsilon}_{ij}^{t-\Delta t}$; $Hist^{t-\Delta t}$

   (m=global iteration counter)

   Calculate : $\bar{\varepsilon}_{ij}^{t,(m)} = \bar{\varepsilon}_{ij}^{t-\Delta t} + \Delta\bar{\varepsilon}_{ij}^{t,(m)}$

2. Initial approximation variables:

$$B_{ijkl}^{(\alpha),t,tr} = B_{ijkl}^{(\alpha),t,tr}(\bar{\sigma}_{ij}^{t-\Delta t}; \quad Hist^{t-\Delta t}), \quad \alpha=1,2,3,4$$

$$\varepsilon_{ij}^{(\alpha),t,tr} = B_{ijkl}^{(\alpha),t,tr}\bar{\varepsilon}_{kl}^{t,(m)}, \quad \Delta\sigma_{ij}^{(\alpha),t,tr} = C_{ijkl}^{(\alpha),t,0}\Delta\varepsilon_{kl}^{(\alpha),t,tr}$$

$$\varepsilon_{ij}^{(\alpha),t,tr} = \varepsilon_{ij}^{(\alpha),t-\Delta t} + \varepsilon_{ij}^{(\alpha),t,tr}$$

3. Iterate for k = 1,2,3. . . (k = local iteration counter)

   Calculate : $C_{ijkl}^{(\alpha),t,(k)} = C_{ijkl}^{(\alpha),t,(k)}(\sigma_{ij}^{(\alpha),t,(k)})$, $\qquad\qquad\qquad\qquad$ (3-35)

$$B_{ijkl}^{(\alpha),t,(k)} = B_{ijkl}^{(\alpha),t,(k)}(\sigma_{ij}^{(\alpha),t,(k)})$$

   Define : $X_{ij}^{t,(k+1)} = X_{ij}^{t,(k)} + \left[\dfrac{\partial R_{ij}^{t,(k)}}{\partial X_{kl}}\right]^{-1}R_{kl}^{t,(k)}$,

   $R_{kl}^{t,(k+1)}, \bar{\sigma}_{kl}^{t,(k+1)}, \bar{C}_{kl}^{t,(k+1)}$

   using Eqs. (3-25), (3-28),(3-9), and (3-10)

   IF $\left\|R_{ij}^{t,(k+1)}\right\| \le Tol$ THEN GOTO 4 and EXIT

   ENDIF GOTO 3

4. Update: $\quad \bar{\sigma}_{ij}^{t,(m)} \leftarrow \bar{\sigma}_{ij}^{t,(k+1)}, \quad \bar{C}_{ijkl}^{t,(m)} \leftarrow \bar{C}_{ijkl}^{t,(k+1)}, \quad Hist^{t}$

At each structural (global) iteration within an incremental time-step $\Delta t^{(m)}$, trial

incremental components of effective strain tensor $\Delta\bar{\varepsilon}_{ij}^{t,(m)}$ are obtained from the FE

structural level. The superscript (m) denotes global iteration counter within the current

incremental time step. The goal is to calculate current total effective stresses $\overline{\sigma}_{ij}^{t,(m)}$ and

effective consistent tangent stiffness $\overline{C}_{ijkl}^{t,(m)}$ from given state variables and history

variables stored from the previous converged solution at time (t- Δt). The history

variables result from solving the time-dependent integral form and inelastic constitutive

relation in the polymeric sub-cells in a recursive-iterative manner. The converged $\overline{C}_{ijkl}^{t,(m)}$

after M global iteration at the current time t will be used to provide incremental trial

strains for the next time step (t+Δt).

3.3. Concurrent time-integration algorithm

The time-integration algorithm within the linearized micromechanical and

corrector scheme, which is compatible with a displacement based FE framework, is

described as follows. The concurrent time-integration is required to link the time-

dependent and inelastic material behavior of the matrix constituent to the viscoelastic-

viscoplastic responses at the structural level and determine stress-strain fields in the

constituents due to a prescribed boundary condition at the structural level. At the FE

structural level, an iterative solution is performed for the nonlinear analyses. This study

uses ABAQUS FE code (2005) solver. Two criteria are checked in the ABAQUS

iterative linear solver, which are force residual and displacement correction. The force

residual vector is defined by:

$$\mathbf{R}_\mathbf{F}^\mathbf{t} = \mathbf{P}^\mathbf{t} - \mathbf{K}^\mathbf{t}\mathbf{u}^\mathbf{t} = \mathbf{0} \tag{3-36}$$

To achieve an equilibrium state, the external force $\mathbf{P}$ and internal force $\mathbf{Ku}$ must be equal

at every time t; where $\mathbf{K}$ is the stiffness matrix of the structure and $\mathbf{u}$ is the displacement

solution at time t. In a nonlinear problem, $\mathbf{R_F}$ will only be approximating to zero. The

displacement residual is:

$$R_\delta^t = \frac{\left\|\delta\Delta\mathbf{u}^t\right\|}{\left\|\Delta\mathbf{u}^t\right\|} \tag{3-37}$$

The residuals in Eqs. (3-36) and (3-37) are monitored at the structural level at

each time increment. The goal is to achieve global (structural), micromechanical

(material), and constituent (viscoelastic-viscoplastic matrix) convergence simultaneously.

Thus, an efficient and accurate numerical algorithm for solving the constitutive material

model becomes necessary. The concurrent micromechanical model allows providing

composite effective properties from the properties of individual constituents and

simultaneously recognizing responses of the individual constituents from the composite

responses. The proposed micromechanical model can be easily coupled with different

constitutive material models, which is suitable for integration within a multi-scale

material framework. The iterative correction scheme for the micromechanical

formulation is summarized in Fig. 3-3. Input to this algorithm is the effective incremental

strain, previous converged effective stress and history variables. The output is the current

effective stress, consistent tangent stiffness matrix and updated history variables.
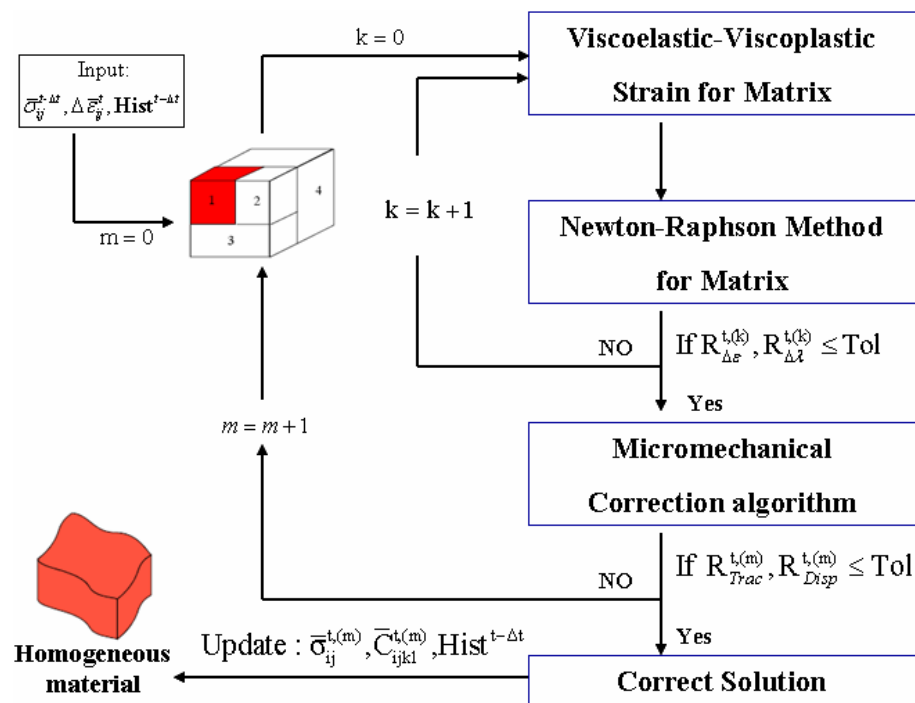
Figure 3-3. Summary of homogenization of particle reinforced composite for viscoelatic-viscoplastic responses (m=micromechanical model iteration counter, k=constituent iteration counter)

3.4 Numerical implementation and verification

The capability of the proposed micromechanical model in predicting effective

elastic, viscoelastic, and viscoplastic behaviors is presented. The proposed

micromechanical model is implemented in a 3D continuum element using a material

subroutine of ABAQUS FE code. Available analytical and experimental works in the

literature on elastic, viscoelastic and viscoplastic responses of solid spherical particle

reinforced composites are used for comparisons. Micromechanical models of Dvorak

and Srinivas (1999), Mori and Tanaka (1973), Differential scheme, and Self consistent

method are also used to verify the effective elastic properties calculated using the

proposed micromechanical model. The calculated linear and nonlinear elastic responses

of particle composites are compared with experimental data of Biwa et al. (2001) and

Cho et al. (2006). The capability of the micromechanical model in predicting nonlinear

viscoelastic responses is verified with the micromechanical and FE models reported by

Levesque et al. (2004) and creep data of Aniskevich and Hristova (2000). The effective

viscoplastic responses are verified with analytical solutions and micromechanical model

of Pierard et al. (2004). Convergence behaviors at the macrostructural (global),

microstructural, and constituent levels are also examined during the nonlinear analyses.

3.4.1. Elastic responses

The effective linear elastic properties of composites with several particle volume

fractions (0–100%) generated using the proposed micromechanical model are first

compared with micromechanical models of Dvorak and Srinivas (1999), Mori and

Tanaka (1973), self consistent model, and differential scheme. In this case, the composite

systems made of silicate carbide particle embedded in the aluminum matrix are used.

Both particle and matrix are modeled as isotropic linear elastic. The in situ material

properties are obtained from Eroshkin and Tsukrov (1995), which are given in Table 3-1.

Figure 3-4 presents effective shear and bulk moduli for several composite volume

fractions. The effective properties calculated from the proposed micromechanical model

are comparable with other micromechanical models.

Table 3-1

Elastic properties of silicon carbide particle and aluminum matrix (Eroshkin and Tsukrov, 1995)

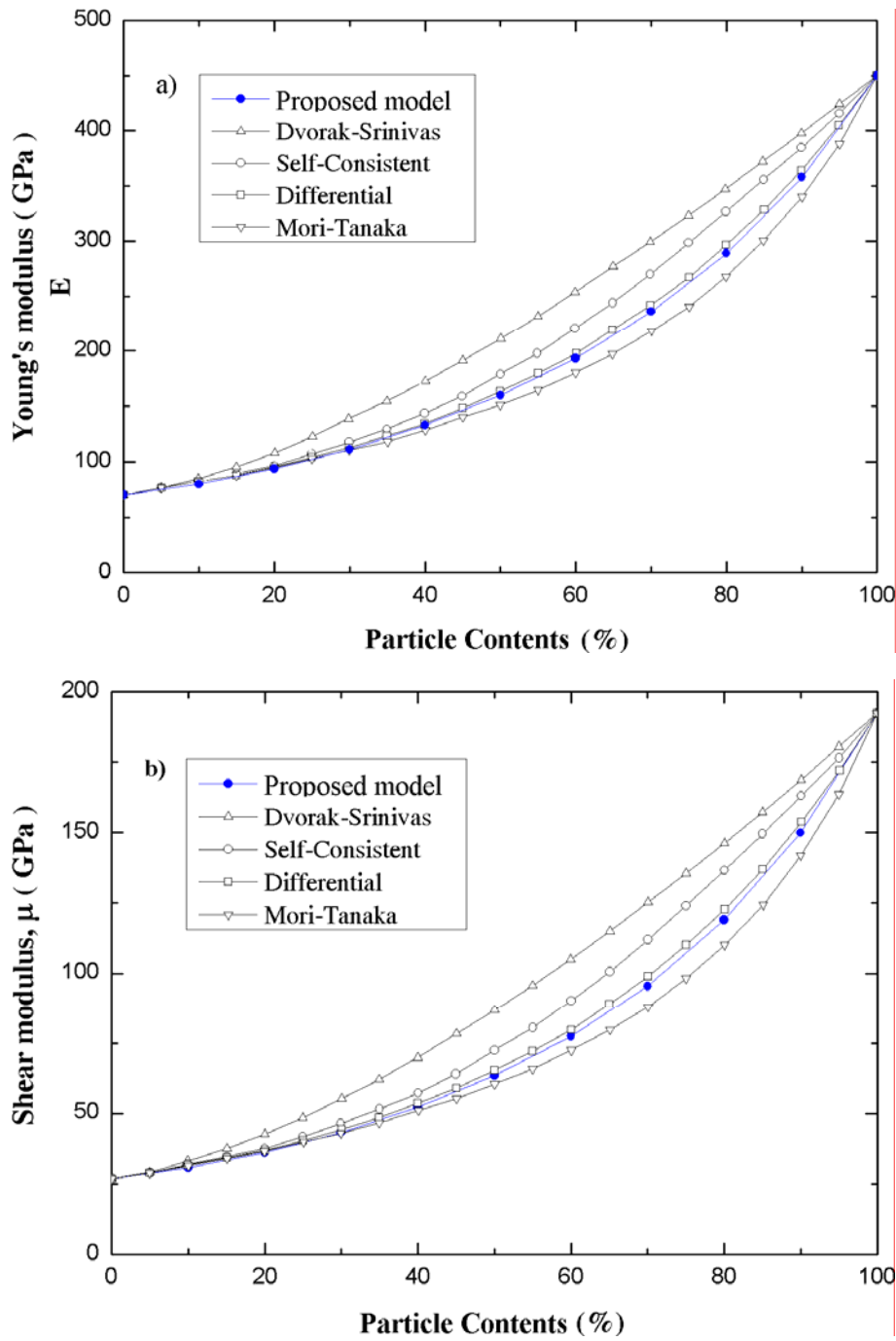| Constituents	E(MPa)	ν
Silicon carbide	450000	0.17
Aluminum	70000	0.30

Figure 3-4. Effective composite (a) Young's and (b) Shear moduli with various Vf.

Figure 3-5 shows comparisons of elastic moduli for 21.6%, 37.2%, and 52.4%

volume contents of rubber particle-toughened PMMA composite. The constituent

properties are obtained from Biwa et al. (2001), which are given in Table 3-2. The

effective Young's, shear, and bulk moduli for several composite volume fractions

obtained from the proposed micromechanical model are comparable with the

experimental data.

Table 3-2

Elastic properties of rubber-toughened PMMA composite (Biwa et al. 2001)

Constituents	Bulk moduli K(GPA)	Shear moduli G(GPa)
Rubber particle	2.71	0.56
PMMA (poly methyl methacrylate)	5.91	2.25
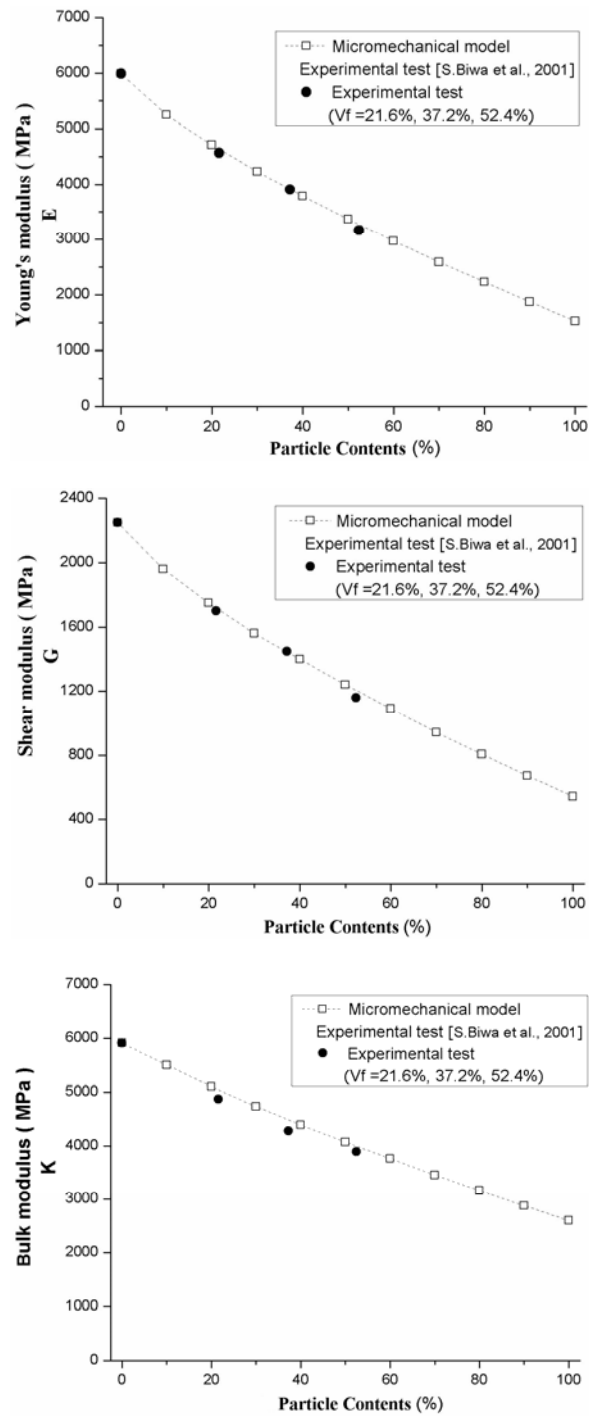
Figure 3-5. Effective composite (a) Young's (b) shear and (c) bulk moduli with different Vf

Next, the linear and nonlinear elastic responses of composite are compared with available experimental data of Cho et al. (2006). The composites consisted of micro size glass beads having volume fraction of 5%. The tested samples have particle diameter vary from 6 μm to 500 μm. The elastic properties for glass and vinylester resin are shown in Table 3-3. Based on the experimental data of unreinforced vinylester resin, the nonlinear stress dependent elastic modulus is modeled using parameter g_0 in Eqs. (2-3) and (2-4), which is fitted using power law function $g_0 = 1 + C\sigma^n$. The coefficient C and power n are calibrated by fitting the uniaxial stress–strain function $\varepsilon = (1 + C\sigma^n)\sigma / E$ with the experimental responses. The calibrated nonlinear parameters for vinylester resin are given in Table 3-3. Table 3-4 shows comparisons of effective initial Young's moduli obtained from the experiment and proposed micromechanical model. The modulus calculated using the proposed micromechanical model is in good agreement with the ones from the experiment with less than 1% error. The effective nonlinear responses for the 5% composite volume fraction are then given in Fig. 3-6. Good prediction is shown by the proposed micromechanical model. It is seen that the effect of particle's size on the linear elastic modulus of the composite is insignificant.

Table 3-3

Elastic properties of glass beads and vinylester resin (Cho et al., 2006)

Constituents	E(MPa)	ν	C	n
Glass bead	10500	0.25		
Vinyester	600	0.30	0.00029	1.603

Table 3-4

Effective composite's Young's moduli with vf = 5%

Constituents	Experiment	Micromodel
$\bar{E}/E_{resin}$	1.067	1.073
% error		0.6
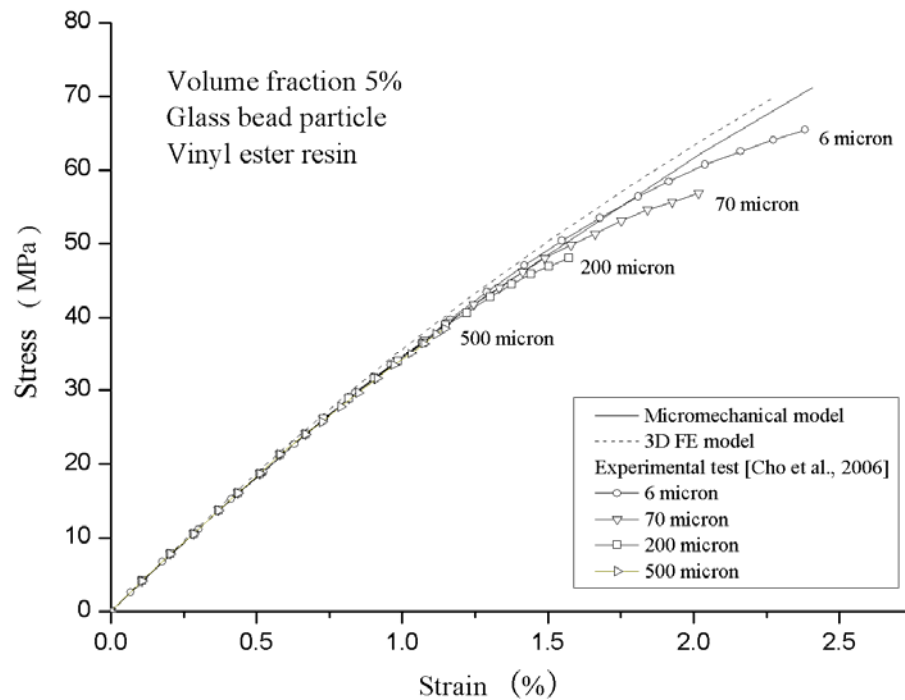
Figure 3-6. Nonlinear stress-strain relations for glass/vinylester composites (VF=5%)

Figures 3-7(a–c) illustrate multi-level residual norm, in a logarithmic scale, for the

nonlinear elastic analyses of the glass/vinylester composite at two stress levels: 40 and

70 MPa. The analysis is performed with the maximum relative incremental time of 0.29,

which is comparable to incremental stress of 20 MPa. As expected, more iterations are

required to minimize the residual at the higher stress level. The convergence behaviors at

the micro level, shown in Fig. 3-7 (b), are reported during the last iteration of the

structural (macro) level, which are iteration numbers 2 and 3 for the stress levels 40 and

70 MPa, respectively. Similarly, the convergence behaviors at the constituent level given

in Fig. 3-7 (c) are shown for the last converged step at the micro level. The residual is

reported from the matrix sub-cell number 2. It is seen that the correction algorithms are

required to minimize residuals at each level. Otherwise, the large residual strains (nearly

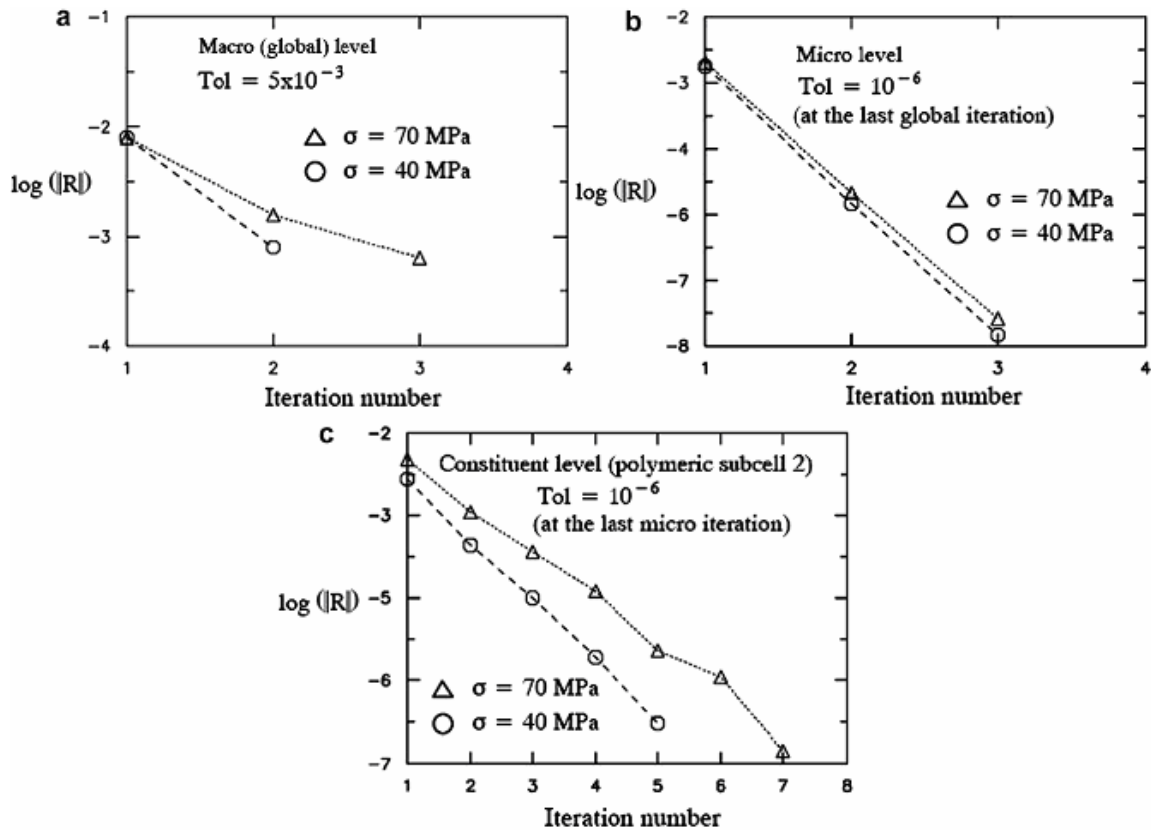1000 micro strain) may cause solutions at the upper level to diverge.

Figure 3-7. Multi-level convergence behaviors at two stresses during the nonlinear analyses of glass/vinylester composites (vf = 5%): a) macro b) micro c) constituent (polymer) levels

The effective elastic properties calculated from the simplified micromechanical

model are also compared with the ones obtained from FE analyses of the detailed RVEs.

Two composite's RVEs, shown in Fig. 3-8, are considered. FE meshes of the cubic

RVEs having spherical inclusions are generated using 3D continuum elements (C3D20),

which are also shown in Fig. 3-8. The first RVE contains only one particle. The second

RVE contains a total of two particles, one particle is placed in the middle and a total of

eight one-eight particles are placed at the corners of the cubic RVE.
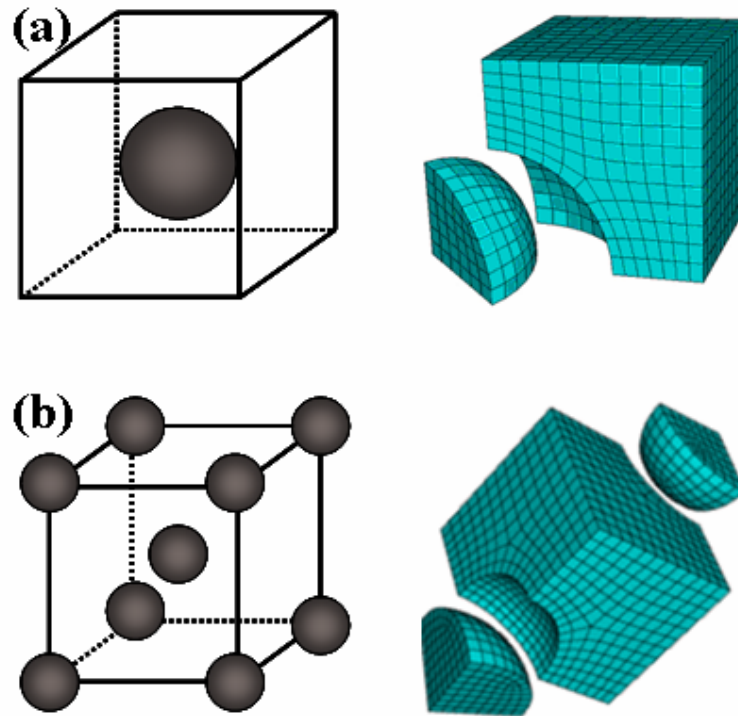

Figure 3-8. Representative cubic volume elements with (a) single inclusion and (b) multiple inclusions. Detailed FE meshes are generated for both RVEs. Symmetric boundary conditions are imposed on the three symmetry planes

The elastic properties of glass particle and polystyrene matrix are given as E_p=70

GPa, ν_p=0.25, E_m=3.5 GPa, and ν_m=0.35. Figure 3-9 shows Young's modulus, shear

modulus, and Poisson's ratio determined using FE models of RVEs with one and two

particles, and the proposed micromechanical model for different particle volume fraction.

The effective elastic properties calculated from the proposed micromechanical model are

comparable to the ones obtained from the detailed FE RVE model with two particles. In

both RVE models, the effective properties characterized from the far field variables and

the ones calculated based on the total strain energy of the RVEs are reported. Except for

the Poisson's ration, the elastic moduli of the proposed micromechanical model lie

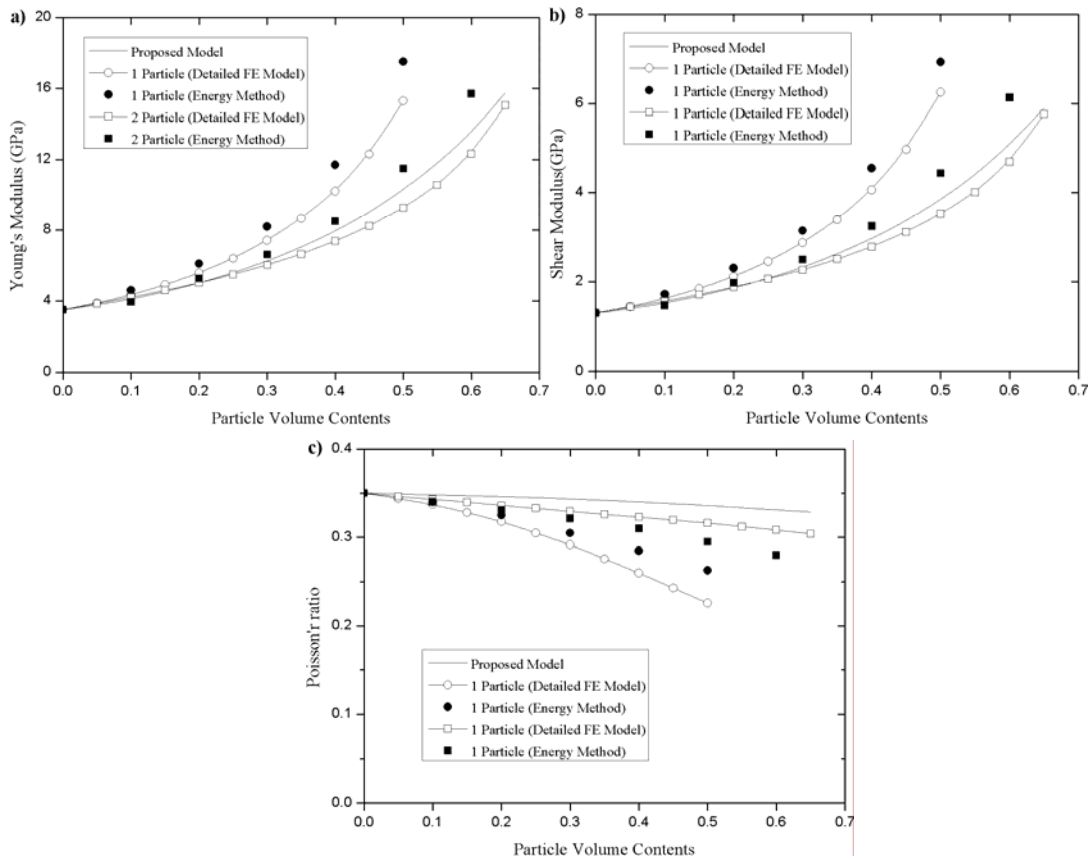between the two values in the RVE with two particles.

Figure 3-9. Effective composite elastic properties with various volume fractions

At fixed particle volume contents, the particle's diameter of the RVE with one particle is larger than the particle's diameter of the RVE having two particles. The unit cell model with two particles can result in higher localized stress and strain distribution due to the inter particle interaction in the matrix region. When the particle sizes are larger or when the volume content of particle increases, the effect of contact between particles on the overall responses of composites become more pronounced. These effects can lead to different values of the mechanical properties, as illustrated in Fig 3-9. In addition, the effects of micro-structural arrangement on the overall behaviors of composites are more significant at higher particle contents. Böhm (2008) reported the effective elastic properties of fiber and particle reinforced composites. The effective elastic properties of unidirectional fiber composites along the fiber axis seem to be independenton the size and arrangement of the fiber in the composites. However, in the transverse fiber direction the size and arrangementof fiber can significantly affect the effective properties especially for higher fiber content. For the particle reinforced composites, the effective elastic properties are strongly dependent on the particle arrangements, especially for a relatively high particle contents. The maximum volume content of the RVE with one particle that can be generated is about 50%. At this volume

content, the particles are in contact with the neighboring particles. For composites with

smaller particle size, higher volume contents can be generated in the RVE with two

particles, i.e., 65%. In addition, nonlinear elastic response of glass/vinylester composites

are also compared to the one generated using the detailed FE model with two particles as

seen in Fig. 3-6.

3.4.2 Viscoelastic behaviors

The accuracy of the proposed micromechanical model for predicting effective

viscoelastic responses is also examined using the micromechanical and FE models

reported by Levesque et al. (2004) and experimental tests conducted by Aniskevich and

Hristova (2000). Levesque et al. (2004) developed a micromechanical model for

analyzing nonlinear viscoelastic responses of glass particles embedded in the

polypropylene matrix. The nonlinear viscoelastic behavior, which follows the Schapery

integral model, is attributed to the matrix constituent and the particle is assumed to be

linear elastic. Table 3-5 gives the in situ linear elastic properties. The time-dependent

material parameters expressed in terms of Prony series function are given in Table 3-6.

The reported nonlinear stress-dependent parameters for the polypropylene matrix are:

$$g_0 = 1 + 9.19 \times 10^{-4} \times (\bar{\sigma}^t - 2.5)^2 H(\bar{\sigma}^t - 2.5)$$
$$g_0 = 1 + 1.03 \times 10^{-3} \times (\bar{\sigma}^t - 15)^2 H(\bar{\sigma}^t - 15)$$
$$g_0 = 1 + 7.92 \times 10^{-3} \times (\bar{\sigma}^t)^2$$
$$a = 1.$$

(3-38)

where H is the Heaviside unit step function.

Table 3-5

Elastic properties of glass particle and polypropylene matrix (Levesque et al., 2004)

Constituents	E(MPa)	ν
Glass	69000	0.3
Polypropylene	2020	0.3

Table 3-6

Pony parameter for polypropylene matrix (Levesque et al., 2004)

N	$\lambda_n(s^{-1})$	$D_n \times 10^{-5}$ (MPa^{-1})
1	0.32	7.971
2	0.032	3.678
3	0.01	2.896
4	0.0032	7.142
5	0.0016	3.076

Both the analytical and detailed FE models of Levesque et al. (2004) are used to

verify the responses from the proposed micromechanical model. Figure 3-10 illustrates

the effective stress–strain responses for composites with particle volume fractions: 10–

30% under a constant loading rate. The results from the proposed micromechanical

model agree very well with the analytical and detailed FE models. The convergence

criteria used for the structural, micromechanical, and constituent levels are similar to the

ones used for the nonlinear elastic analyses, as described above. In this case, equilibrium

at the structural scale for all stress levels and volume fractions is achieved immediately

without performing any iteration. This is perhaps due to a relatively low stress level and

an efficient stress correction algorithm at the micromechanical level. Convergence

behavior at the micro level for composite with volume fraction 10% is given in Fig. 3-11.

The residuals are reported for two stress levels: 10 and 20 MPa. It is concluded that the

effectiveness and accuracy of the correction algorithm at the micro level help

accelerating structural convergence. Figure 3-12 compares the effective composite

behaviors under several loading rates generated using the micromechanical model and

the FE model. A composite system with 20% particle volume fraction is used.

Convergence problem at the macro level has occurred during the analyses at high stress

and loading rate. It should be noted that all the analyses are performed without

tightening incremental time or modifying tolerance and the default convergence criteria

in ABAQUS are used. This leads to large time increments with very tight convergence

criteria, which potentially causes divergence in the nonlinear analyses. To overcome the

divergence, several numerical treatments can be done such as: reducing time increments,

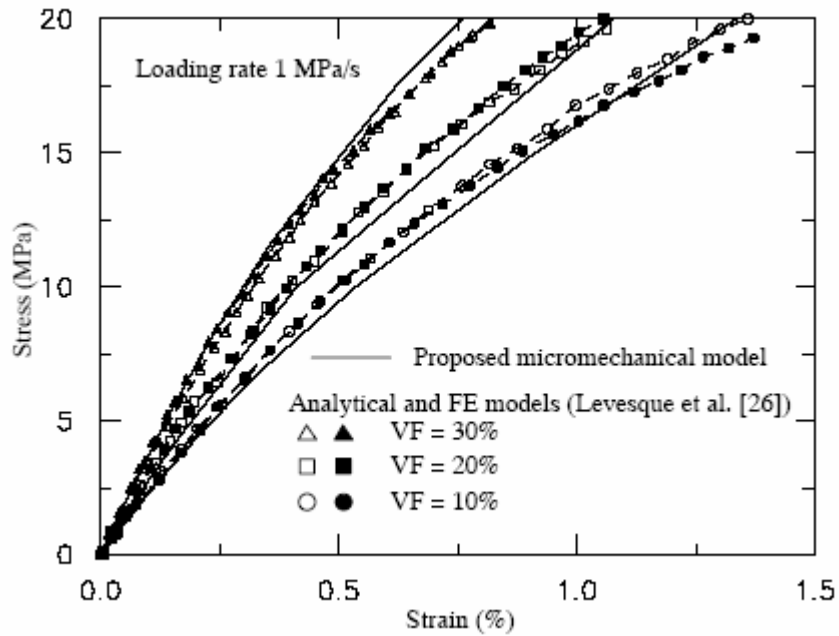adding more iteration, relaxing tolerance, using different numerical solver, and so on.

Figure 3-10. Nonlinear stress–strain relations for various glass particle Vf
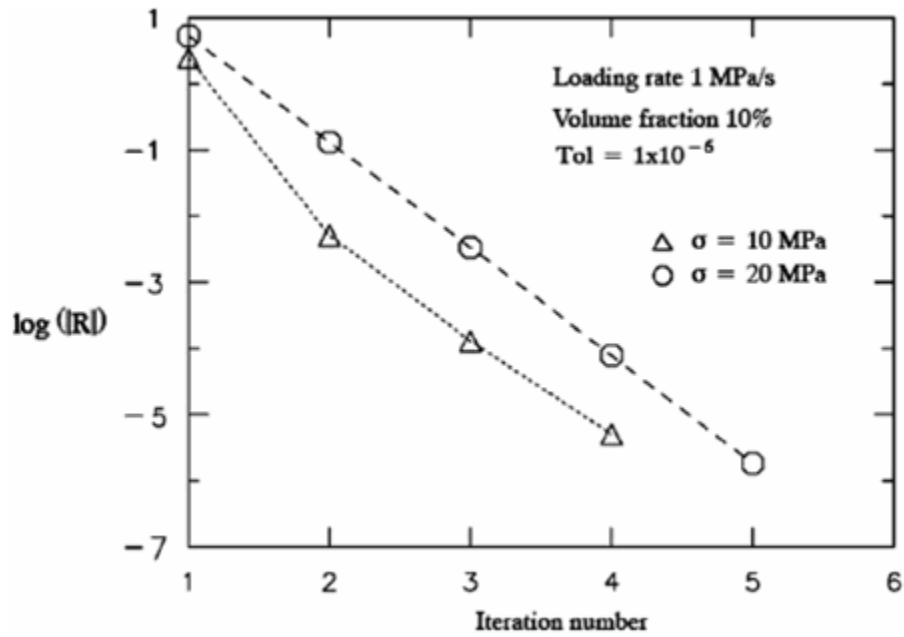
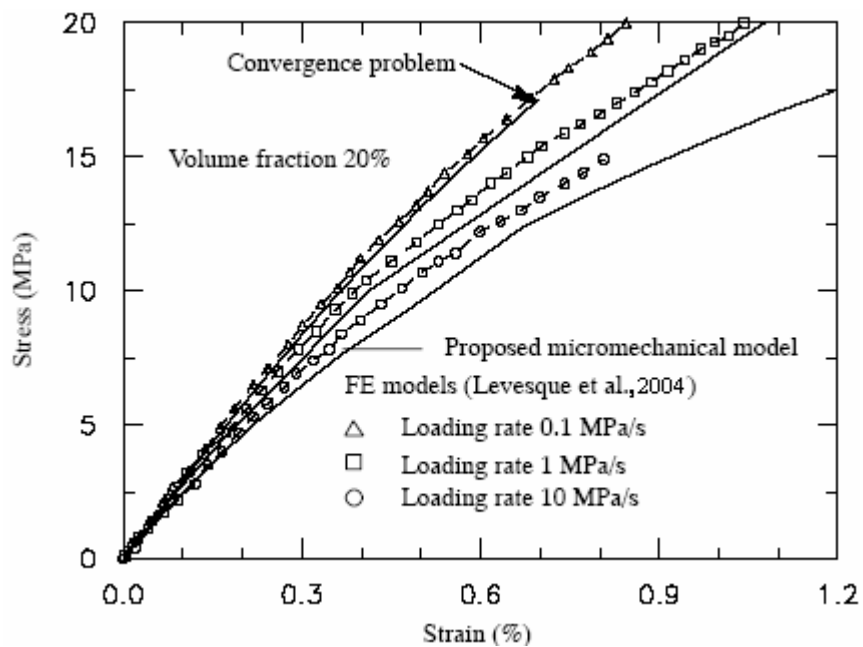Figure 3-11. Residual error at the micro level during the analyses in Fig. 3-9

Figure 3-12. Effect of loading rate on nonlinear stress–strain relations

Next, the long term creep data (4.1 months) on polyester resin reinforced with

diabase and marble spherical particles, reported by Aniskevich and Hristova (2000), are

also used to validate the proposed micromechanical model. The diabase and marble

reinforcements are made of linear elastic materials and the polyester resin follows a

linear viscoelastic response. The linear elastic properties of the constituents are given in

Table 3-7.

Table 3-7
Elastic properties of diabase and marble particles and polyester resin (Aniskevich and
Hristova, 2000)

Constituents	E(MPa)	ν
Glass	8800	0.26
Marble	440000	0.25
Polyester	5800	0.35

Table 3-8

Effective Young's moduli for diabase/polyester and marble/polyester systems

Composites	Effective Young's modulus(MPa)	
	Micromechanical model	Experiment
Diabase/polyester with vf		
0.28-0.08	8200	11000±1000
0.28	9700	
0.28+0.08	11600	
Marble/polyester with vf		
0.28-0.08	8500	9800±1200
0.28	10300	
0.28+0.08	12700	

Table 3-9

Prony parameters for polyester resin

N	$\lambda_n(s^{-1})$	$D_n \times 10^{-5} (MPa^{-1})$
1	1.	4.50
2	10^{-1}	3.00
3	10^{-2}	5.40
4	10^{-3}	7.60
5	10^{-4}	16.0
6	10^{-5}	22.0
7	10^{-6}	25.0

The measured composites' volume fractions were 0.28 ± 0.08, which indicate

large variability. The composites' effective Young's moduli calculated using the

proposed micromechanical model and the ones obtained from the experimental tests is

presented in Table 3-8. It is seen that the micromechanical model with upper bound

volume fraction gives closer prediction of the effective modulus for the

diabase/polyester systems. The modulus for the marble/ polyester system is predicted

with a lower bound volume fraction of 0.2. The linear viscoelastic behavior for the

polymeric resin is then calibrated using the reported creep data of unreinforced polyester

resin, shown in Fig. 3-13. The calibrated Prony parameters are given in Table 3-9.

Finally, micromechanical model predictions of the composite's long-term (4.1 months)

transient compliances are illustrated in Fig. 3-14. The volume fractions of 0.36 and 0.2

are used for diabase/polyester and marble/polyester composites, respectively. Good

agreement with the experimental tests of Aniskevich and Hristova (2000) is shown for

both diabase/polyester and marble/polyester systems. Once again, all the analyses are

performed without controlling incremental time or relaxing tolerance and the default

convergence criteria in ABAQUS are used. In this case, the maximum incremental time

during the analyses is 2000 h. Figure 3-14 also presents the long-term responses of

diabase/polyester from the proposed micromechanical model without iterative correction

scheme at the micro level. It is seen that using only linearized micromechanical relations

lead to significant mismatch in predicting long-term material responses.
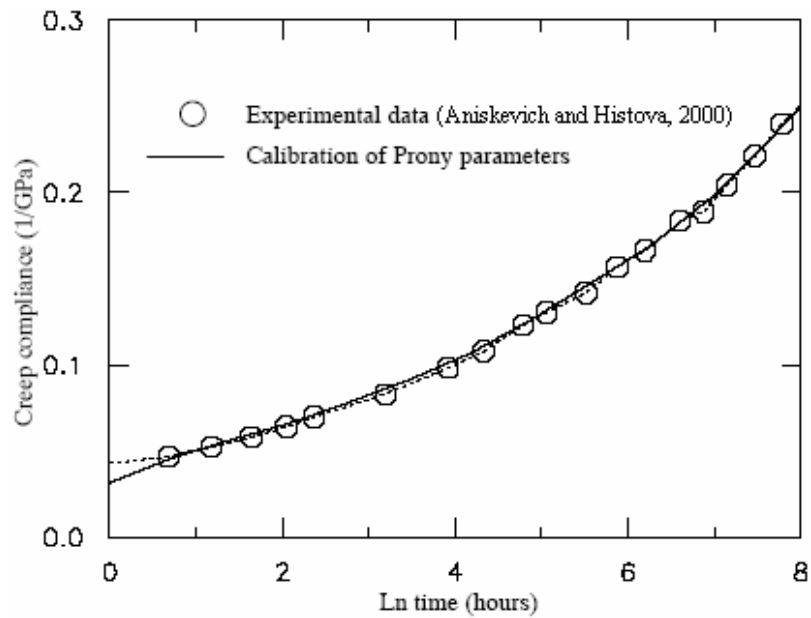

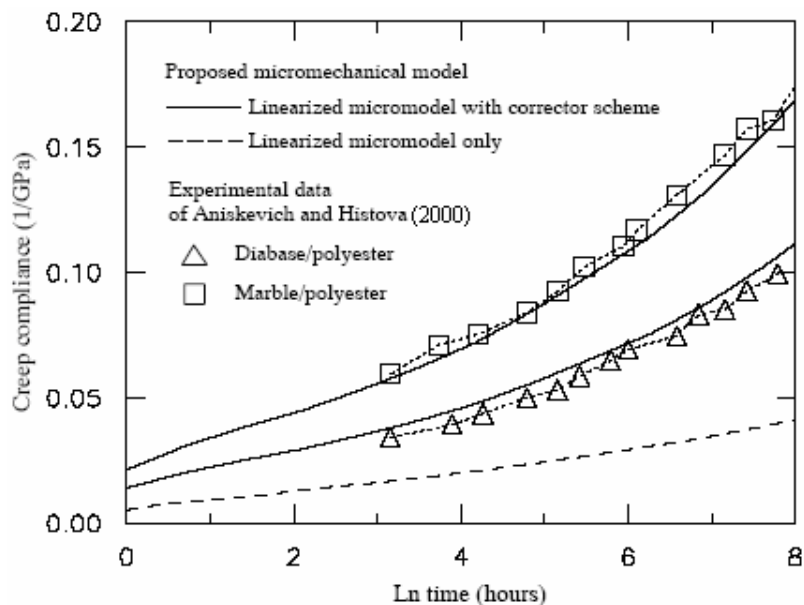Figure 3-13. Long term creep compliance for polyester resin

Figure 3-14. Long term creep compliance for polyester reinforced composites

3.4.3. Viscoplastic behaviors

Experimental data on viscoplastic polymer composites are currently available for

composites with fiber reinforcements. Current studies on viscoplastic behaviors of

particle reinforced composites are mainly done for metal matrix composites. To verify

the proposed micromechanical model in simulating viscoplastic responses, particle

reinforced composites with metal matrix are used. Metal at high temperature exhibits

elastic-viscoplastic behaviors. A viscoplastic micromechanical model of metal matrix

composites, proposed by Pierard et al. (2007) is used for comparison. Both particles and

matrix exhibit viscoplastic responses. The Valanis viscoplastic model is used for the

viscoplastic inclusion and matrix. Uniaxial loadings at a strain rate, $10^{-3} s^{-1}$ is applied to

composites with 30% particle volume fraction. The elastic properties and Valanis's

viscoplastic parameters in Eq. (2-41) and (2-54) are given in Table 3-10. Figure 3-15

presents the stress-strain behaviors for each constituents and composites subject to a

$10^{-3} s^{-1}$ strain rate. The proposed micromechanical model is comparable to the Hill, and

Eshelby models, and the affine homogenization model of Pierard et al. (2007).

Table 3-10
Elastic properties viscoplastic properties (Pierard et al., 2007)

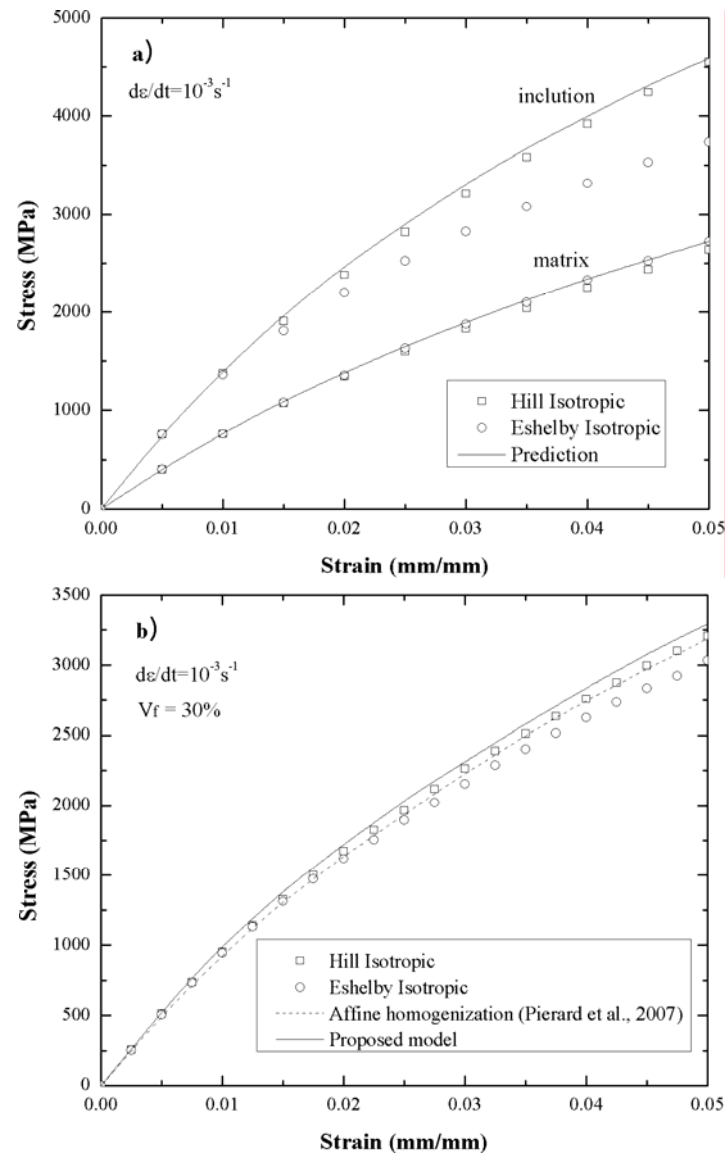| Constituents	E(GPa)	ν	S_y^o	a	b
Particle	400	0.286	7000	0.4	0.00001
Matrix	70	0.33	5000	0.5	0.000015

Figure 3-15. Stress-Strain relation for 10^{-3} strain rate a) matrix and inclusion responses b) composite response of 30% Vf

3.4.4. Viscoelastic-Viscoplastic behaviors

The proposed micromechanical model for the combined viscoelastic-viscoplastic response is examined in terms of its accuracy and efficiency. Experimental data on the

combined viscoelastic-viscoplastic behaviors of particle reinforced composites are

lacking. A FE unit-cell model with two-particles (Fig. 3-8b) that is assumed to closely

represent a microstructure of heterogeneous composite is generated to verify the

viscoelastic-viscoplastic responses of the proposed micromechanical model. Composites

with glass bead particles and HDPE polymer are studied. The glass bead is assumed to

be linear elastic and its mechanical properties are given in Table 3-5. The Schapery-

Perzyna and Schapery-Valanis models are considered. The material properties for the

HDPE are given in section 2.3. FE unit-cell models are generated for composites with

20%, 30% and 50% particle contents. Continuum C3D8R elements are used. Total

numbers of element and node of 20% particle content are 8385 and7168, the 35%

particle content are 9253 and 7936, and the 50% particle content are 11737 and 10206,

respectively. Periodic boundary conditions are imposed to the unit-cell model. Creep-

recovery loading is simulated by applying a constant stress of 10 MPa for 1000 seconds

and removing the load. The numerical algorithm of the combined Schapery-Valanis

model or Shapery-Perzyna model (Chapter II) is used for the matrix elements in the unit-

cell FE model. As expected adding linear elastic particles reduces creep and plastic

strains. Figure 3-16 presents creep-recovery responses for composites with different

particle contents. The responses obtained from the proposed micromechanical model are comparable to the one of the FE unit-cell models. As expected, adding linear elastic particles reduces creep and plastic strains. Figure 3-17 reports the magnitude of the residual in the constituents during the creep-recovery loading of composite with 20% particle volume contents. This is the Frovenios norm of the residual vectors in the matrix constituent. The convergence behaviors at the constituent level are obtained at the time, 0.0045, 1974, and 2449.345 sec. The residuals of the micromechanical model are reported from the matrix sub-cell number 2, which has the highest average local effective stress and initial residual. The residual of the FE unit-cell model is monitored at matrix element number 289, which is in contact with the particle element and has the highest local average stress and residual as illustrated in Fig. 3-17. It is seen that the efficient stress-correction algorithm at the micromechanical model leads to less iteration number at the constituent level, which accelerates the convergence and reduce computational cost.
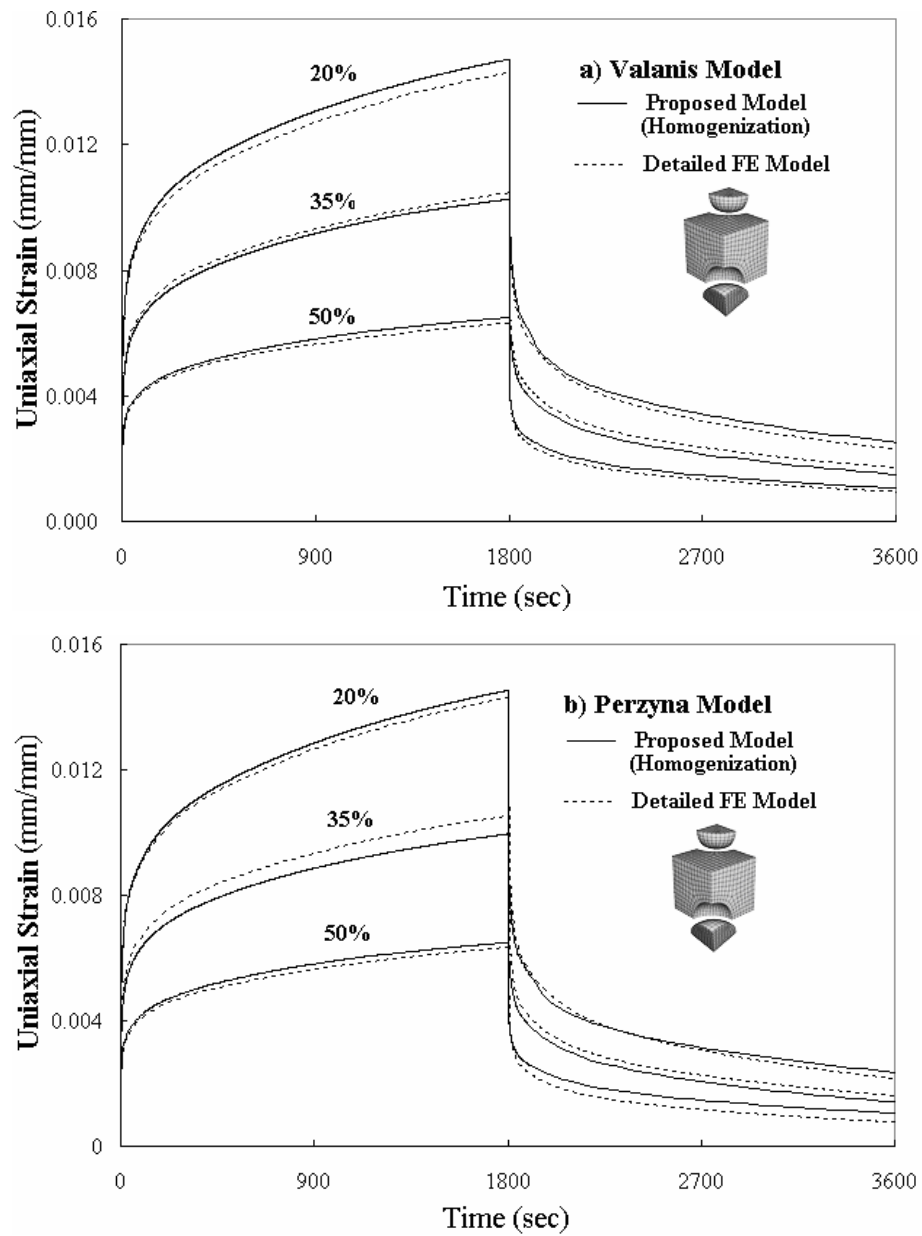
Figure 3-16. Creep recovery responses for different volume fraction, a) Valanis Model b) Perzyna Model
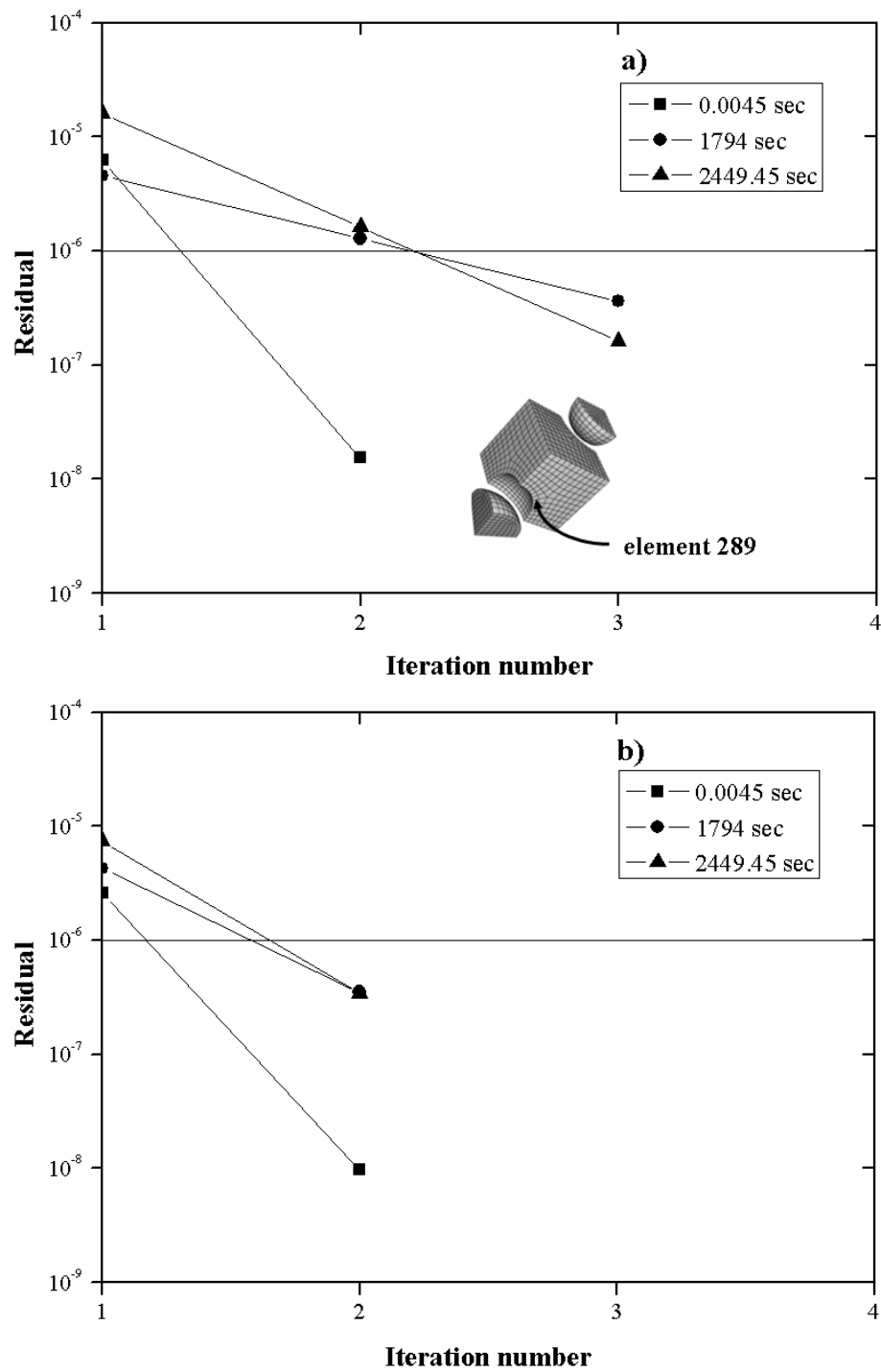
Figure 3-17. Convergence behaviors at three times of glass bead/HDPE composite
(a) Detailed FE unit-cell model (b) Micromechanical model

Large scale nonlinear structural analysis of particle reinforced composites often requires high computing time. In addition, generating FE meshes for composite structures with detailed microstructural characteristics is quite challenging. This study uses the homogenized micromechanical model of particle reinforced composites to analyze the effective viscoelastic and viscoplastic responses of a homogenized composite bar, which can be considered as a relatively large-scale structure. Figure 3-18 illustrates two FE models that represent homogenized composite and heterogeneous composite microstructures. The heterogeneous composite model incorporates detailed particle geometries. We examine the overall response and local field variables of the homogenized and heterogeneous composites. The longitudinal axis of the bar is along the z-axis. The origin of the coordinate is placed on the left side of the bar. The bar has a length, L=1 mm and a square cross-section with a side length, S=0.1 mm. The particles with diameters, 280 μm, are modeled by uniformly placing them in a homogeneous matrix medium. Composites with different particle contents are subjected to a uniaxial creep-recovery loading. The prescribed boundary conditions are given as:

$$
\begin{aligned}
&u_x(0, y, z, t) = 0 \quad u_y(x, 0, z, t) = 0 \quad u_z(x, y, 0, t) = 0 \\
&u_x(S, y, z, t) = \bar{u}_1 \quad u_y(x, S, z, t) = \bar{u}_2 \quad u_z(x, y, L, t) = \bar{u}_3 \\
&\sigma_{zz}(x, y, L, t) = 10 \text{ MPa or } 30 \text{ MPa}
\end{aligned}
\tag{3-40}
$$

The Schapery-Valanis model is used for the HDPE matrix, while the glass particle is linear elastic. The FE model of the homogenized composite consists of ten C3D8R elements while the heterogeneous composite consists of 8960 elements and 11201 nodes. Figure 3-19 shows responses of the composite bars having 20%, 30%, and 50% particle contents subject to a 10 MPa creep-recovery loading. Figure 3-20 shows the creep-recovery responses under 30 MPa. The proposed micromechanical model gives good prediction of the overall viscoelatic-viscoplastic responses. Table 3-11 shows CPU times required for the creep-recovery analyses using the proposed micromechanical model in the homogenized composite bar and the heterogeneous FE models of the composite bar. The heterogeneous composites require higher computing time than the homogenized composite bar.
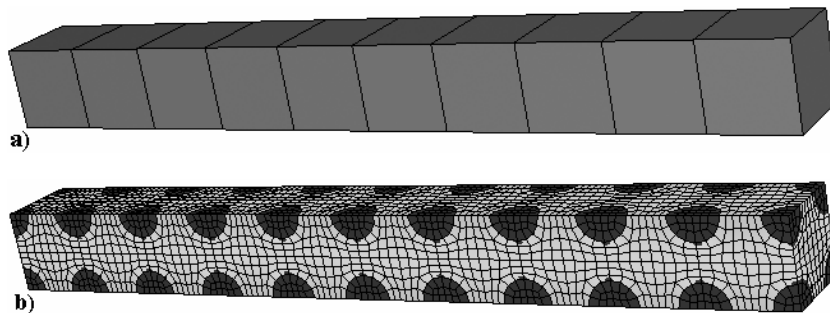

Figure 3-18. FE meshes of a) homogenized composite bar (#element=10, # node=44) and b) heterogeneous composite bar (# element=8960, # node=11201)
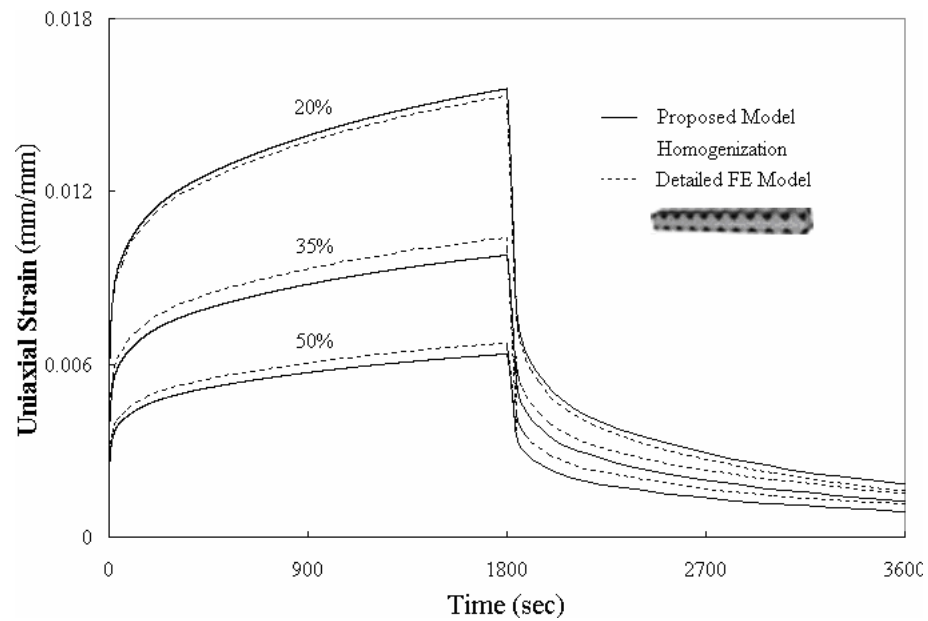
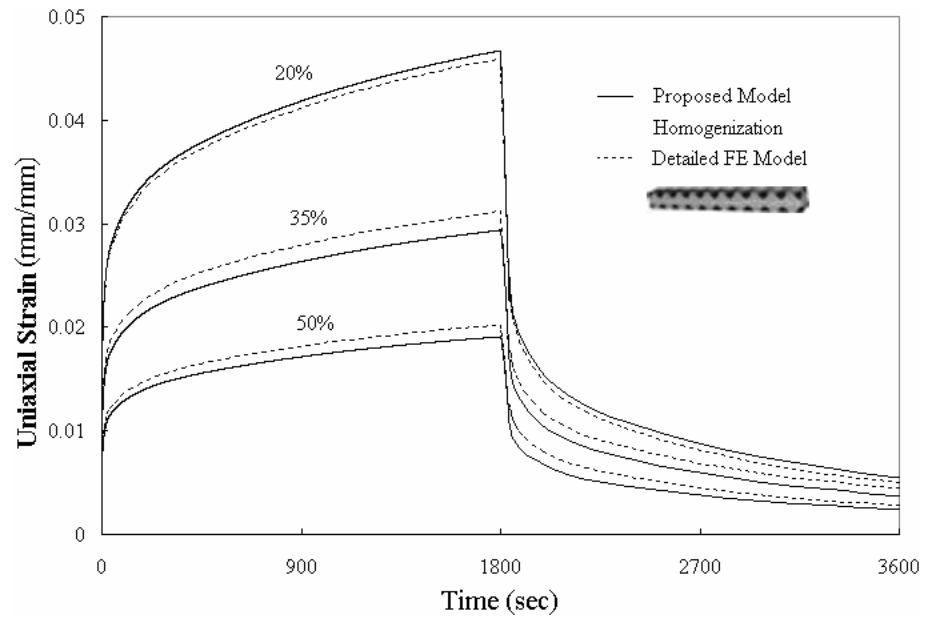Figure 3-19. Creep responses of Valanis model and detailed FE Model under 10 MPa

Figure 3-20. Creep responses of Valanis model and detailed FE Model under 30 MPa

Table 3-11

Comparison of CPU time in homogenized and heterogeneous composite bars

	Total elements	Total nodes	CPU time (sec)
Homogenized bar (20% Vf)	10	44	65.8
Homogenized bar (35% Vf)	10	44	44.6
Homogenized bar (50% Vf)	10	44	65.3
Heterogeneous bar(20% Vf)	8960	11201	13360(3.71hour)
Heterogeneous bar(35% Vf)	8960	11201	13498(3.75hour)
Heterogeneous bar(50% Vf)	8960	11201	11072(3.06hour)

Figures 3-21 and 3-22 illustrate local maximum principal strain and stress contours of

the homogenized and heterogeneous composite bars having 20% particle volume

contents at three different times. The scale factor of 10 is used. It is seen that the

homogenized composites give prediction of the average (effective) responses but they

are limited in characterizing local field variables such as stress concentrations at the

particle-matrix inter-phase and at the region between particles. The field variables

obtained in the homogenized composites represent average field variables of the matrix

and particle constituents.

a) Homogenized model

t=0.0001 sec

t=1800

t=2070

b) Heterogeneous model

t=0.0001 sec

t=1800

t=2070

9.0×10^{-2} 4.5×10^{-2} 0
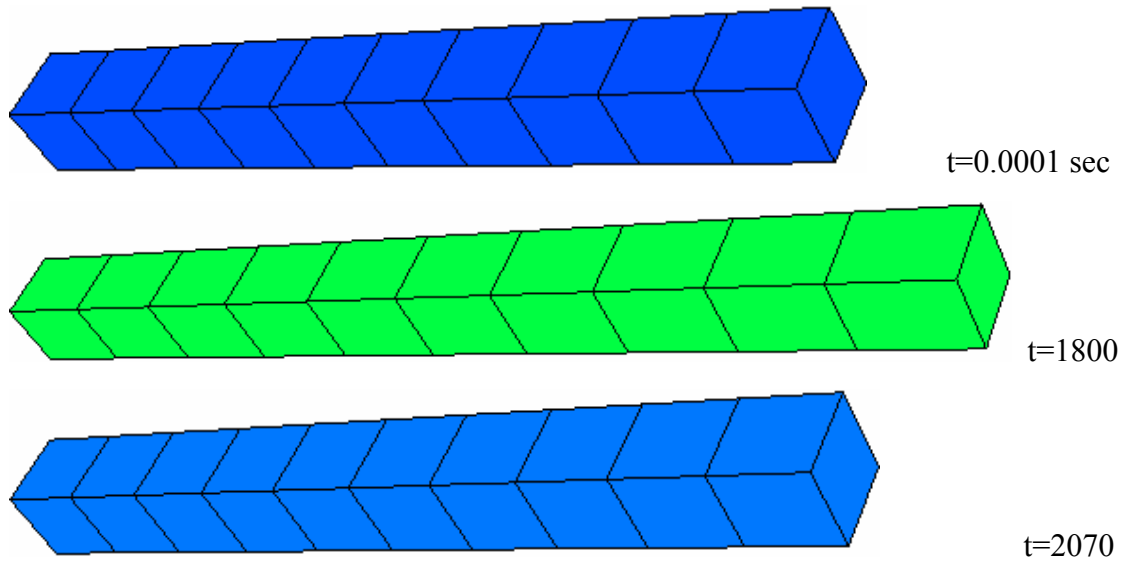
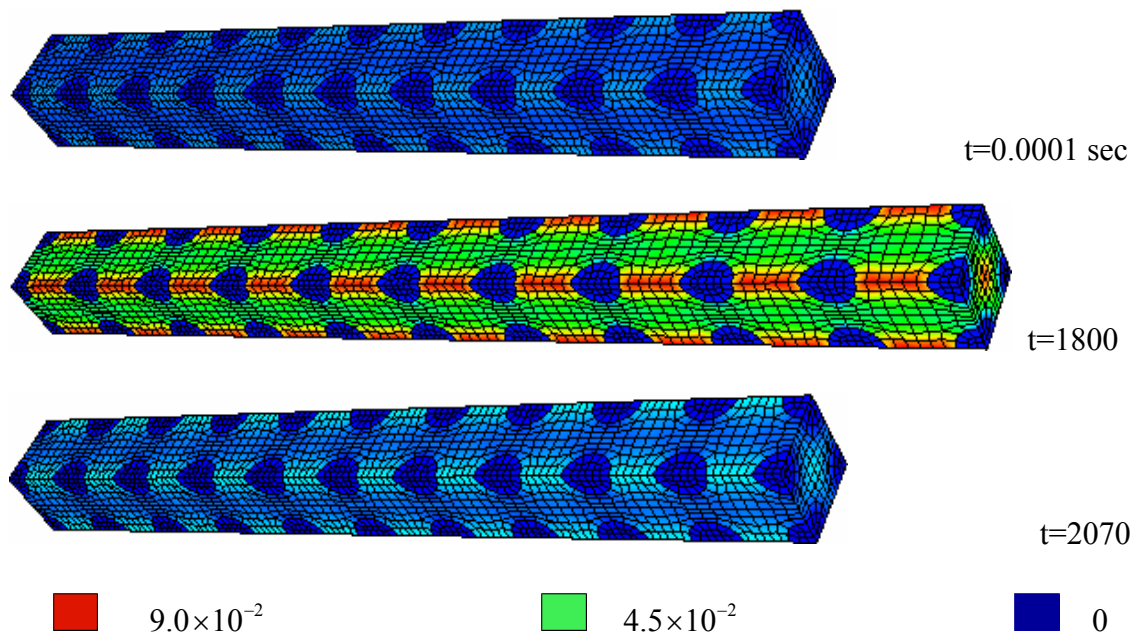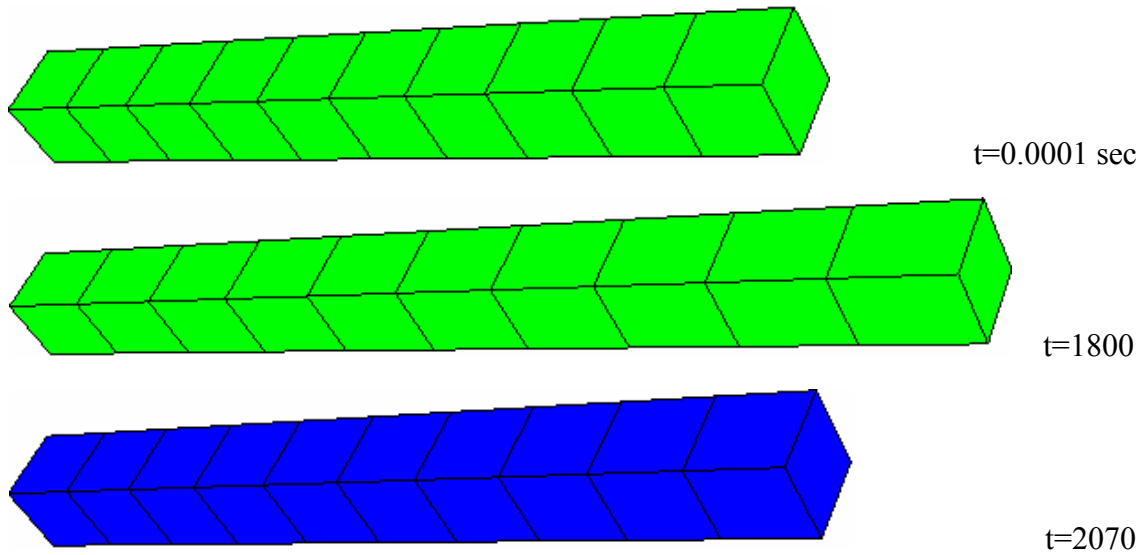Figure 3-21. Maximum principal strain distribution of creep-recovery loading under 30 MPa a) Proposed model b) heterogeneous model

a) Homogenized model

t=0.0001 sec

t=1800

t=2070

b) Heterogeneous model

t=0.0001 sec

t=1800

t=2070

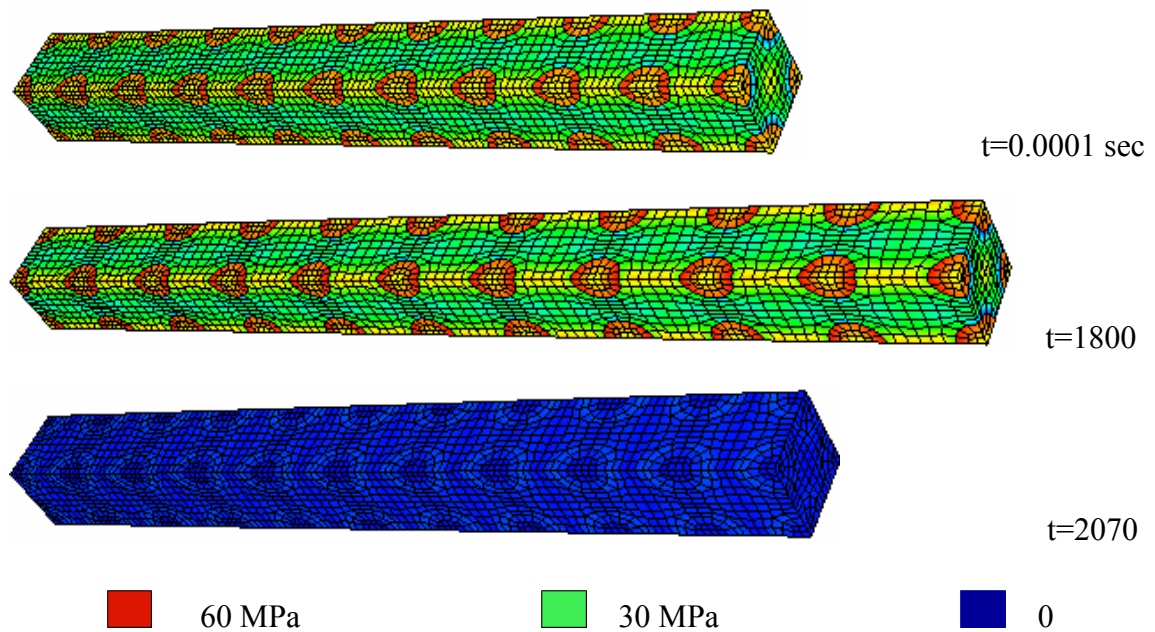60 MPa   30 MPa   0

Figure 3-22. von-Misses stress distribution of creep-recovery response under 30 MPa
a) Proposed model b) heterogeneous model

CHAPTER IV

ANALYSES OF TIME-DEPENDENT AND INELASTIC BEHAVIORS OF FIBER

AND PARTICLE HYBRID COMPOSITES

Polymers have been utilized in many engineering applications due to their

relatively low-cost and light-weight as compared to metal and ceramics. Polymers are

known for their time-dependent characteristic, poor impact resistance, and low fracture

toughness which are the major drawbacks in using polymers. Particles are added to

increase toughness and reduce time-dependent characteristics, while fibers are widely

used to enhance strength and stiffness. The combined fiber and particle reinforced matrix

forms a hybrid composite. Polymer and aluminum, which are often used as matrix in the

hybrid composites, can exhibit time dependent and inelastic responses. The time-

dependent behavior becomes more pronounced at elevated temperatures and high

stresses. Available studies on micromechanical formulations of hybrid composite

systems focus on predicting effective linear elastic properties. This study introduces an

integrated micromechanical and FE model for predicting time-dependent and inelastic

responses of hybrid composites. The studied hybrid systems consist of unidirectional

fiber reinforcements embedded in a matrix system having solid spherical particle fillers.

Fibers can be in the forms of long or short fibers as shown in Figs. 4-1a and 4-1b. The

simplified micromechanical model of a particle reinforced composite discussed in

Chapter III is used to obtain effective properties of the homogenized matrix system. This

matrix system is integrated with unit-cell and representative volume element (RVE)

models of unidirectional fiber reinforced composites, which are generated using FE.

Constitutive equations for viscoelastic and viscoplastic deformations are incorporated for

the homogeneous polymer constituent in the matrix systems. Limited experimental data

available in the literatures are used to validate the proposed modeling framework.

Hybrid composites can be modeled in details by incorporating all heterogeneities.

Governing equations of the deformation in viscoelastic-viscoplastic hybrid composites

subject to prescribed boundary conditions can be formed. This effort is rather impractical

as real micro-structural characteristics of composite materials, such as existence of voids,

spacing between inclusions, and shape of inclusions, would vary with locations.

Furthermore, finding exact analytical solutions to governing equations are not always

possible. A more practical approach is to define an idealized microstructure of

composites and find solutions to boundary value problems (BVP) of the idealized

microstructure. For this purpose, several assumptions have to be made that limits the

predictive capability of the solutions. The idealized microstructure is generated by

selecting RVE of heterogeneous material. In literatures, there are two significantly

different approaches in defining RVE (Hill., 1963, Drugan and Willis, 1996). The first

definition requires the RVE to include all possible micro-structural characteristics of the

composites. This definition generally leads to a large RVE and it requires computational

tools for solving governing equations of the deformation in the RVE. The second

definition considers the smallest micro-structural characteristic that can give sensible

prediction of the overall composite response. The size of RVE according to the second

definition depends on the constitutive material models, external boundary conditions,

and mismatches in the properties of the constituents. In order to obtain effective

properties of composites, homogenization methods, which are often performed on a unit-

cell, are formulated. The unit-cell model is not necessarily the same as RVE and it is

usually defined as the smallest geometrical model that is repeatable in the RVE. For

example, a unit-cell model, having a square matrix with a single heterogeneity, is often

used to obtain effective properties of unidirectional fiber composites. The chosen unit-

cell model assumes a periodic micro-structural arrangement, which simplifies analytical

solutions, but it contradicts with real microstructures of materials. It should be noted that

a unit-cell can give sensible predictions of effective properties, i.e., elastic deformation,

however, local field variables of the constituents in the RVE depend strongly on the

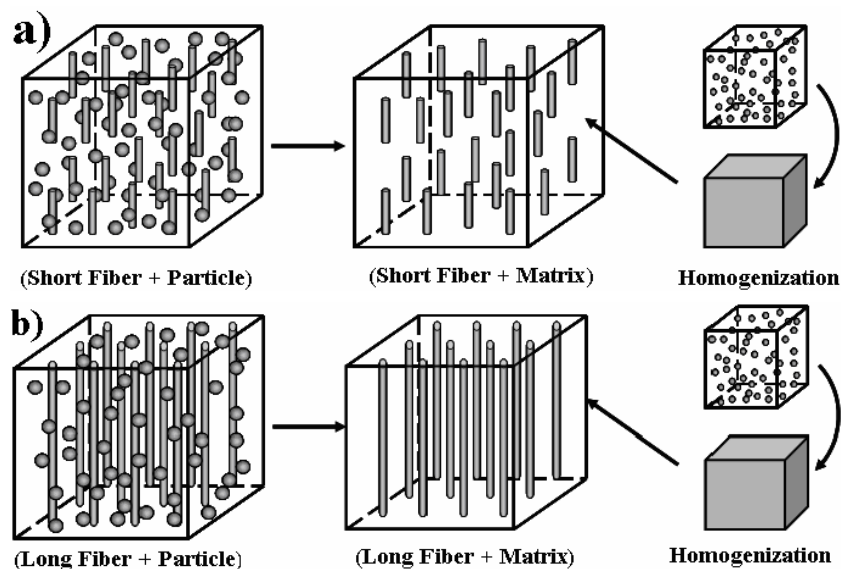micro-structural arrangements, e.g. in plastic deformation.

Figure 4-1. Hybrid composite systems a) with short fiber and particles b) with long fiber and particle

In this chapter, unit-cell models are defined for short and long fiber hybrid

composites, with an intention to provide effective responses of hybrid systems.

Furthermore, FE meshes of RVEs of unidirectional long fiber hybrid composites with

random and regular fiber arrangements are generated. The effective properties and local

field variables determined from the heterogeneous RVEs and unit-cell models are

compared.

4.1 Unit-cell models of hybrid composites

The integrated micromechanical models of particle reinforced composites and FE

model of a unit-cell fiber composite are numerically implemented. Unit-cell models of

short fiber and long fiber hybrid reinforced composites are generated using 3D

continuum elements. The properties of matrix are obtained using the simplified

micromechanical model of a particle reinforced composite (Chapter III). The simplified

micromechanical model is implemented in the user material subroutine (UMAT) of

ABAQUS FE. The fiber and particle are assumed to be linear elastic, while the polymer

constituent follows viscoelastic-viscoplastic behaviors.

4.1.1. Short fiber hybrid composite

Figure 4-2 shows a unit cell model of short fiber and particle reinforced hybrid

composite. Periodic boundary conditions are applied to the unit cell model and perfect

bonding condition is assumed at the interface layer. The size of fibers is in micro-scale.

The effective elastic, viscoelastic, and viscoplastic properties obtained from the unit-cell

models are compared to available experimental data and other homogenization schemes.
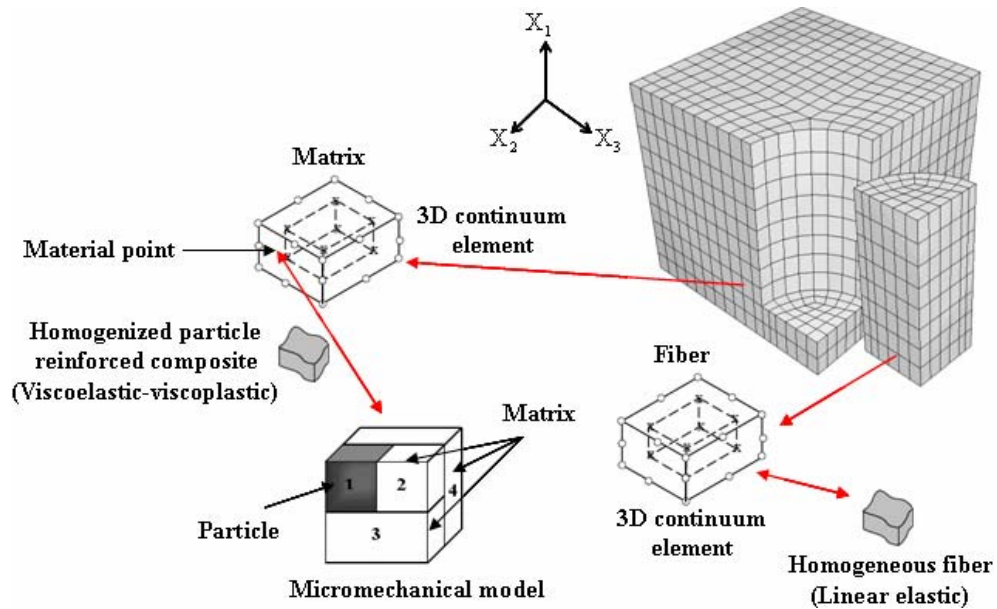

Figure 4-2. FE mesh of heterogeneous short fiber reinforced composite with homogenized particle reinforced matrix

Elastic responses

The elastic modulus obtained from the proposed approach is compared with the

analytical solutions reported by Fu et al. (2002). The hybrid composite consists of glass

fiber, calcite particle, and ABS matrix. The fiber length and radius are 336 μm and 6.9

µm, respectively, and particle diameters are between 13~37 µm. Elastic properties of the

constituents are given in Table 4-1. The integrated micromechanical and FE unit-cell

models are generated for hybrid composites having 10% and 30% total volume contents

of particles and fibers. The elastic properties determined using the proposed model are

compared to the ones generated using the rule of hybrid mixture (RoHM) and a laminate

analogy approach (LAA) as illustrated in Fig. 4-3. The elastic moduli generated using the

proposed approach agrees well with the RoHM and LAA results. Vf (fiber) indicates a

volume content of short fibers and Vf (total) denotes total volume contents of short

fibers and particles. Figure 4-4 shows effective Poisson ratios determined using the

proposed model. As the ratio of Vf(fiber)/Vf(total) increases, the contents of short fibers
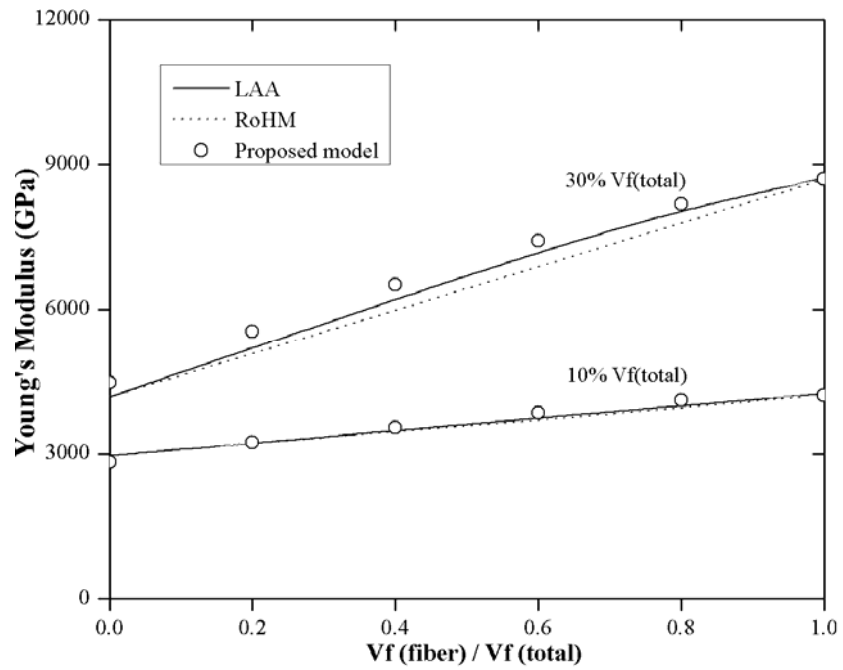
increase leading to stiffer composites.

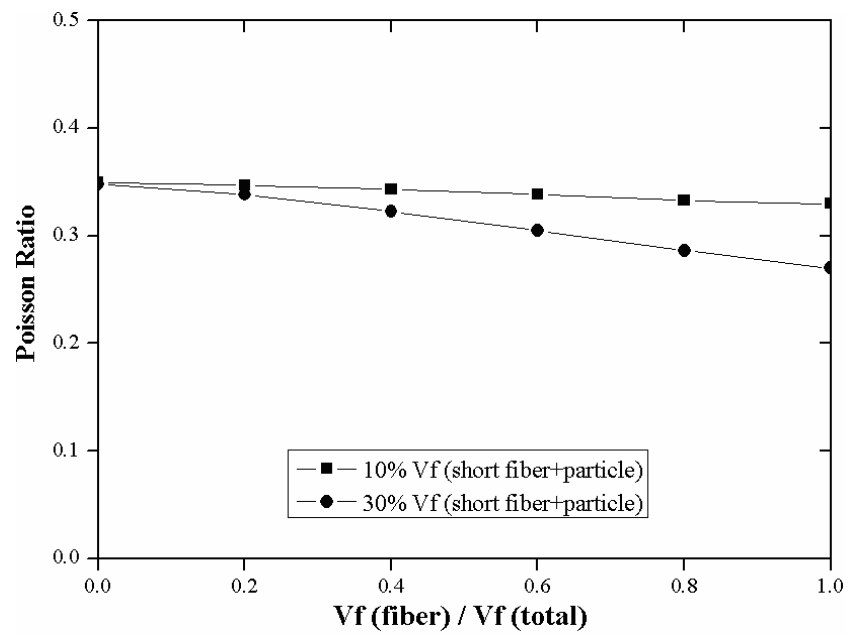Figure 4-3. Effective elastic moduli of hybrid composite

Figure 4-4. Effective Poisson ratio of hybrid composite

Table 4-1

Elastic properties of particle/short fiber/ABS composites

Mechanical Properties	Material type		
	Calcite particle	ABS matrix	Short glass fiber
Young's modulus E (GPa)	167	2.39	75
Poisson ratio, ν	0.25	0.35	0.25

The effective elastic moduli generated using the integrated micromechanical and unit-cell FE framework of hybrid composite are verified using experimental data for a combined polypropylene (PP), ethylene propylene rubber (EPR), and short glass fiber (SGF) hybrid composite (Zebarjad et al., 2001). The elastic properties for the PP matrix, EPR particles and SGF are given in Table 4-2. Figure 4-5 illustrates effective elastic moduli of hybrid composites at several fiber and particle combinations. The homogenization scheme gives reasonable predictions.
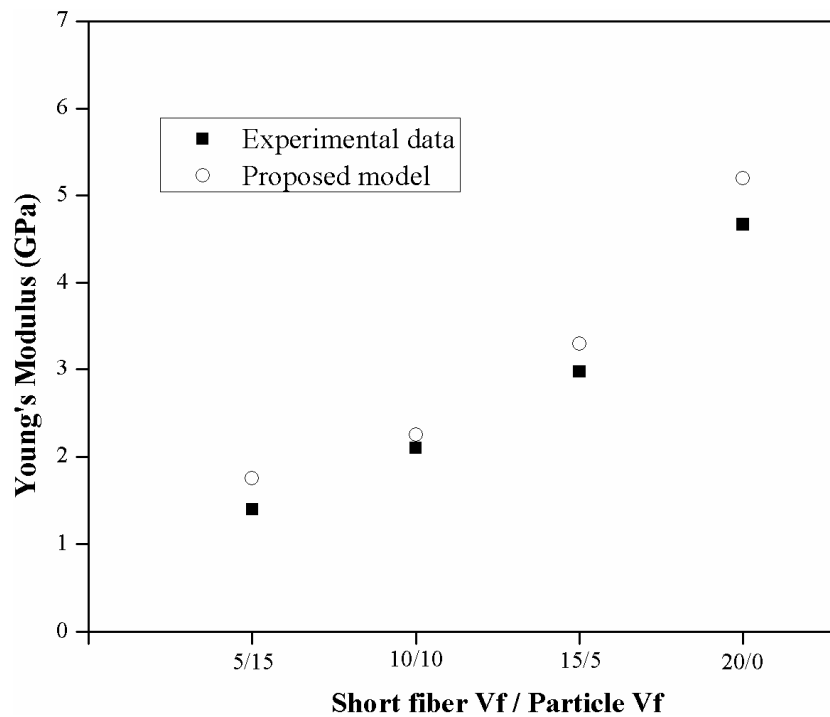
Figure 4-5. Comparison for the elastic modulus of PP-EPR-SGF hybrid composite

Table 4-2

Elastic properties of the phases in PP-EPR-SGF hybrid composite

Mechanical Properties	Material type		
	PP	EPR	SGF
Young's modulus E(GPa)	1.25	3.0	70
Poisson ratio, v	0.42	0.42	50.23

Time dependent responses

The time dependent response obtained using the proposed model is verified using

experimental data reported by Arunachaleswaran et al. (2007). As time-dependent data

of polymer hybrid composites with short fibers are not available, experimental data on

metal based hybrid composites are used to verify the proposed modeling approach. The

studied hybrid composite consists of alumina short fiber (Saffil), particle (SiC), and

matrix (alloy AE42). The fibers have an average diameter of 8 μm and an average length

of 180 μm. The particles have an average diameter of 30 μm. The viscoelastic

parameters for the matrix are characterized by matching the creep response of the matrix

in Fig. 4-6. The elastic properties of constituents are given Table 4-3, and the time-

dependent parameters of the matrix are given in Table 4-4. Creep strains of hybrid

composite having 10% short fiber + 10% particles and 10% short fiber + 15% particle

subject to a constant stress of 100 MPa at 240°C are illustrated in Fig. 4-6. Overall good

predictions of creep responses are observed.

Table 4-3

Elastic properties of the phases in AE42-Saffil-SiC hybrid composite

Mechanical Properties	Material type		
	AE42	SiC	Saffil
Young's modulus E (GPa)	45	450	300
Poisson ratio, v	0.3	0.3	0.25

Table 4-4

Prony series coefficients for the AE42 matrix

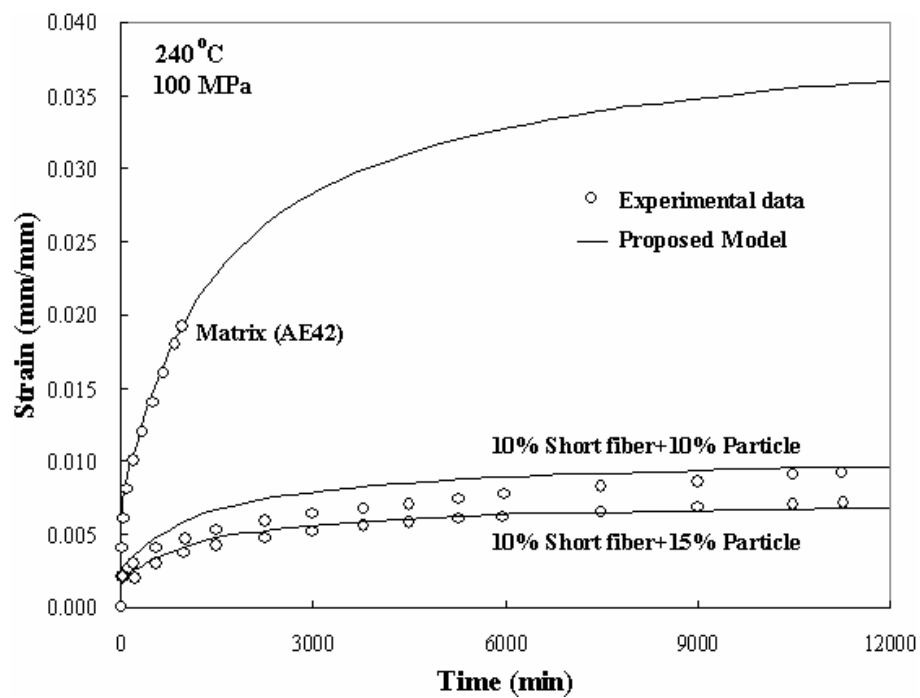| n	$\lambda_n \, (\text{min}^{-1})$	$D_n \times 10^{-4} \, (\text{MPa}^{-1})$
1	1	0.111
2	0.07	4.000
3	0.001	1.500
4	0.0002	1.500

Figure 4-6. Comparison with experimental data at 240°C and 100 MPa

A combined viscoelastic-viscoplastic response of hybrid composites is examined

using the proposed modeling approach. In this study, short fiber and particle are assumed

to be linear elastic, while polymer matrix exhibits a combined viscoelastic-viscoplastic

response. The time-integration algorithm for the combined viscoelastic-viscoplastic

model is used for the high density polyethylene (HDPE) constituent. The

micromechanical model of particle reinforced composite is implemented in the UMAT

subroutine of the ABAQUS FE code. The viscoelastic and viscoplastic parameters of the

HDPE are calibrated from experimental data of Lai and Bakker (1995). The elastic

properties of short fiber, particle, and HDPE constituents are given in Table 4-5. The

viscoelastic properties for HDPE constituent are given in Table 4-6. The viscoplastic

parameters η_p and n of the Perzyna model in Eqs. (2-26) and (2-27) are given Table 4-7.

The integrated micromechanical and FE unit-cell models are used to predict creep-

recovery responses of hybrid systems subject to a 40 MPa constant load. Two hybrid

systems are studied. The first system consists of 10% volume contents of short fiber and

10% volume contents of particle (10/10), and second system has 10% and 15% volume

contents of short fiber and particle (10/15), respectively. Responses of hybrid systems

subject to a 40 MPa tensile stress applied in the axial fiber and transverse fiber directions

are monitored.

Table 4-5

Elastic properties of the phases in Short fiber-Glass particle-HDPE hybrid composite

Mechanical Properties	Material type		
	HDPE	Glass Particle	Glass Short Fiber
Young's modulus E(GPa)	4.535	69	70
Poisson ratio, v	0.3	0.3	0.3

Table 4-6

Prony series coefficients for the HDPE polymer

n	$\lambda_n (sec^{-1})$	$D_n \times 10^{-4} (MPa^{-1})$
1	1	2.23
2	10^{-1}	2.27
3	10^{-2}	1.95
4	10^{-3}	3.50
5	10^{-4}	5.50
6	10^{-5}	5.50

Table 4-7

Viscoplastic parameters of Perzyna model

η_p	n
35	1.36

Figure 4-7 illustrates von-Misses stress and maximum principal strain distributions

of two hybrid systems (10/10) and (10/15) due to loading along the axial fiber direction.

In this case, to maintain uniform deformation in the direction of the applied load, the

stiffer fibers experience higher stresses. The matrix regions surrounding the side length

of fiber show low stresses at the locations away from the fiber and relatively high

stresses close to the fiber/matrix inter-phases. The localized stresses (stress

concentration) near the inter-phase regions could potentially cause damage/debonding.

Furthermore, stresses in the matrix regions under the edge of the fiber are much more

pronounced. If only unreinforced polymers are considered, these stress levels may cause

matrix failure. Thus, adding particle fillers is expected to increase stiffness and failure

strength of the matrix. It is noted that the present study does not take into consideration

failure/damage due to localized stress/strain. However, the present study can be used as

preliminary parametric studies for designing hybrid composite materials or structures by

identifying critical area for damage to initiate. In Figs. 4-7(c-d), it is seen that the strains

below the fiber's edge are pronounced even after removal of the applied stresses. Adding

more particle fillers in the matrix slightly reduces the strains. Figure 4-8 shows von-

Misses stress and strain fields when the composite are loaded in the transverse fiber

direction. The matrix region experiences higher stresses compared to the stresses due to

loading is in the axial fiber direction. The matrix of (10/10) hybrid system having 10%

particle reinforcement is softer than the matrix of (10/15) hybrid system having 15%

particle reinforcement. Figure 4-9 shows stress and strain fields in the matrix constituent

of the (10/10) hybrid composite. Figs. 4-9(a-b) illustrate the von-Misses stress

distributions due to loading along the axial fiber direction and transverse fiber direction.

When the external load is removed, the residual stress is seen at the inter-phase region

with the magnitude between 16-25 MPa. Figs. 4-9(c-d) illustrate the maximum principal

strain distributions due to loading along the axial fiber direction and transverse fiber

direction. It is observed that the time-dependent and plastic deformations in the matrix

constituent could lead to non-negligible residual stress is the matrix region even after

removed of the external load. This residual stress becomes pre-existing stress (pre stress)

when the hybrid composite is being subjected to the next loading histories. Thus, under

the transverse loading, adding particle fillers can significantly improve performance of

hybrid composites. Both stress and strain discontinuities are observed at the inter-phase

regions. It should be noted that the perfect bond between fiber and matrix is imposed by

traction continuity and displacement compatibility conditions. Thus, continuity in strains

is not guarantee unless this condition is imposed.

Figure 4-7. von-Misses Stress (in MPa) and maximum principal strain distribution of hybrid composite under axial loading a) stress distribution (10/10) b) stress distribution (10/15) c) strain distribution (10/10) d) strain distribution (10/15)
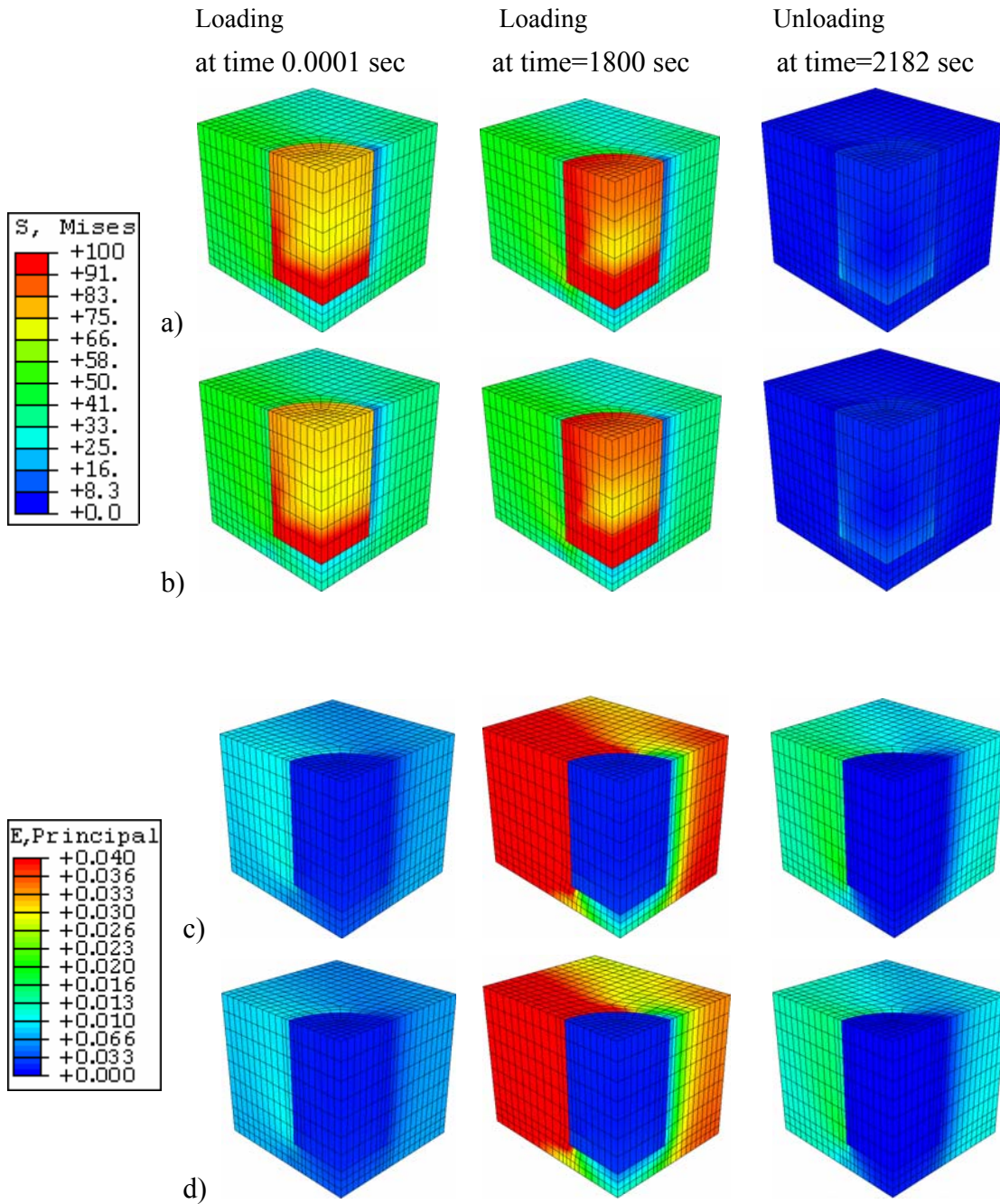
Figure 4-8. von-Misses Stress (in MPa) and maximum principal strain distribution of hybrid composite under transverse loading a) stress distribution (10/10) b) stress distribution (10/15) c) strain distribution (10/10) d) strain distribution (10/15)
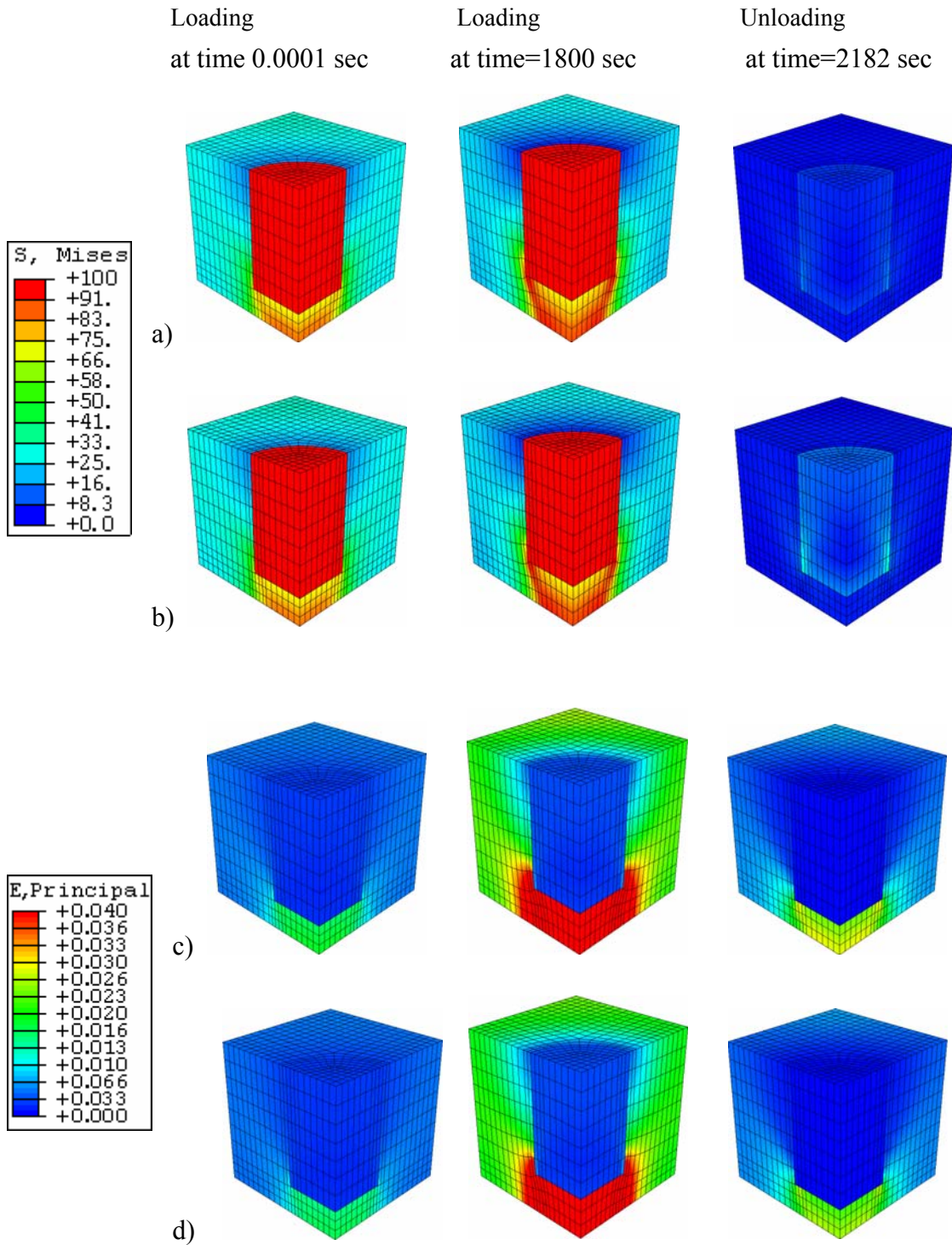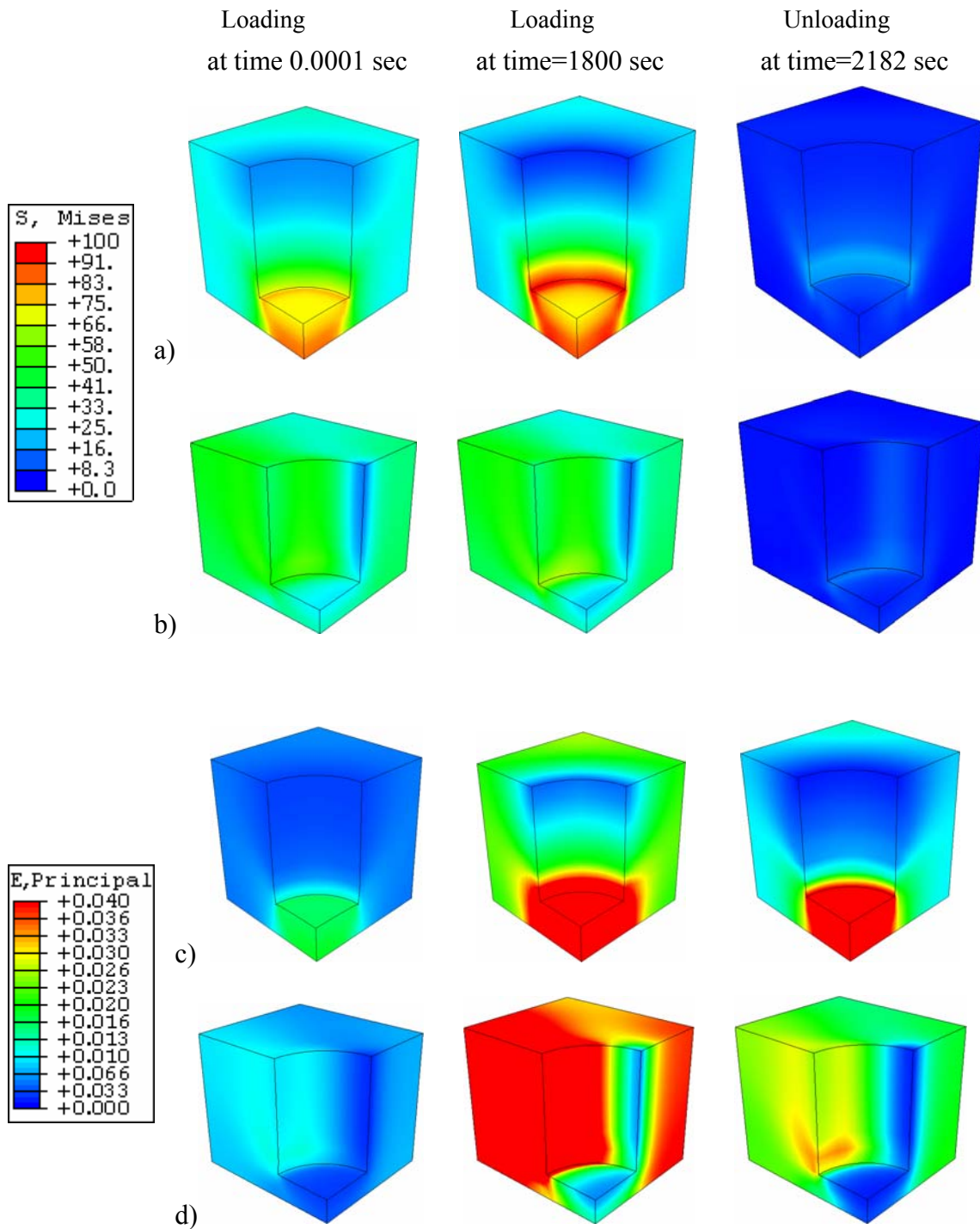
Figure 4-9. von-Misses Stress (in MPa) and maximum principal strain distribution of hybrid composite (10/10) under axial loading and transverse loading a) stress distribution (axial loading) b) stress distribution (transverse loading) c) strain distribution (axial loading) d) strain distribution (transverse loading)

Figure 4-10 illustrates the creep-recovery responses for the two hybrid systems

loaded along the axial fiber direction. The creep strain of total 20% volume content of

fibers and particles is more pronounced than the one with 25% total fiber and particle

volume content. Adding particles can reduce the time-dependent behavior of hybrid

systems but insignificantly changes the elastic (instantaneous) strains. When the

composite is loaded in the axial fiber direction, fibers generally carry most of the

mechanical load and only small portion of the load is transferred to the matrix, resulting

in small plastic deformations (less than 0.25%). It is also seen that adding particles to the

hybrid composites insignificantly reduces the plastic deformation. Figure 4-11 illustrates

creep-recovery response of the two hybrid systems loaded in the transverse fiber

direction. Similar behaviors as in Fig. 4-10 are observed. Higher strains and plastic

deformations are exhibited when loading is applied in the transverse fiber direction.
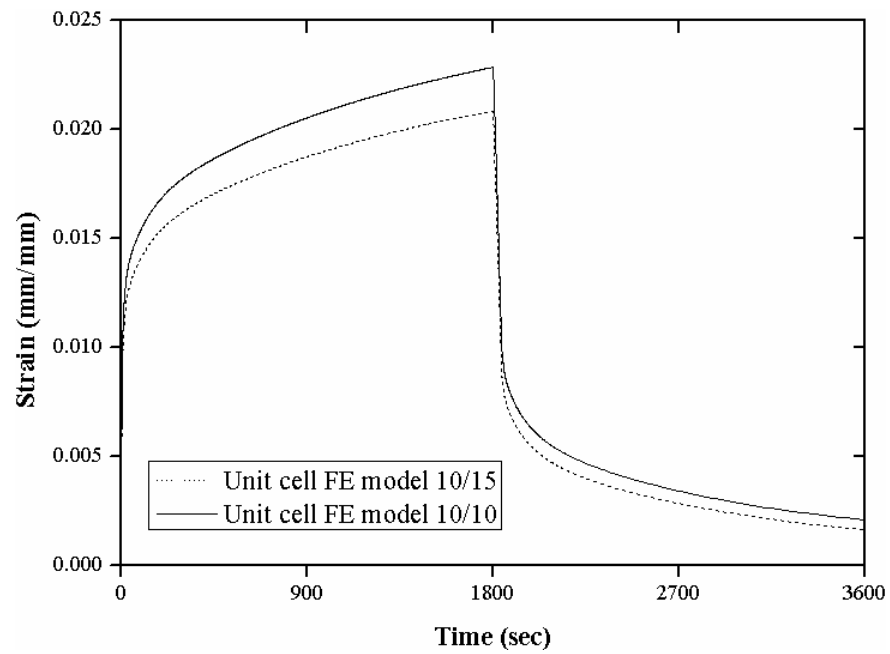
Figure 4-10. Creep-recovery responses of Short fiber-particle-HDPE hybrid composite (loading in the axial fiber direction)
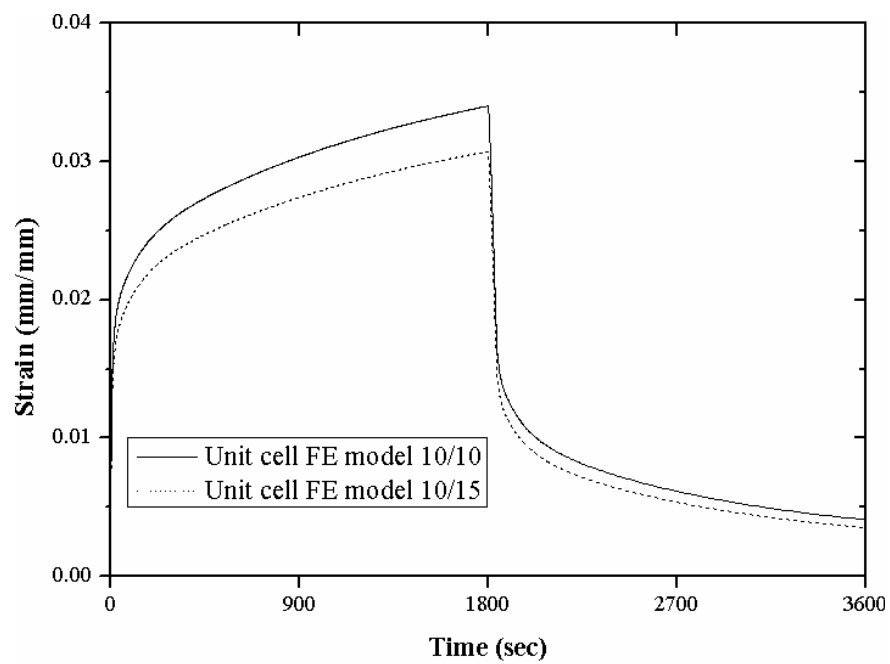
Figure 4-11. Creep-recovery responses of Short fiber-particle-HDPE hybrid composite (loading in the transverse fiber direction)

The proposed modeling approach is also used to simulate stress-strain responses due to quasi-static loadings at different rates: 0.01, 0.1, 1.0MPa/s. Figure 4-12 shows predictions of the stress-strain responses under three different stress rates in the axial fiber direction. The combined viscoelastic-viscoplastic response is more pronounced for a slow loading. It is seen that increasing total volume contents of the elastic reinforcements reduces the maximum strain, but insignificantly decreases the permanent deformation. Figure 4-13 shows the stress-strain responses during the transverse loading at different rates. The permanent deformations are more pronounce when the composite are loaded in the transverse fiber direction because higher stresses are exhibited in the matrix.
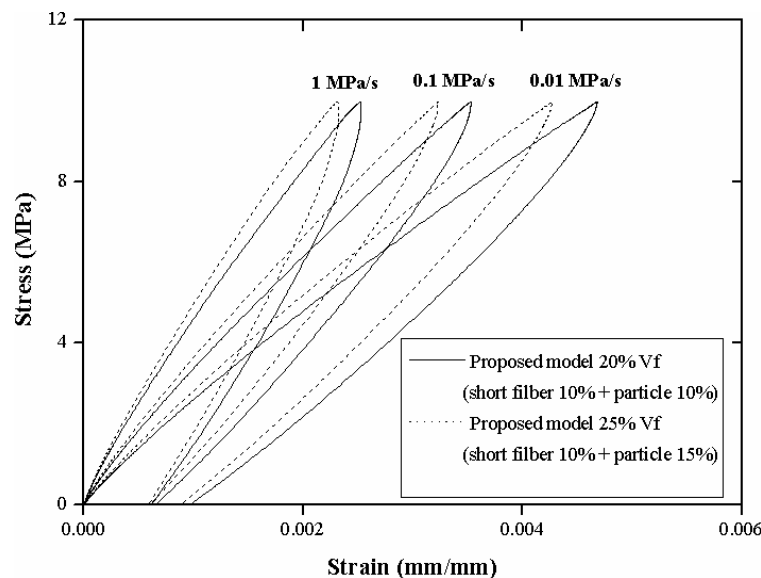
Figure 4-12. Stress-Strain relation under different loading rate (axial fiber direction)
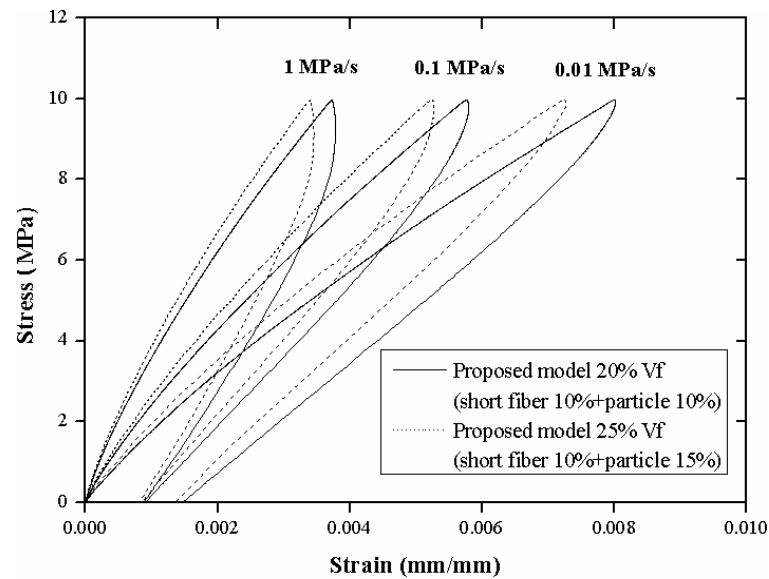
Figure 4-13. Stress-Strain relation under different loading rate (transverse direction)

4.1.2. Long-fiber hybrid composite

A hybrid composite having unidirectional long-fiber and particle filler is studied as illustrated in Fig. 4-1b. The integrated micromechanical model of particle reinforced composites and FE unit cell model of long fiber composites is numerically implemented. Figure 4-14 presents the unit-cell model of hybrid composite generated using FE. The properties of matrix are obtained using the homogenization method of particle reinforced composite as mentioned in section 4.1.1. The elastic and time-dependent responses of hybrid systems with different fiber and particle contents are examined.
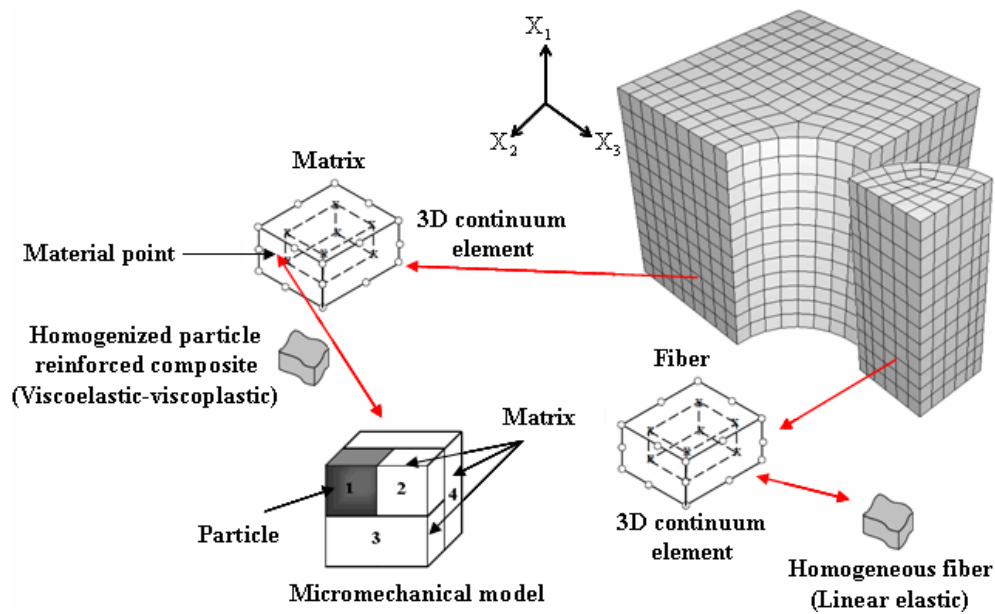
Figure 4-14. FE mesh of heterogeneous long fiber reinforced composite with homogenized particle reinforced matrix

Elastic responses

The elastic modulus obtained from the proposed modeling approach is compared with the experimental data reported by Hartikainen et al. (2005). The hybrid composite consists of long glass fiber (LGF), polyoefin particle, and polypropylene (PP) matrix. The fiber length in the tested specimen is 11 mm. The mean particle diameter is 2.0 μm. Elastic properties of the constituents are given in Table 4-8. The integrated micromechanical and FE unit-cell models are generated for hybrid composites having (0% long fiber and 7.7% particle content: 0/7.7), (3.7/0), (4.2/7.4), (12.9/0), and

(14.6/6.6). The effective elastic moduli in the axial fiber direction are given in Fig. 4-15.

The elastic moduli calculated using the proposed approach agrees well with the

experimental data. Errors about 5% are observed for the (12.9/0) and (14.6/6.6) hybrid

systems.

Table 4-8

Elastic properties of the phases in long fiber- particle-PP hybrid composite

Mechanical Properties	Material type		
	PP	Polyoefin Particle	Long glass fiber
Young's modulus E (GPa)	4.535	3.2	65
Poisson ratio, v	0.3	0.32	0.21
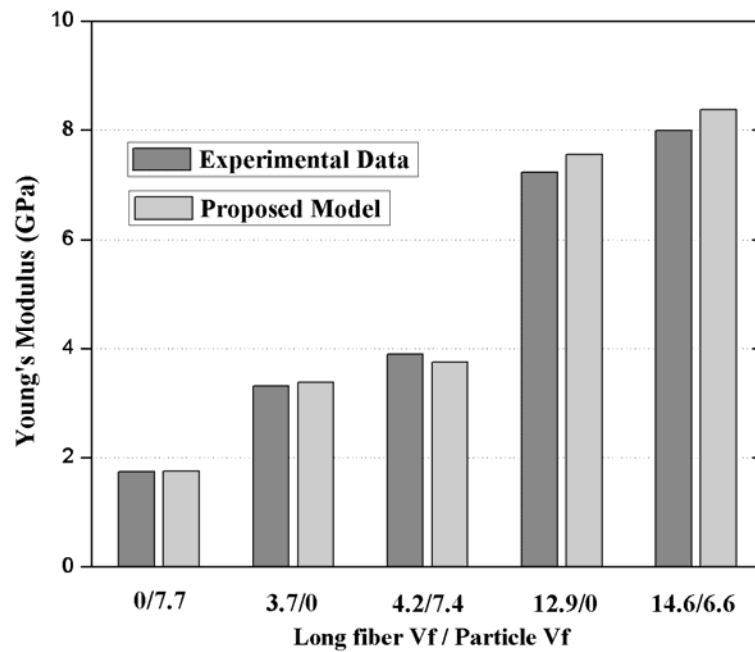
Figure 4-15. Young's modulus of long glass fiber and particle hybrid composite

Time dependent responses

A combined viscoelastic-viscoplastic response of hybrid composites having long

fiber and particle is numerically examined using the proposed modeling approach.

Hybrid composites having long glass fibers and polyoefin particles constituents are

studied. Experimental data of combined viscoelastic-viscoplastic responses of long fiber-

particle hybrid composites are currently lacking. The elastic and time dependent

properties of the constituents are reported in the Tables 4-5 and 4-6. The viscoplastic

material constants of the Perzyna model, η_p and n in Eqs. (2-26) and (2-27) are given in

Table 4-7. The integrated micromechanical and FE unit-cell models are used to predict

creep-recovery responses subject to a 40 MPa tension stress. The constant stress is

applied for 1800 sec and recovery is monitored for another 1800 sec. Three hybrid

systems are studied. The first system consists of 10% volume contents of long fiber and

30% volume contents of particle (10/30). The second and third systems are 20/20 and

30/10 hybrid composites, respectively. Figure 4-16 illustrates the von-Misses stress and

maximum principal strain distribution of (10/30) hybrid system subject to loading along

the axial fiber and transverse fiber directions. When the composite is loaded in the

transverse direction of fiber, overall stress in the matrix is higher than the one due to

axial loading in fiber direction. The local stresses in the composite region show nearly

uniform values except in the small region near the fiber/matrix inter-phase (Fig. 4-15b).

Uniform strains are shown when the composites are loaded in the axial fiber direction

(Fig. 4-15c), resulting in higher stresses in the stiffer fibers (Fig. 4-15a). Figure 4-17

illustrates von-Misses stress and maximum principal strain distribution in the matrix

constituent of the (10/30) hybrid composite subject to loading along the axial fiber and

transverse fiber directions. More pronounced residual strain is seen in the matrix regions

due to loading in the transverse fiber direction, loading to residual stresses (between 0-

16 MPa).

Figure 4-18 illustrates the overall creep-recovery responses due to loading in the

axial fiber direction (40 MPa). Overall permanent deformations after a complete removal

of the load are negligible as most of the load is carried by the linear elastic fibers. It is

seen that the composites with higher contents of long fibers show less creep strains since

smaller stress is carried by the matrix. Figure 4-19 shows creep-recovery responses on

hybrid systems loaded in the transverse fiber direction. Significant time-dependent

responses are exhibited due to the higher stresses in the matrix region. It is seen that all

hybrid systems show similar responses. Hybrid systems with higher fiber contents result

in smaller stresses in the matrix constituents. To maintain similar overall responses of

hybrid composites, the less particles are needed when the composites have more fibers.

Thus, one can vary the compositions of the constituents in the hybrid composites to

achieve desired performance. Later in this chapter, the responses from the unit-cell

model will be compared to the one of RVE in order to access the validity in determining

effective behaviors and local field variables using the unit-cell model.

Loading   Loading

Unloading

at time 0.0001 sec   at time=1800 sec   at time=2182 sec
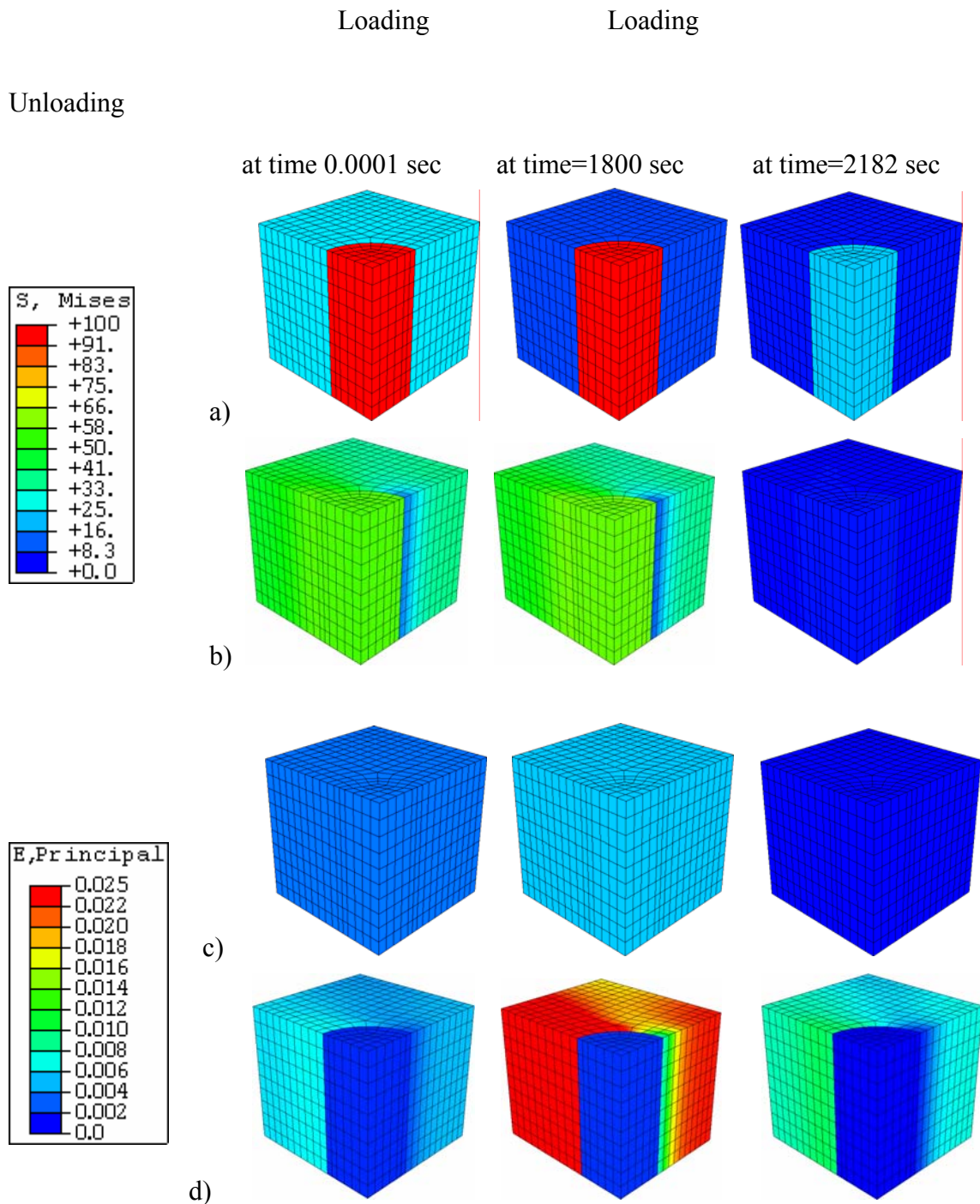
Figure 4-16. von-Misses Stress (in MPa) and maximum principal strain distribution of hybrid (10/30) under 40 MPa axial and transverse creep-recovery loading a) stress distribution under axial loading b) stress distribution under transverse loading c) strain distribution under axial loading d) strain distribution under transverse loading
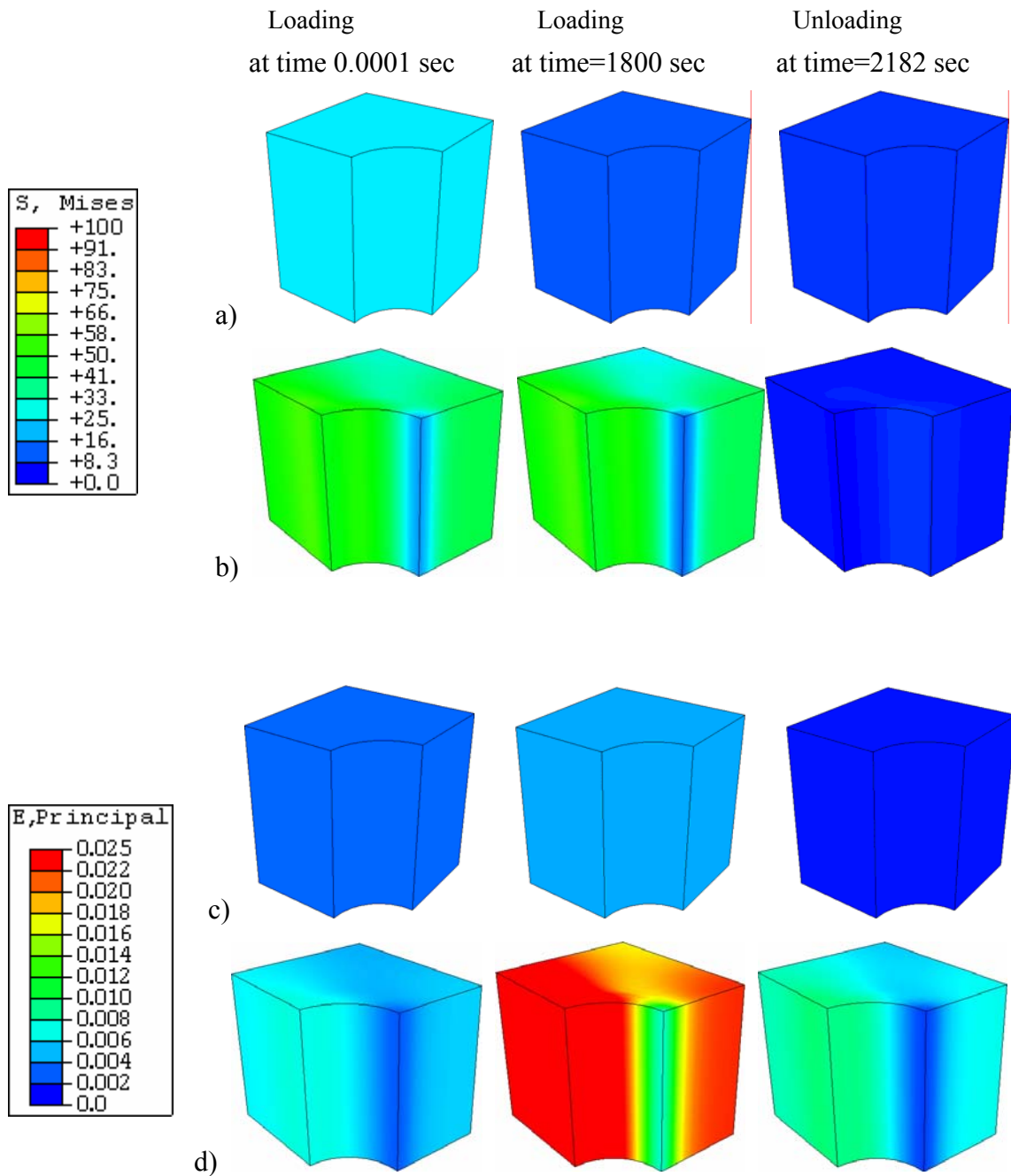
Figure 4-17. von-Misses Stress (in MPa) and maximum principal strain distribution of matrix (10/30) under 40 MPa axial and transverse creep-recovery loading a) stress distribution under axial loading b) stress distribution under transverse loading c) strain distribution under axial loading d) strain distribution under transverse loading
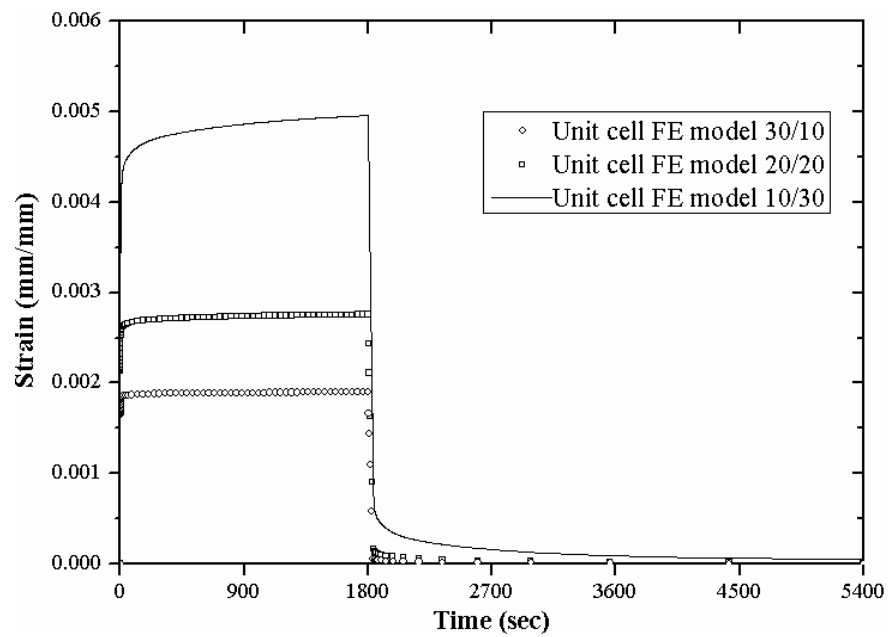
Figure 4-18. Creep-recovery responses of Long fiber-particle-PP hybrid composite (unidirectional loading)
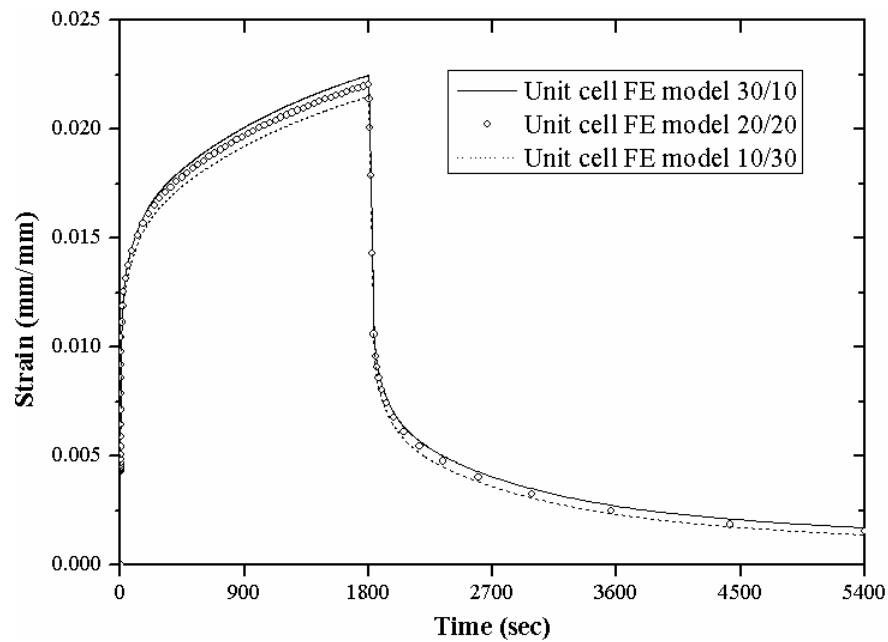
Figure 4-19. Creep-recovery responses of Long fiber-particle-PP hybrid composite (transverse loading)

4.2   RVE Models of Unidirectional Long-Fiber Hybrid Composites

In this section, RVE models are generated for hybrid composites having uniform

and random arrangements of unidirectional long-fibers. Figure 4-20 illustrates FE mesh

of a RVE of a hybrid system. The effective responses of the homogenized matrix are

obtained from the micromechanical model of particle reinforced composites and are

incorporated at the material points within matrix elements in the RVE-FE model. The

purpose of this study is to compare the effective responses obtained using FE unit-cell

and FE-RVE models. Local stress and strain fields are also monitored.
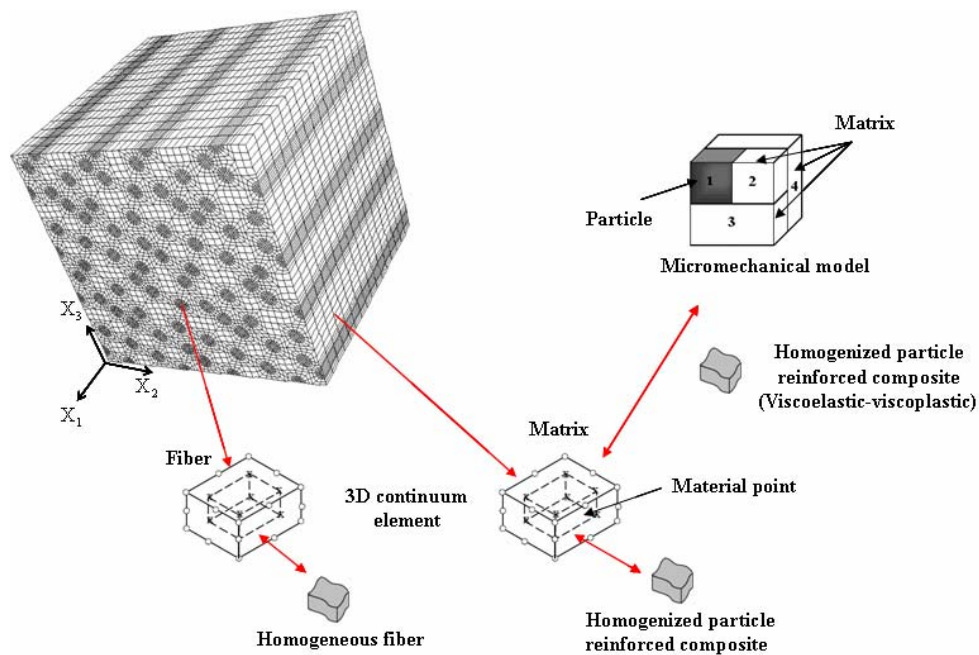
Figure 4-20. FE microstructures for heterogeneous and homogenized particle reinforced composite system

The hybrid systems are made of glass long-fiber, glass particle and HDPE polymer constituents. The elastic properties and time dependent properties of the constituents are given in Tables 4-5 and 4-6. The viscoplastic material constants of the Perzyna model are given in Table 4-7. The integrated micromechanical and FE-RVE models are used to simulate creep-recovery responses subject to a constant 40 MPa stress for eight hybrid systems: 10% volume contents of uniform fibers and 20% volume contents of particles (10/20 u), (20/10 u), (20/40 u), (50/10 u), 10% volume contents of random fiber and 20% volume contents of particles (10/20 r), (20/10 r), (20/40 r), (50/10 r). Figure 4-21 shows cross-sectional area of the RVE models of random and uniform fiber distributions of 10%, 20%, 50% fiber contents. Responses of hybrid systems subject to loading in the axial and transverse fiber directions are examined. The fibers of Fig 4-21b) are distributed randomly with the following rule. The cross section of the 10% and 20% fiber contents are checkered with 19 perpendicular and horizontal lines, and the 50% fiber contents has 31 perpendicular and horizontal lines. The 10% random arrangement contains 2 fibers per perpendicular and horizontal line, the 20% and 50% random arrangements have 4 and 6 fibers, respectively. The center points of the fibers are placed

along the lines. Finally, the detailed fiber meshes are generated randomly by fixing the

diameter of the fibers.
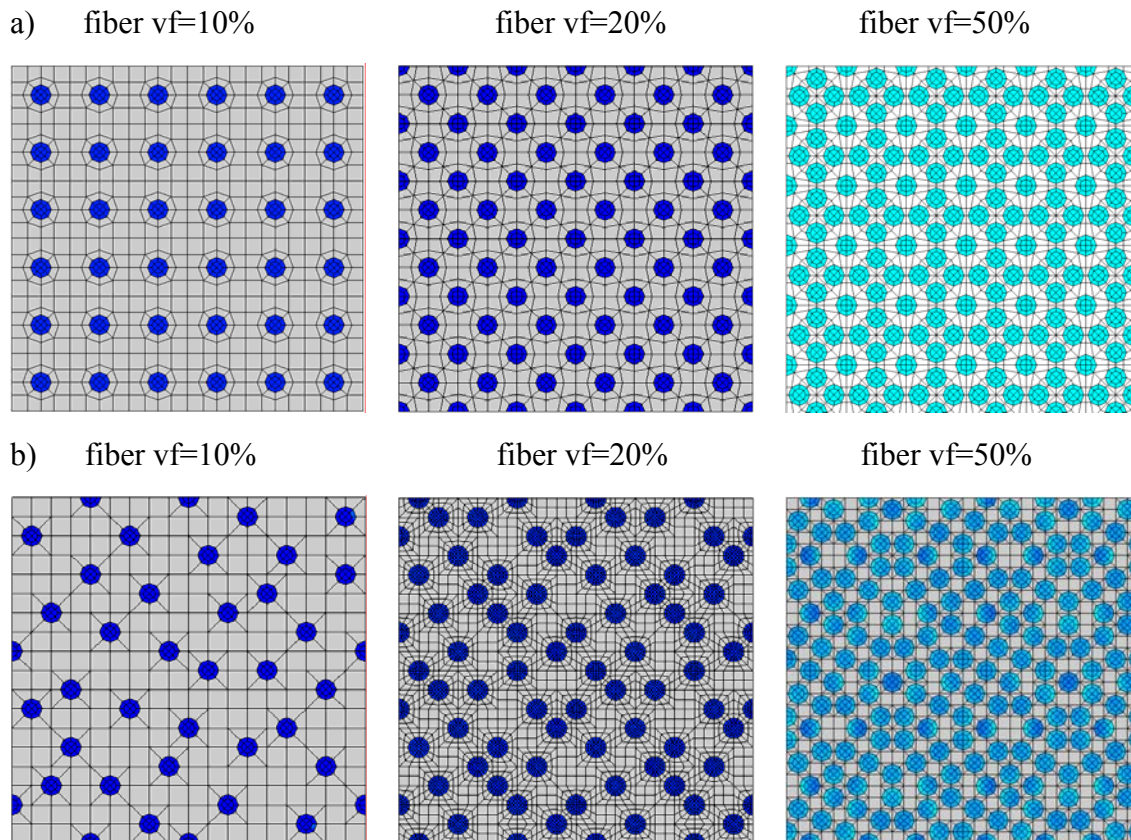
Figure 4-21. Cross-section of hybrid with long fiber: a) Uniform fibers   b) Random
fibers

Figure 4-22 shows the creep-recovery responses due to a prescribed loading in the

axial fiber direction (40 MPa). Responses of the hybrid systems having 10% fiber + 20%

particles and 20% fiber + 10% particles are reported. Responses obtained from the FE-

unit cell model and FE-RVE models with random and uniform fiber arrangements are

comparable with slight discrepancies. The time-dependent responses from the unit-cell

are slightly lower than the ones of the RVEs. Figure 4-23 shows the responses of 60%

total volume fraction of hybrid systems subject to a uniaxial loading in the fiber

direction (40 MPa). When loaded in the axial fiber direction, continuous long fibers

generally carry most of the mechanical load and only small portion of the load is

transferred to the matrix. In these two graphs, the permanent deformations are

insignificant due to a relatively low stress exhibited in the matrix. Table 4-9 present the

instantaneous strains in the RVE and unit-cell models monitored at time=0.001. From

the above table, it is seen that the instantaneous response in the unit-cell and RVE

models differ by less than 4.29%. The difference in the response at t=1800 second

increase to max 8.39% (Table 4-10). The limitation in the unit-cell FE model in

capturing detailed field variables result in lower response prediction as the constituent

properties are dependent on the localized stresses field. Figures 4-24 and 4-25 show the

viscoelastic-viscoplastic responses of transverse loading for 30% and 60% total volume

fraction of the fibers and particles. The responses of the transverse loading are softer due

to higher stresses in the matrix, and permanent deformations are more pronounced.

Some discrepancies are observed in the responses of the RVE and unit-cell models. This is due to the fact that in the RVE models, it is possible to incorporate localized stresses between fibers, which result in higher overall strain responses. Table 4-11 presents the instantaneous strains in the RVE and unit-cell models monitored at time=0.001. The difference in the instantaneous strain responses during the transverse loading is less than 8.36%. As time progresses, the deviations become larger which is shown by nearly 19% difference in the response at t=1800 second for the hybrid composite with 50% fiber contents (Table 4-12). Thus, it can be concluded that the unit-cell model, which results in lower overall responses, is limited in capturing localized stresses in the matrix. The stress-dependent behaviors in the matrix constituent make the deviations more severe.

Figures 4-26 and 4-27 illustrate the von-Misses the stress and maximum principal strain distribution of (20/10 r and 50/10 r) hybrid composites subject to loading along the axial fiber and transverse fiber directions. This conditions cause low stress levels and insignificant plastic deformation in the matrix. The uniform strains are shown (Fig. 4-26c). While, when the composite is loaded in transverse direction of fiber, the overall stress distribution in the matrix is higher than fiber directional loading, and results in the softer responses in Figs. 4-24 and 4-25.

Figure 4-22. Creep recovery responses of 30% Vf for unidirectional loading

Figure 4-23. Creep recovery responses of 60% Vf for unidirectional loading

Table 4-9

Instantaneous axial strain response at t=0.001 second

	(10/20)	(20/10)	(20/40)	(50/10)
Unit-cell	8.0380E-04	5.5884E-04	4.6149E-04	2.8163E-04
RVE random	8.2469E-04	5.6014E-04	4.6231E-04	2.9145E-04
	(2.60% error)	(0.23% error)	(0.17% error)	(3.49% error)
RVE uniform	8.2469E-04	5.8053E-04	4.8127E-04	2.9058E-04
	(2.60% error)	(3.88% error)	(4.29% error)	(3.18% error)

Table 4-10

Instantaneous axial strain response at t=1800 second

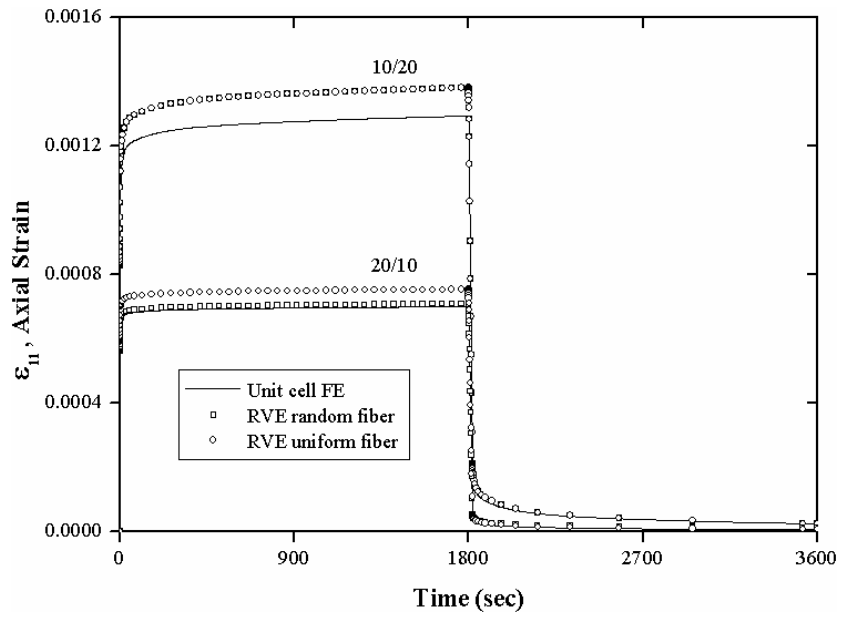|	(10/20)	(20/10)	(20/40)	(50/10)
Unit-cell	1.2931E-03	6.9894E-04	6.6584E-04	2.8959E-04
RVE random	1.3807E-03	7.0783E-04	6.6779E-04	3.1389E-04
	(6.77% error)	(1.27% error)	(0.29% error)	(8.39% error)
RVE uniform	1.3807E-03	7.5294E-04	7.0944E-04	3.1284E-04
	(6.77% error)	(7.73% error)	(6.55% error)	(8.03% error)
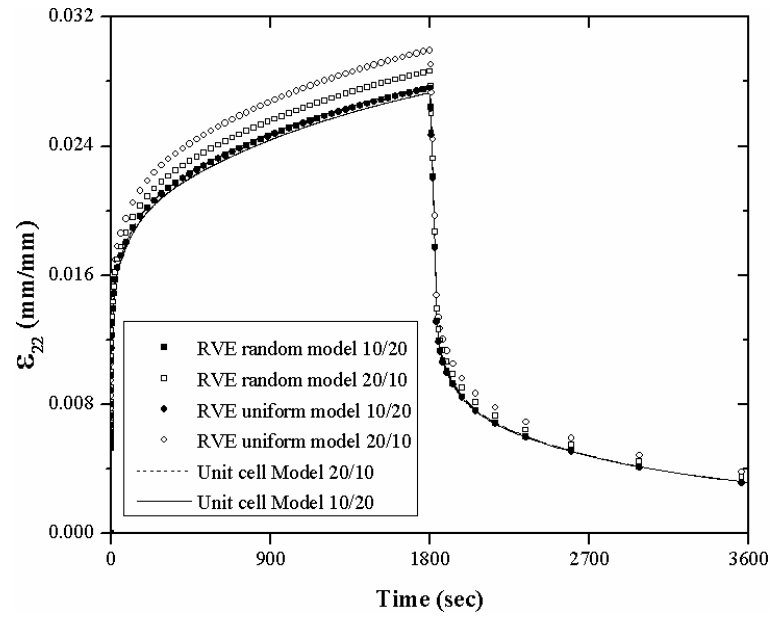
Figure 4-24. Creep recovery responses of 30% Vf for transverse loading
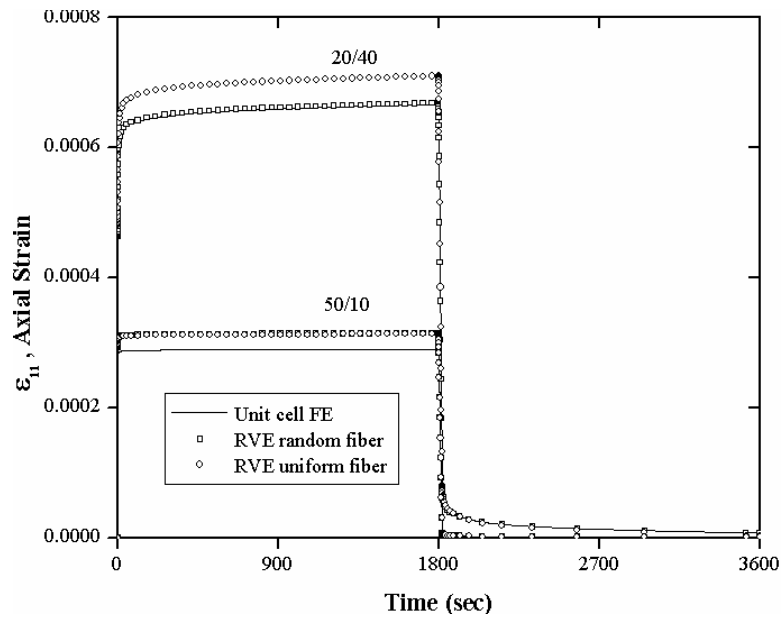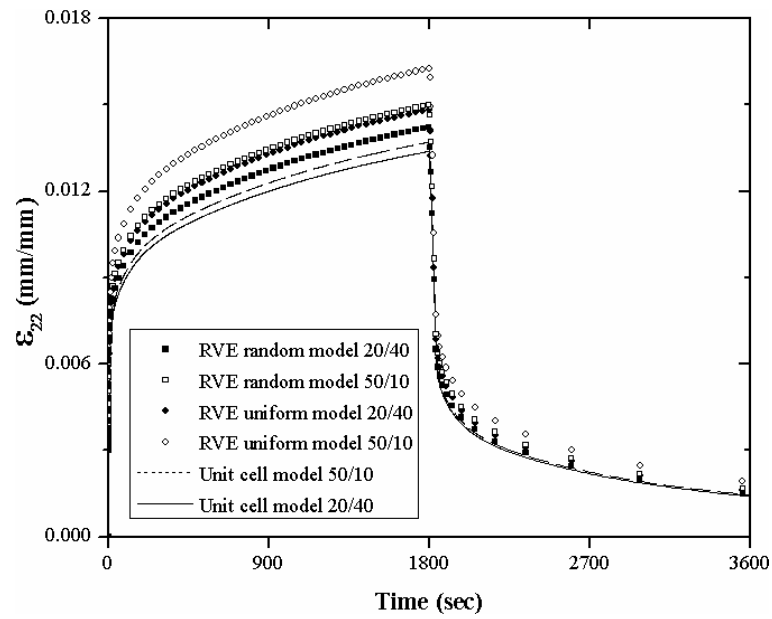

Figure 4-25. Creep recovery responses of 60% Vf for transverse loading

Table 4-11

Instantaneous transverse strain response at t=0.001 second

	(10/20)	(20/10)	(20/40)	(50/10)
Unit-cell	5.2192E-03	5.2484E-03	2.9459E-03	2.9502E-03
RVE random	5.2879E-03	5.3771E-03	3.0169E-03	3.1652E-03
	(1.32% error)	(2.45% error)	(2.26% error)	(7.29% error)
RVE uniform	5.2964E-03	5.4153E-03	3.1214E-03	3.1968E-03
	(1.48% error)	(3.18% error)	(5.96% error)	(8.36% error)

Table 4-12

Instantaneous transverse strain response at t=1800 second

	(10/20)	(20/10)	(20/40)	(50/10)
Unit-cell	2.7302E-02	2.7578E-02	1.3378E-02	1.3706E-02
RVE random	2.7598E-02	2.8637E-02	1.4210E-02	1.4989E-02
	(1.08% error)	(3.84% error)	(6.22% error)	(9.36% error)
RVE uniform	2.7745E-02	2.9935E-02	1.4809E-02	1.6254E-02
	(1.62% error)	(8.55% error)	(10.7% error)	(18.6% error)

Loading
at time 0.0001 sec

Loading
at time=1800 sec

Unloading
at time=2182 sec

S.Misses
MPa
+80
+73
+66
+60
+53
+46
+40
+33
+26
+20
+13
+66
+00

a)

b)

E,Principal
+0.06
+0.05
+0.05
+0.04
+0.04
+0.03
+0.03
+0.02
+0.02
+0.01
+0.01
+0.005
+0.000

c)

d)
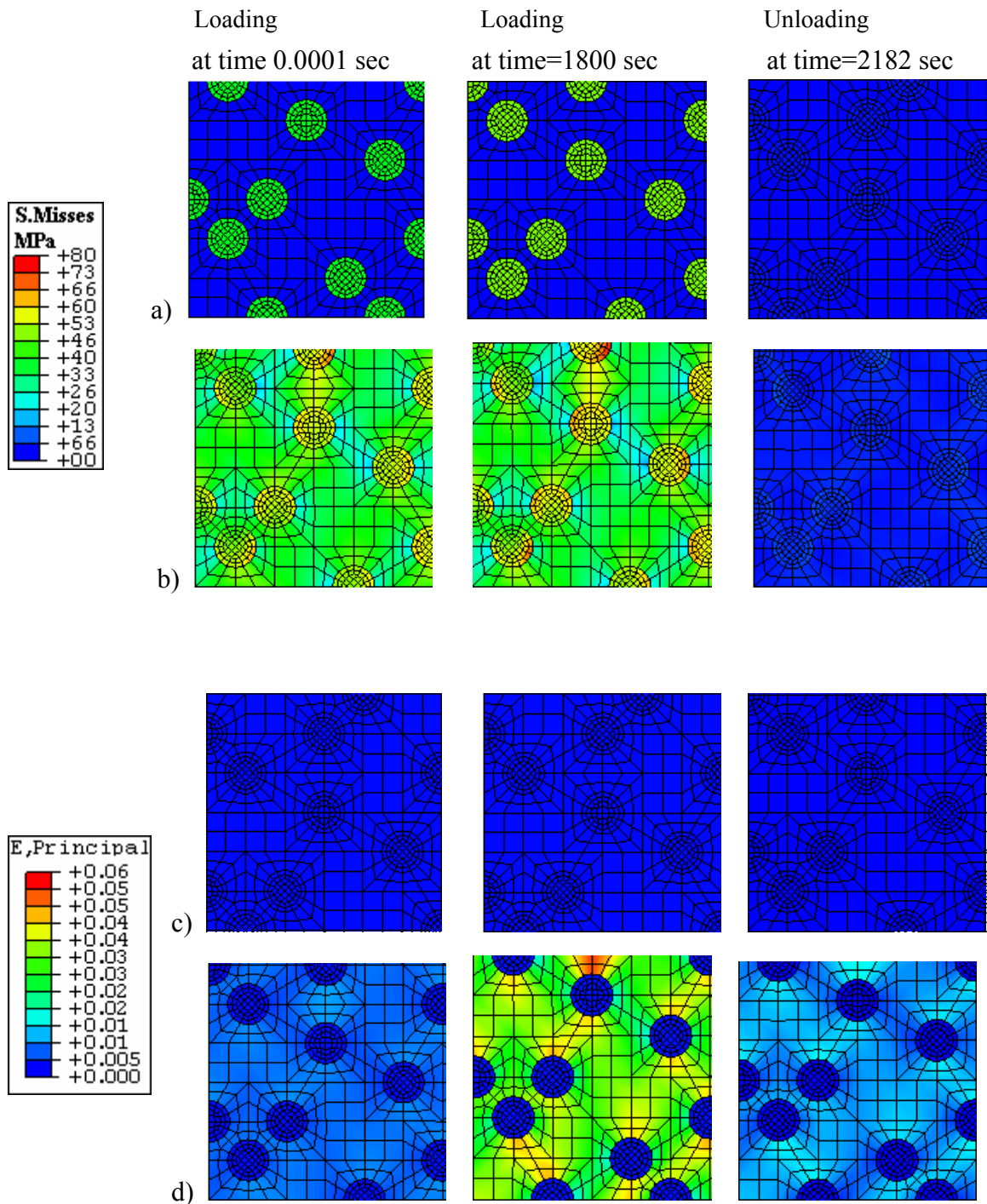
Figure 4-26. von-Misses Stress (in MPa) and maximum principal strain distribution of hybrid (20/10 r) under 40 MPa axial and transverse creep recovery loading a) stress distribution under axial loading b) stress distribution under transverse loading c) strain distribution under axial loading d) strain distribution under transverse loading
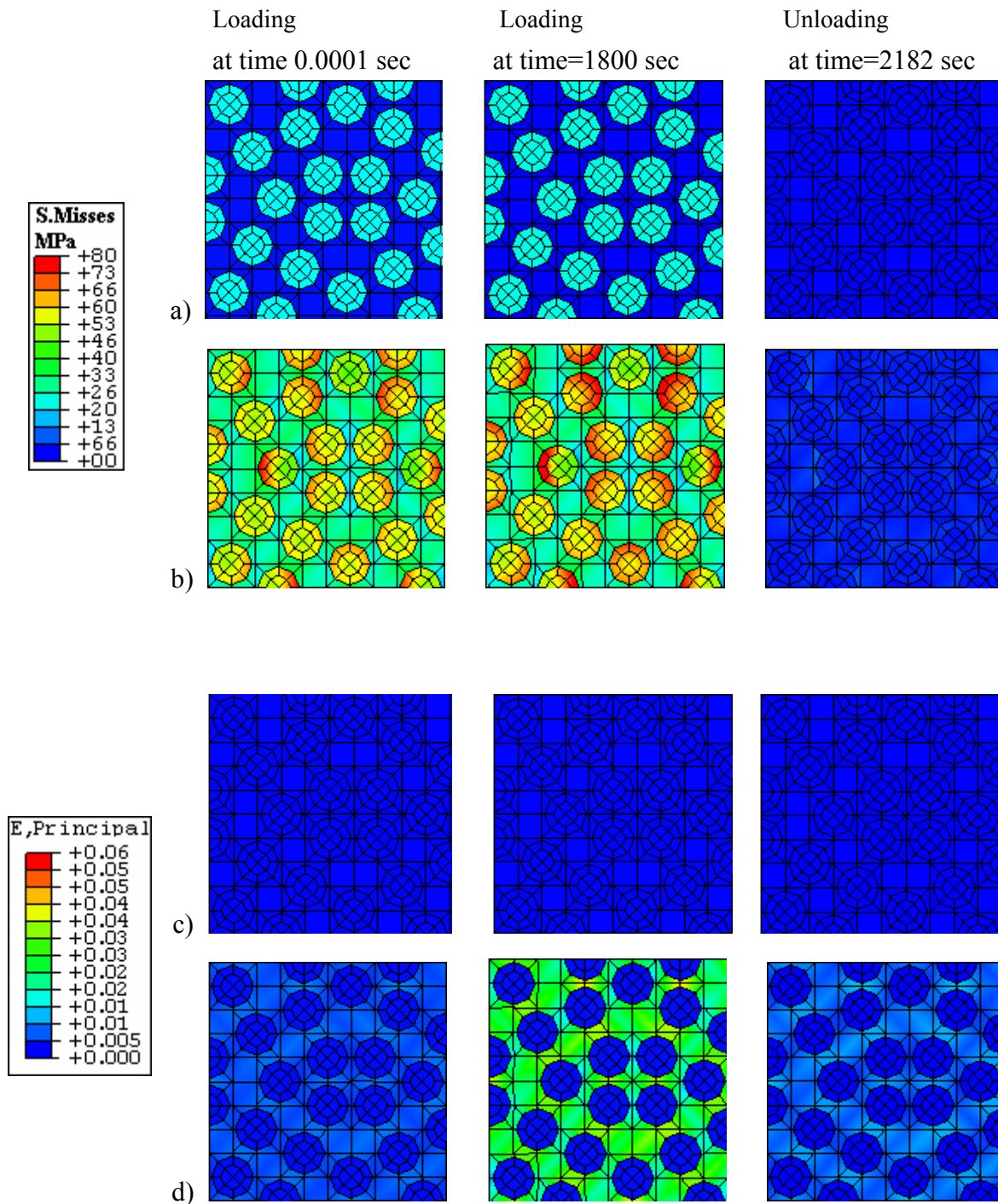
Figure 4-27. von-Misses Stress (in MPa) and maximum principal strain distribution of hybrid (50/10 r) under 40 MPa axial and transverse creep-recovery loading a) stress distribution under axial loading b) stress distribution under transverse loading c) strain distribution under axial loading b) strain distribution under transverse loading

CHAPTER V

CONCLUSION AND FUTURE RESEARCH

5.1 Conclusion

A simplified micromechanical model of particle reinforced polymer composites have been developed for combined viscoelastic-viscoplastic responses. The viscoelastic-viscoplastic responses are due to the existence of polymer matrix. The proposed micromechanical model provides the capability of predicting the overall time-dependent and inelastic responses of particle reinforced composite and quantifying stress-dependent behavior of the polymer constituent. The proposed micromechanical model has been used to provide effective properties of matrix, having filler particles dispersed in a homogeneous polymer, in the fiber-particle hybrid composites. Multiple time integration algorithms have been developed to solve the time-dependent and inelastic constitutive model in the polymer constituent, to link the nonlinear behavior of the polymer constituent to the micromechanical model, and to integrate the micromechanical model to the FE framework. The research findings and conclusions are discussed as follows:

1)   A time integration algorithm is formulated for solving a viscoelastic-viscoplastic

constitutive equation of polymers (Chapter II). The polymers are assumed to be

isotropic. A total strain is additively decomposed into recoverable viscoelastic and

irrecoverable viscoplastic strains. The Schapery integral model is used for the 3D

isotropic nonlinear viscoelastic responses. For the viscoplastic strain, two viscoplastic

constitutive models are considered, which are the Perzyna model, having a rate-

dependent yield surface and static yield condition, and the Valanis endochronic model

based on the irreversible thermodynamics without a yield surface. The chosen

constitutive material models are driven by observing overall (macroscopic) behaviors

of homogeneous polymers without an intention to capture changes in the

macromolecular structures of the polymers during loadings. Linearized solutions of

the nonlinear constitutive equations are obtained and an iterative scheme is added to

minimize errors arising from the linearization. The presented constitutive material

model and the solution method are suitable only for small deformation gradient

problems. The inclusion of viscous material parameters allows predicting time-

dependent responses subject to different loading rates. It should be mentioned that the

capability of the presented constitutive model in capturing responses of polymers due to high loading rates, such as impact loading, is still questionable.

2) In Chapter III, the homogenization method has been presented for modeling time-dependent and inelastic responses of polymer composites having solid spherical reinforcements. It is assumed that the particles of the same size and shape are uniformly distributed in a homogeneous polymer such that the gradient of the particle volume content is nearly zero. Each particle is fully surrounded by matrix and contact between particles is not being considered. A one eighth unit-cell model consisting of four sub-cells is generated and the homogenization for the stress and strain fields is defined in terms of the average strains and stresses in the sub-cells. A periodic boundary condition is imposed to the unit-cell model. Strain concentration matrices are used to relate the strains in the particle and matrix constituents to the effective strains of the composites. The traction continuity and displacement compatibility at the sub-cells' interfaces are imposed to formulate linearized micromechanical relations. Due to the nonlinear and time-dependent responses in the matrix sub-cells, the linearized micromechanical relations will usually violate the constitutive equations or the nonlinear constitutive relations will violate the traction and

displacement continuity conditions. The iterative corrector scheme is also formulated

to minimize errors from the linearization. The proposed homogenization scheme is

compatible with a displacement based FE framework and can sensibly predict overall

time-dependent responses of particle reinforced composites having low to medium

particle contents, i.e., less than 50%.

3)   The proposed micromechanical model has been successfully employed for modeling

matrix systems, having particle fillers, in fiber-particle reinforced hybrid composite

(Chapter IV). The studied hybrid systems consist of unidirectional fiber

reinforcements embedded in a matrix system having solid spherical particle fillers.

The simplified micromechanical model of particle reinforced composite is used to

obtain effective properties of the matrix system. This matrix system is integrated to

unit-cell models of unidirectional fiber reinforced composites, which are generated

using the FE code. Constitutive equations for viscoelastic and viscoplastic

deformations are used for the homogeneous constituents in the matrix systems.

Limited experimental data and analytical solutions have been used to verify time-

dependent and inelastic response of hybrid composites.

5.2 Future Research

The current study can be extended as follows:

1) The time-dependent and inelastic constitutive models can be modified to include the effects of environments, such as hostile thermal condition, on the viscoelastic-viscoplastic responses of polymers. It is also possible to take into account the dissipation of energy in the current viscoelastic-viscoplastic material models which is converted into heat. A general integral form of the time-dependent constitutive material model can be extended to include new history-dependent material parameters to account for macromolecular changes, such as scission, in the polymers during loadings, which has been presented by Wineman and Min (2002).

2) Interphase subcells can be added to the micromechanical model to simulate traction separation type damage between the particle and matrix subcells.

3) The study of hybrid composites can be extended for randomly oriented short fiber-particle reinforced hybrid composite.

4) It is also possible to add a higher level homogenization scheme for obtaining effective responses of fiber and matrix systems in the hybrid composites.

REFERENCES

ABAQUS User's Manual, Version 6.5, (2005), Hibbitt, Karlsson,, Sorensen, Inc.

Aboudi, J., 1991. Mechanics of Composite Materials: A Unified Micromechanical
Approach. Elsevier.

Aboudi, J., Pindera, M.J., Arnold, S.M., 1996. Thermoelastic theory for the response of
materials graded in two directions. Int. J. Solids, Structures 33, 931-966.

Aboudi, J., 2005. Micromechanically established constitutive equations for multiphase
materials with viscoelastic-viscoplastic phases. Mechanics of Time-dependent
Materials 9, 121-145.

Alberola, N.D., Mele. P., 1996. Viscoelasticity of polymers filled by rigid or soft
particles: theory and experiment. Polymers Composites 17, 751-759.

Aniskevich, K., Hristova, J., 2000. Creep of polyester resin filled with mineral. J. Alied
Polymers Sci. 77, 45-52.

Arunachaleswarran, A., Pereira, I.M., Dieringa, H., Huang, Y., Hort, N., Dhindaw, B.K.,
Kainer, K.U., 2007. Creep behavior of AE42 based hybrid composites. Materials
Science, Engineering A 460-461, 268-276.

Bathe, K.J., 1996. Finite element procedure. Englewood Cliffs, NJ: Prentice Hall.

Barello, R.B., Levesque, M., 2008. Comparison between the relaxation spectra obtained
from homogenization models, finite elements simulation for the same composite. Int.
J. of Solid, Struc. 45, 850-867.

Belayachi, N., Benseddiq, N., Aait-Abdelaziz, M., 2008. Behaviour of the heterogeneous

glassy polymers: computational modeling, experimental approach. Composites Science, Technology 68, 367-375.

Biwa, S., Ito, N., Ohno, N., 2001. Elastic properties of rubber particles in toughened PMMA: Ultrasonic, micromechanical evaluation. Mechanics of Materials, MOM 33, 717-728.

Bodner, S.R., Partom, Y., 1975. Constitutive equation for elastoviscoplastic strain hardening material. ASME J. Al. Mech. 385–389.

Bohm, H.J., 2008. A short introduction to basic aspects of continuum micromechanics. ILSB-Arbeitsbericht Report 206. CDL-FMD report 3-1998.

Chailleux, E., Davies. P., 2003. Modeling the nonlinear viscoelastic-viscoplastic behavior of aramid fiber yarns. Mech. Time-dependent Matl. 7, 291-301.

Chailleux, E., Davies. P., 2005. A nonlinear viscoelastic-viscoplastic model for the behavior of polyester fibers. Mech. Time-dependent Matl. 9, 147-160.

Chawla, N., Ganesh, V.V., Wunsch, B., 2004. Three-dimensional, 3D) microstructure visualization, finite element modeling of the mechanical behavior of the SiC particle reinforced aluminum composites. Scripta Materialia 51, 161–165.

Chen, X.H., Mai, Y.W., 1998. Micromechanics of rubber-toughened polymers. J. Materials Science 33, 3529-3539.

Cho, J., Joshi, M.S., Sun, C.T., 2006. Effects of inclusion size of mechanical properties of polymeric composites with micro, nano particles. Composite Sci. Technol., (in press).

Christensen, R. M., 1971. Theory of viscoelasticity. New York: Academic Press.

Christensen, R.M., 1969. Viscoelastic properties of heterogeneous media. J. Mech. Phys. Solids 17, 23–41.

Christensen, R.M., Lo, K.H., 1979. Solutions for effective shear properties in three phase sphere, cylindrical models. J. Mech. Phys. Solids 27, 4, 315–330.

Colak, O., 2005. Modeling deformation behavior of polymers with viscoplasticity theory based on overstress. Int. J. Plasticity 21, 145-160.

Danielsson,M., Parks, D.M., Boyce, M.C., 2007. Micromechanics, macromechanics, constitutive modeling of the elasto-viscoplastic deformation of rubber-toughened glassy polymers. Int. J. Mech., Phys. of Solids 55, 533-561.

Dommelen, J.A.W., Brekelmans, W.A.M., Baaijens, F.P.T., 2002. Micromechanics of particle-modified semi-crystalline materials. Fifth World Congress on Computational Mechanics, Vienna, Austria.

Drozdov, A., 1999. A constitutive model in viscoelastoplasticity of glassy polymers. Polymer 40, 3711-3727.

Drozdov, A.D., Christiansen, J.deC., 2008. Thermo-viscoelastic, viscoplastic behavior of high-density polyethylene. Int. J. of Solids and Structures 45, 4274-4288.

Drugan, W.J., Willis, J.R., 1996. A micromechanics-based nonlocal constitutive equation, estimates of representative volume element size for elastic composites. Journal of the Mechanics, Physics of Solids 44, 497-524.

Dvorak, G.J., Srinivas, M.V., 1999. New estimates of overall properties of heterogeneous solids. J. Mech. Phys. Solids 47, 899–920.

Eroshkin, O., Tsukrov, I., 1995. On micromechanical modeling of particulate composites

with inclusions of various shapes. Int. J. Solids Struct. 42, 409–427.

Eshelby, J. D., 1957. The determination of the elastic field of an ellipsoidal inclusion, and related problem. Proc. Roy. Soc., London A241, 376-396.

Findley,W.N., Lai, J.S., Onaran, K., 1976. Creep and relaxation of nonlinear viscoelastic materials. New York: Dover Publication.

Frank, G.J., 1998. A constitutive model for the mechanical responses of glassy polymers. Ph.D. Thesis, University of Dayton, Dayton, OH.

Frank, G.J., Brockman, R.A., 2001. A viscoelastic-viscoplastic constitutive model for glassy polymers. Int. J. Solids, Structures 38, 5149-5164.

Friend, C.M., Horsfall, I., Burrows, C.L., 1991. The effect of particulate: fibre ratio on the properties of short-fibre/particulate hybrid MMC produced by perform infiltration. J. of Mat. Sci. 26, 225-234.

Fu, S.Y., Xu, G., Mai, Y.W., 2002. On the elastic modulus of hybrid particle/short-fiber/polymer composites. Composites: Part B 33, 291-299.

Ghosh, S., Mukhopadhyay, S.N., 1991. A two-dimensional automatic mesh generator for finite element analysis of random composites. Compt. & Structures 41, 245-256.

Ghosh, S., Mukhopadhyay, S.N., 1993. A material based finite element analysis of heterogeneous media involving Dirichlet tessellations. Comput. Methods Al. Mech.Engrg. 101, 211-247.

Ghosh, S., Mallett, R. L., 1994. Voronoi cell finite element. Compt. & Structures 501, 33-46.

Ghosh, S., Moorthy, S., 1995. Elastic-plastic analysis of arbitrary heterogeneous

materials with the Voronoi cell finite element method. Comput. Methods Al. Mech. Engrg. 121, 373-409.

Ghosh, S., Lee, K.H., Moorthy, S., 1995. Multiple scale analysis of heterogeneous elastic structures using homogenization theory, voronoi cell finite element method. Int. J. Solids Structures 32, 1, 27-62.

Green, E., Rivlin, R.S., 1957. The Mechanics of nonlinear materials with memory. Arch. Rational Mech. Anal. 1, 1-21.

Haj-Ali, Muliana, 2004. Numerical finite element formulation of the Schapery nonlinear viscoelastic material model. Int. J. Numerical Meth. in Eng. 59, 1, 25-45.

Haj-Ali, R.M., Muliana, A.H., 2003. Micromechanical models for the nonlinear viscoelastic behavior of pultruded composite materials. Int. J. Solids, Structures 40, 1037-1057.

Haj-Ali, R.M., Kilic, H., Zureick, A.H., 2001. Three-dimensional micromechanics-based constitutive framework for analysis of pultruded structures. Journal of Engineering Mechanics 127, 7, 653-660.

Haj-Ali, R.M., Muliana, A.H., 2004a. A multi-scale constitutive framework for the nonlinear analysis of laminated composite materials, structures. Int. J. Solids Struct. 41, 3461–3490.

Haj-Ali, R.M., Muliana, A.H., 2004b. Numerical finite element formulation of the Schapery nonlinear viscoelastic material model. Int. J. Numer. Meth. Eng. 59, 1, 25–45.

Haj-Ali, R.M., Pecknold, D.A., 1996. Hierarchical material models with microstructure

for nonlinear analysis of progressive damage in laminated composite structures, Struct. Res. Ser. No. 611, UILU-ENG-96-2007, Department of Civil Engineering, University of Illinois at Urbana-Champaign.

Hall, R.B., 2005. A thermodynamic framework for viscoplastic based on overstress. ASME J. Engrg. Mater. Technol. 127, 369-373

Halpin,J.C., Jerine,K., Whitney, J.M., 1971. The laminate analogy for 2, 3 dimensional composite materials. J. Composite Materials 5, P36-49.

Harper, B.D., Weitsman, Y., 1985. Characterization method for a class of thermorheologically complex materials. J. Rheology 29, 49–66.

Hashin Z., 1970. Complex moduli of viscoelastic composites-2 fiber reinforced materials. Int J Solid Structures. 68, 797–807.

Hashin Z., 1966. Viscoelastic fiber reinforced materials. AIAA 4, 1411.

Hashin Z, Rosen Walter B., 1964. Elastic moduli of fibre-reinforced materials. J Alied Mechanics 223–232.

Hashin, Z., 1983. Analysis of composite materials - A survey. ASME J. Al. Mech. 50, 481–505.

Hashin, Z., Shtrikman, S., 1962. On some variational principles is anisotropic, nonhomogeneous elasticity. J. Mech. Phys. Solids 10, 335–342.

Haythornthwaite, R.M., 1968. A more rational approach to strain-hardening data. Engineering Plasticity, Cambridge: Cambridge University Press.

Heeres, O.M., Suiker, A.S. J., de Borst, R., 2002. A comparison between the Perzyna viscoplastic model, the consistency viscoplastic model. European J. Mech. A, 21, 1-

12.

Henriksen, M., 1984. Nonlinear viscoelastic stress analysis–A finite element approach. Computer Structures 18, 133-139.

Hill, R., 1963. Elastic properties of reinforced solids: Some theoretical principles. J. Mech.Phys. Solids 11, 357-372.

Hill, R., 1965. A self consistent mechanics of composite materials. J. Al. Mech. Phys. Solids 13, 213-222.

Hornberger, K., Stamm, H., 1989. An implicit integration algorithm with a projection method for viscoplastic constitutive equations. Int. J. Numer. Meth. Engrg. 28, 2397-2421.

Hutchinson, J.W., 1976. Bounds, self-consistent estimates for creep of polycrystalline materials. Proc. Roy. Soc. London A348, 101-127.

Ju, W., 1990. Consistent tangent moduli for a new class of viscoplasticity. Journal of Engineering Mechanics 116, 1764-1779.

Ju, J.W., 1992. On algorithmic tangent moduli for a class of viscoplastic models. AMD 135, Plastic Flow Creep 31, 67-78.

Ju, J.W., Chen, T.M., 1994. Micromechanics, effective elastoplastic behavior of two phase metal matrix composites. Journal of Engineering Materials Technology 116, 310-318.

Ju, J.W., Tseng, K.H., 1996. Effective elastoplastic behavior of two-phase ductile matrix composites: a micromechanical framework. Int. J. Solids Struct. 33 4267–4291.

Ju, J.W., Tseng, K.H., 1997. Effective elastoplastic algorithm for ductile matrix

composites. J. Engng. Mech. **123,** 3, 260–266.

Kanaun, S.K., Jeulin.D., 2001. Elastic properties of hybrid composites by the effective
field aroach. J. of the Mechanics, Physics of Solids 49, 2339-2367.

Kari, S., Berger, H., Rodriguez-Ramos, R., Gabbert, U., 2005. Computational evaluation
of effective material properties of composites reinforced by randomly distributed
spherical particles. Composite Structures (in press).

Kari, S., Berger, H., Rodriguez-Ramos, R., Gabbert, U., 2007. Computational evaluation
of effective material properties of composites reinforced by randomly distributed
spherical particles. Compos. Struct. 77, 223–231.

Kennedy, T. C., 1998. Nonlinear viscoelastic analyses of composite plates, shells.
Composite Structures 41, 265-272.

Kerner, E.H., 1956. The elastic, thermo-elastic properties of composite media. Proc.
Phys. Soc. 69, 8B, 808–813.

Khan, A.S., Huang, S., 1995. Continuum theory of plasticity. New York: Wiley-Interscience.

Kim, J.S., Muliana, A.H., 2009. A time-integration method for the viscoelastic-
viscoplastic analyses of polymers and finite element implementation. Int. J. Numer.
Mech. Engng. 1-26

Kinloch, A.J., Maxwell, D., Young, R.J., 1985. Micromechanics of crack propagation in
hybrid-particulate composites. J. Matr. Sci. Letter 4, 1276–1279.

Kojic, B. 2005. Inelastic analysis of solids, structures. New York: Springer.

Krempl, E., Ho, K., 2000. An over stress model for solid polymer deformation behavior
applied to Nylon66. ASTM--STP 1357, 118-137.

Lai, J., Bakker, A., 1995. An integral constitutive equation for nonlinear plasto-viscoelastic behavior of high-density polyethylene. Polymer Engr. Sci. 35, 1339-1347.

Lai, J., Bakker, A, 1996. 3-D Schapery representation for nonlinear viscoelasticity, vinite element implementation. Computational Mechanics 18, 182-191.

Landau, H.H., Weiner, J.H., Zwicky, E.E., 1960. Thermal stress in a viscoelastic-plastic plate with temperature dependent yield stress. J. Alied Mechanics, Trans. ASME 27, 297-302.

Leiden, J., Woodhams, R.J., 1974. The strength of polymeric composites containing spherical fillers. J. Alied Polymer Sci. 18, 1639.

Levesque, M., Derrien, K., Mishnaevski, L., Baptiste, D., Gilchrist, M. D., 2004. A micromechanical model for nonlinear viscoelastic particle reinforced polymeric composite materials: Undamaged state. Composites A 35, 905-913.

Levesque, M., Gilchrist, M.D., Bouleau, N., Derrien, K., Baptiste, D., 2007. Numerical inversion of the Laplace–Carson transform applied to homogenization of randomly reinforced linear viscoelastic media. Computational Mechanics 40, 4, 771–789.

Levy, A., Pifko, A. B., 1981. On computational strategies on problems involving plasticity, creep. Int. J. Numer. Meth. Engrg. 17, 747-771.

Li, J., Weng, G.J., 1993. Effective viscoelastic behavior, complex moduli of a class of isotropic polymer matrix composites. ASME, MD Publication, Mater. Mech. Issue, 46, 207–225.

Liu, J. et al, 1998. Hybrid mesoporous materials with functionalized monolayers. Chem.

Eng. Technol., 21, 1.

Lockett, F. J., 1972. Nonlinear viscoelastic solids. New York: Academic Press.

Mareau, C., Favier, V., Berveiller, M., 2009. Micromechanical modeling coupling time-independent, time-dependent behaviors for heterogeneous materials. IJSS, 46, 223-237.

McLaughlin, R., 1977. A study of the differential scheme for composite materials. Int. J. Eng. Sci. 15, 237–244.

Megnis, M., Varna, J., 2003. Micromechanics based modeling of nonlinear viscoplastic response of unidirectional composite. Composites Science and Technology 63, 19-31.

Mondal, A.K., Kumar, S., 2008. Impression creep behaviour of magnesium alloy-based hybrid composite in the longitudinal direction. Composites Science and Technology 68, 3251-3258.

Mori, T., Tanaka, K., 1973. Average stress in matrix, average elastic energy of materials with misfitting inclusions. Acta Metall. 21, 571–574.

Muliana, A. H., Khan, A. K., 2006. A time integration scheme for stress-temperature behaviors of adhesive polymer. Computer Method in Alied Mechanics Engineering (submitted).

Muliana, A. H., Kim, J. S., 2007. A concurrent micromechanical model for nonlinear v iscoelastic behaviors of particle reinforced composites. Int. J. Solids and Structures 44, 6891-6913.

Mura, T., 1987. Micromechanics of defects in solids. Dordrecht: Martinous Nijhoff Publishers.

Naghdi, P. M., Murch, S. A., 1963. On the mechanical behavior of viscoelastic/plastic solids. J. Allied Mechanics 30, 321-327.

Nemat-Nasser, S., Hori, M., 1999. Micromechanics: overall properties of heterogeneous materials. 2nd Ed., Burlington, MA: Elsevier.

Oh, K.H., Han, K.S., 2007. Short-fiber/particle hybrid reinforcement: Effects on fracture toughness, fatigue crack growth of metal matrix composites. Composite Science, Technology 67, 1719-1726.

Park, S.W., Schapery, R.A., 1997. A viscoelastic constitutive model for particulate composite with growing damage. Int. J. Solids Struct. 34, 8, 931–947.

Perzyna, P., 1966. Fundamental problems in viscoplasticity. Advances in Allied Mechanics 9, 243-377.

Perzyna, P., 1971. Thermodynamic of rehological materials with internal changes, J. Mech. 10, 391-408.

Perzyna, P., Wojno, W., 1975. Unified constitutive equations for elastic. Viscoplastic Materials 24, 85-94.

Pierard, O., Lorca, J., Segurado, J., Doghri, I., 2007. Micromechanics of particle-reinforced elasto-viscoplastic composites: Finite element simulations versus affine homogenization. International Journal of Plasticity 23, 1041-1060.

Pipkin, A. C., 1972. Lectures of viscoelasticity theory. New York: Springer-Verlag.

Poon, H., Ahmad, F., 1999. A finite element constitutive update scheme for anisotropic, viscoelastic solids exhibiting non-linearity of the Schapery type. International Journal of Numerical Method in Engineering 46, 2027-2041. 297-302.

Rajagopal, K.R., Srinivasa, A.R., 2005. A note on a correspondence principle in nonlinear viscoelastic materials. Int. J. Fracture. 131, 47–52.

Schapery, R. A., 1969. On the characterization of nonlinear viscoelastic materials. polymer engineering, Science 9, 4, 295-310.

Schapery, R. A., 1997. Nonlinear viscoelastic, viscoplastic constitutive equations based on thermodynamics. Mechanics of Time-Dependent Materials 1, 209.

Schapery, R.A., 1969. On the characterization of nonlinear viscoelastic materials. Polym. Eng. Sci. 9, 4, 295–310.

Seelig, T., Van der Giessen, E., 2002. Localized plastic deformation in ternary polymer blends. IJSS 39, 3505-3522.

Simo, J.C., Hughes, T., J., R., 1998. Computational inelasticity. New York: Springer-Verlag.

Takahashi, S., Katoh, T., Taguchi, S., Watanabe, T., 1983. Glass-fiber, graphite flake reinforced polyimide composite diaphragm for loudspeakers. J. Audio Eng. Soc. 31, 10, 723–728.

Tsou, A.H., DelleFave, D.L., 1996. Creep of a glass-flake-reinforced epoxy adhesive for space alications. Polymer 37(24), 5381-5386.

Valanis, K.C., 1971. A theory of viscoplasticity without a yield surface. Part 1, general theory. Arch. Mech. 23, 517-533.

Wang, W.M., Sluys, W. J., de Borst, R., 1997. Viscoplasticity for instabilities due to strain softening, strain-rate softening. Int. J. Numer. Meth. Engrg. 40, 3839-3864.

Weng, G.J., 1993. A self-consistent relation for the time-dependent creep of polycrystals. Int. J. Plasticity 9,191-198.

Willis, J.R., 1977. Bounds, self-consistent estimates for the overall properties of anisotropic composites. J. Mech. Phys. Solids 25, 185–202.

Wong, F.C., Ait-Kadi, A., 1995. Mechanical behavior of particulate composites: experiments, micromechanical predictions. J. Alied Polymer Sci. 55, 263-278.

Wong, F.C., Ait-Kadi, A., 1995. Mechanical behavior of particulate composites: experiments, micromechanical predictions. J. Al. Polym. Sci. 55, 263–278.

Yang, L., Wang, L., Zhu, Z., 1994. Micromechanical analysis of the nonlinear elastic, viscoelastic constitutive relations of a polymer filled with rigid particles. Acta Mechanica Sinica. 10, 2, 176–185.

Yang, W., Shi, Li, Z. M, Xie, B.H, Feng, J.M., Yang, M. B, 2004. Mechanical properties of glass bead-filled linear low-density polyethylene. J. Elastomers, Plastics 36, 251-26

Yilmazer, U., 1992. Tensile, flexural, impact properties of a thermoplastic matrix reinforced by glass fiber, glass bead hybrids. Composite Science and Technology 44, 119-125.

Young, R.J., Maxwell, D.L., Kinloch, A.J., 1986. The deformation of hybrid-particulate composites. J. Mater. Sci. 21, 380–388.

Zebarjad, S.M., Bagheri, R., Lazzeri, A., 2001. Hybrid –GF–EP. Part 1. Deformation mechanism. Plast Rubber Compos, 30, 370.

Zienkiewicz, O. C., Cormeau, I. C., 1972. Viscoplasticity solution by finite element process. Archive of Mechanics 25, 873-889.

Zienkiewicz, O.C., Cormeau, I.C., 1974. Viscoplasticity-plasticity and creep in elastic

solids: A unified numerical solution approach. Int. J. Numer. Meth. Engrg. 8, 821-845.

VITA

Name: Jeong-Sik Kim

Address: Texas A&M University
                   Department of Mechanical Engineering
                   3123 TAMU
                   College Station, TX 77845-3123
                   c/o Hanifah Muliana

Email Address: jeongsik77@hotmail.com
                   tojeongsik@gmail.com

Education: B.S., Mechanical Engineering, Donga University, South Korea, 1998
                   M.S., Mechanical Design Engineering, Pusan National Univeristy,
                       South Korea, 2001
                   Ph.D., Mechanical Engineering, Texas A&M University,College
                       Station, USA, 2009